Trends in Mathematics
Research Perspectives CRM Barcelona Vol.4

Montserrat Corbera
Josep Maria Cors
Jaume Llibre
Andrei Korobeinikov
Editors

Extended Abstracts Spring 2014

Hamiltonian Systems and Celestial Mechanics

Virus Dynamics and Evolution

CRM CENTRE DE RECERCA MATEMÀTICA

Birkhäuser

Trends in Mathematics

Research Perspectives CRM Barcelona

Series editors

Enric Ventura
Antoni Guillamon

Since 1984 the Centre de Recerca Matemàtica (CRM) has been organizing scientific events such as conferences or workshops which span a wide range of cutting-edge topics in mathematics and present outstanding new results. In the fall of 2012, the CRM decided to publish extended conference abstracts originating from scientific events hosted at the center. The aim of this initiative is to quickly communicate new achievements, contribute to a fluent update of the state of the art, and enhance the scientific benefit of the CRM meetings. The extended abstracts are published in the subseries Research Perspectives CRM Barcelona within the Trends in Mathematics series. Volumes in the subseries will include a collection of revised written versions of the communications, grouped by events.

More information about this series at http://www.springer.com/series/4961

Extended Abstracts Spring 2014

Hamiltonian Systems and Celestial Mechanics

Montserrat Corbera
Josep Maria Cors
Jaume Llibre
Editors

Virus Dynamics and Evolution

Andrei Korobeinikov
Editor

Birkhäuser

Editors
Montserrat Corbera
Departament de Tecnologies Digitals,
Campus Torre dels Frares
Universitat de Vic
Vic, Spain

Josep Maria Cors
Departament de Matemàtica Aplicada III
Universitat Politècnica de Catalunya
Manresa, Spain

Jaume Llibre
Departament de Matemàtiques
Universitat Autònoma de Barcelona
Barcelona, Spain

Andrei Korobeinikov
Centre de Recerca Matemàtica
Barcelona, Spain

ISSN 2297-0215 ISSN 2297-024X (electronic)
Trends in Mathematics
ISBN 978-3-319-22128-1 ISBN 978-3-319-22129-8 (eBook)
DOI 10.1007/978-3-319-22129-8

Library of Congress Control Number: 2015954093

Mathematics Subject Classification (2010): First part: 34C25, 34C29, 65P30, 70H05; Second part: 92D15, 92D25, 92D30

Springer Cham Heidelberg New York Dordrecht London

Printed on acid-free paper

Springer International Publishing AG Switzerland is part of Springer Science+Business Media (www.birkhauser-science.com)

Contents

Part I
Hamiltonian Systems and Celestial Mechanics

Editors

Montserrat Corbera
Josep Maria Cors
Jaume Llibre

Foreword

From January to July 2014, the Research Programme *Central Configurations, Periodic Orbits and beyond in Celestial Mechanics* took place at the Centre de Recerca Matemàtica (CRM), in Bellaterra, Barcelona. It was coordinated by Montserrat Corbera (Universidad de Vic, Spain), Josep Maria Cors (Universitat Politècnica de Catalunya, Spain), and Jaume Llibre (Universitat Autònoma de Barcelona, Spain).

During these intense seven months, several scientific events took place, including an international conference (the HAMSYS-2014), three advanced courses, and a weekly seminar, all of them with the active participation of many visitors invited to attend from several countries abroad. Of course, additionally, all participants had numerous occasions to host informal but fruitful conversations among themselves, discussing mathematical ideas which, in many cases, gave rise to new and interesting results; altogether in a very dynamic and productive research atmosphere.

In this volume of the subseries Research Perspectives CRM-Barcelona (published by Birkhäuser inside the series Trends in Mathematics), we present fifteen Extended Abstracts corresponding to selected talks given by participants in the Research Programme. More than half of them come from talks at the *Conference on Hamiltonian Systems and Celestial Mechanics 2014 (HAMSYS2014)* (held from June 2nd to 6th, 2014), and the rest come from talks at the weekly seminar held along the first semester of 2014. We hope the presentation of this material under the present Extended Abstract form will give to the authors the opportunity to

quickly communicate their recent research: most of the short articles here are brief and preliminary presentations of new results not yet published in regular research journals.

We would like to express our gratitude to CRM for hosting and supporting our research programme. Also our warm thanks to the CRM staff, its director, Joaquim Bruna, and all the secretaries for providing great facilities and a very pleasant working environment. Finally, thanks are due to all those who attended the talks, for their interest, their active participation, and their enthusiasm towards mathematics.

Vic, Spain — Montserrat Corbera
Manresa, Spain — Josep Maria Cors
Barcelona, Spain — Jaume Llibre

On the Force Fields Which Are Homogeneous of Degree −3

Alain Albouy

Soon after establishing the famous properties of the $1/r^2$ law of force, Newton described a spiraling orbit of a particle under a central force in $1/r^3$. He also noticed that the addition of a force in $1/r^3$ to another force results in a kind of precession of the orbit, see [14, Book 1, Proposition 44]. In 1842, Jacobi [8] gave general results about the force fields which are homogeneous of degree -3 and derived from a potential. More recently, Montgomery [12] gave an impressive description of the dynamics of the planar 3-body problem with a force in $1/r^3$. Such homogeneity of the force also appears in Appell's projective dynamics, where the force is considered together with a constraint, see [2].

Here we deduce a very elementary property: the dynamics defined by a force field which is homogeneous of degree -3 can always be reduced, by simply constraining it. This remark is indeed an elegant foundation of Appell's projective dynamics. We will see how does it relate to other known properties.

Proposition 1 *Let $\Omega \subset V$ be an open semi-cone in a finite dimensional real vector space V, and $f\colon \Omega \to V$ be a vector field which is positively homogeneous of degree -3. The dynamics of the ordinary differential equation $\ddot{q} = f(q)$ is reduced by one degree of freedom (i.e., by two dimensions) by constraining it to any hypersurface transverse to the rays, the constraint being imposed by means of a central reaction.*

Here *semi* and *positively* refer to the fact that we are only concerned with the *half*-lines drawn from the origin of the vector space, called *rays*. The term *reaction* refers to the familiar mechanical system formed by a particle moving on a surface. In this familiar situation the reaction is normal to the surface. But in our proposition the reaction is *central*, i.e., "radial", i.e., carried by the ray. The existence and uniqueness theorems for the solution of such kind of constrained system are easy.

A. Albouy (✉)
IMCCE, CNRS, Observatoire de Paris, Paris, France
e-mail: albouy@imcce.fr

M. Corbera et al. (eds.), *Extended Abstracts Spring 2014*, Trends in Mathematics 4,
DOI 10.1007/978-3-319-22129-8_1

Their proofs do not depend on the particular choice concerning the direction of the reaction, provided that this direction is fixed in advance and transverse to the hypersurface.

Proof We write the equation of the hypersurface $h(q) = 1$, where $h\colon \Omega \to]0, +\infty[$ is a positively homogeneous function of degree 1. We denote by $q_1 = q/h(q)$ the central projection of q on the hypersurface. We will show that q_1 follows some trajectory of the system defined by the constraint and by the force field f.

We start with the given equation $\ddot{q} = f(q)$. We compute $\dot{q}_1 = h^{-2}(h\dot{q} - \dot{h}q)$. Instead of differentiating again with respect to the time t, we introduce a change of time depending only on the position q. The corresponding differentiation on any quantity r is denoted by r' and the change of time is defined by the formula $r' = h^2\dot{r}$. We get $q_1' = h\dot{q} - \dot{h}q$, $q_1' = h\ddot{q} - \ddot{h}q$ and $q_1'' = h^3\ddot{q} - h^2\ddot{h}q$. But $h^3\ddot{q} = h^3 f(q) = f(q_1)$ according to the degree of homogeneity of the force field f. The final equation is $q_1'' = f(q_1) + \lambda q_1$, where $\lambda = -h^3\ddot{h}$. The value of λ should be rather thought of as determined by the constraint: q_1 remains on the hypersurface, which determines uniquely the value of the multiplier λ. □

This reduction process is not standard. The reduction by two dimensions does not involve a constant of motion. We can describe it as the effect of two vector fields Y and Z related with the vector field X defined by our ordinary differential equation. The three vector fields are characterised by $\partial_X q = \dot{q} = p$, $\partial_X p = \dot{p} = f(q)$, $\partial_Y q = q$, $\partial_Y p = -p$, $\partial_Z q = 0$, $\partial_Z p = q$. The Lie brackets $[X, Y] = 2X$, $[Y, Z] = 2Z$, $[Z, X] = Y$ show that the subspaces generated at each (q, p) by X, Y and Z form an integrable distribution in the sense of the Frobenius [–Stefan–Sussmann] theorem. Note also that these brackets define a Lie algebra sl_2. The three-dimensional integral manifolds intersect our constraint along curves, which are the trajectories of the constrained system.

A force field f with degree of homogeneity α defines an X which satisfies the commutation relation $[X, Y_\beta] = (1-\beta)X$, where Y_β is defined by $\partial_{Y_\beta} q = q$, $\partial_{Y_\beta} p = \beta p$, and where $2\beta = \alpha + 1$. If $\alpha \neq -3$, nothing replaces the vector field Z, and we can only reduce by one dimension.

Proposition 1 is the fastest way to introduce projective dynamics. If we start with a dynamics defined by a force field on an affine space of dimension n, we can embed this space as an affine hyperplane in a vector space V of dimension $n + 1$, and extend the force to V by homogeneity of degree -3. Then we constrain this homogeneous force field to another hypersurface (another "screen"), thus producing another system which is very simply related with the initial one. Many dynamical properties are thus preserved by central projection. We already know that many geometrical properties are also preserved by central projection, and this remark is the foundation of projective geometry. Thus, we should similarly consider that there is a projective dynamics, which extends projective geometry to the motions generated by force fields.

Applying this construction to the two fixed centres problem allows deducing the well-known integrability of this problem from purely geometric considerations.

By choosing a convenient quadric as the other screen, the question reduces to considerations on the intersections of a plane with two cylinders, see [2].

Facts related to Proposition 1 are known in the case where f is derived from a potential, see [3, pp. 161, 169, 172] and [5]. The following observation may be new.

Proposition 2 *If the vector space V is endowed with an inner product, if the force field f of Proposition 1 is the gradient of a function $U\colon \Omega \to \mathbb{R}$ with respect to this inner product, and if we constrain f, by means of a central reaction, to the intersection S of Ω with the unit sphere, then the multiplier λ associated to the constraint is the energy multiplied by -2.*

Here, the central reaction is normal. We have a natural constrained system on S. The potential is the restriction of U to S. If we start with such a natural system on S, we form the unique extension of the potential in a function U on Ω which is positively homogeneous of degree -2. Note that $f = \nabla U$ will not be tangent to the sphere, which does not affect the dynamics but does affect the value of the multiplier λ.

Proof To determine λ in the equation $\ddot{q} = \nabla U + \lambda q$ we differentiate twice the constraint $\langle q, q\rangle = 1$. We get $0 = \langle q, \dot{q}\rangle$ and $0 = \langle q, \nabla U + \lambda q\rangle + \langle \dot{q}, \dot{q}\rangle = -2U + \lambda + \langle \dot{q}, \dot{q}\rangle$. □

Proposition 2 plays an interesting role in the relation discovered by Knörrer between the Neumann potential on the sphere and the geodesics on an ellipsoid, see [6, 9]. We will exhibit an intermediate problem which clarifies this relation as well as the integrability of the Neumann potential. Consider a symmetric positive definite $G\colon V \to V^*$ and the vector field on $\Omega = V \setminus \{0\}$

$$f(q) = \frac{Mq}{\langle Gq, q\rangle^2},$$

where $M\colon V \longrightarrow V$ is such that $GM = {}^tMG$. In words, the linear map M is symmetric with respect to the inner product G. We may make explicit this symmetry in two ways: through a symmetric $B\colon V \to V^*$ such that $M = G^{-1}A$, or through a symmetric $B\colon V \to V^*$ such that $M = B^{-1}G$. For simplicity of exposition we assume that A is positive definite (and then so is $B = GA^{-1}G$).

The formula $M = G^{-1}A$ suggests to endow V with the inner product G and to observe that f is, up to a central force, the gradient of the function $\langle Gq, q\rangle^{-2}\langle Aq, q\rangle/2$. By constraining the dynamics to the sphere $\langle Gq, q\rangle = 1$, we get the Neumann potential.

The formula $M = B^{-1}G$ suggests to endow V with the inner product B and to observe that f is the gradient of the function $-\langle Gq, q\rangle^{-1}/2$. Constraining the dynamics to $\langle Bq, q\rangle = 1$, we get our intermediate problem, whose integrability was established by Braden, see [7, 17]. This is a natural system on the sphere, defined by a potential which is the inverse of a quadratic form (while the Neumann potential is a quadratic form).

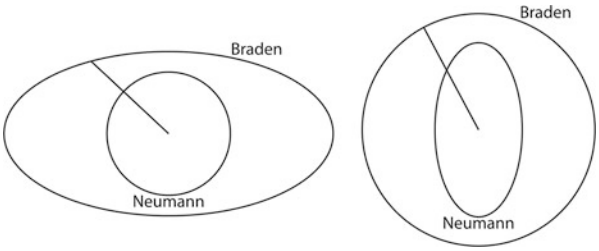

We can deduce the integrability of both the Neumann potential and our intermediate problem from their correspondence through central projection and change of time. They are *quasi-bi-Hamiltonian* systems, as already claimed about the Neumann potential in [1, 4, 15]. This last reference also connects this remark to the works [10, 11, 16].

Let us consider the Jacobi problem on the ellipsoid. The motion of a particle Q on the ellipsoid $\langle AQ, Q\rangle = 1$ embedded in the Euclidean vector space (V, G), under the potential $\nu\langle GQ, Q\rangle/2$, is defined by the equation

$$\ddot{Q} = \mu MQ + \nu Q.$$

Here, μ is a multiplier. The case $\nu = 0$ defines the geodesic motion on the ellipsoid. The addition of this potential was already considered by Jacobi, and again by Moser [13] in connection with Knörrer's work. Differentiating the constraint three times, we find Joachimsthal's constant of motion in the form $\eta = \mu\langle AQ, MQ\rangle^2$. The motion of $q = MQ$ is constrained by $\langle Bq, q\rangle = 1$ and satisfies the equation

$$\ddot{q} = \frac{\eta}{\langle Gq, q\rangle^2} Mq + \nu q.$$

This constraint and this equation also define our intermediate problem. But η and ν have a different interpretation in both problems. In the Jacobi problem, ν is a parameter and η is a multiplier which appears to be a constant of motion. In our intermediate problem $\eta = 1$ and ν is a multiplier which, according to Proposition 2, is a constant of motion. Any orbit of a problem is an orbit of the other problem for some choice of a parameter.

This is similar to what was explained by Knörrer and Moser, except that they needed a change of the time parameter and we did not. The motion on a sphere under the inverse of a quadratic potential is thus closer to the Jacobi problem than the motion on the sphere under a quadratic potential.

The introduction of our intermediate problem allows decomposing the Gauss map $Q \mapsto MQ/\|MQ\|$ introduced by Knörrer, into two steps: $Q \mapsto q \mapsto q/\|q\|$. Knörrer's change of time appears in the second step as associated to the central projection from our intermediate problem to the Neumann problem. It satisfies the rule, discovered by Appell, which associates a change of time to a central projection.

Acknowledgements This work benefited from discussions with Alexey Borisov, Alain Chenciner, Yuri Fedorov, Božidar Jovanović, Hans Lundmark and Ivan Mamaev.

References

1. A. Albouy, "Projective dynamics of a classical particle or multiparticle system". *Oberwolfach reports* **4–3** (2007), 1926–1928.
2. A. Albouy, "There is a projective dynamics". *EMS Newsletter* **89** (2013), 37–43.
3. A. Albouy and A. Chenciner, "Le problème des *N* corps et les distances mutuelles". *Inventiones Mathematicae* **131** (1998), 151–184.
4. M. Błaszak, "Bi-Hamiltonian separable chains on Riemannian manifold". *Physics Letters A* **243** (1998), 25–32.
5. A.V. Borisov, A.A. Kilin, and I.S. Mamaev, "Multiparticle systems. The algebra of integrals and integrable cases". *Regular and Chaotic Dynamics* **14** (2009), 18–41.
6. A.V. Borisov and I.S. Mamaev, "Isomorphisms of geodesic flows on quadrics". *Regular and Chaotic Dynamics* **14** (2009), 455–465.
7. H.W. Braden, "A completely integrable mechanical system". *Letters in Mathematical Physics* **6** (1982), 449–452.
8. C.G.J. Jacobi, "Lectures on Dynamics", transl. K. Balagangadharan, New Delhi, Hindustan Book Agency, 2009, lecture 4.
9. H. Knörrer, "Geodesics on quadrics and a mechanical problem of C. Neumann". *J. Reine Angew. Math.* **334** (1982), 69–78.
10. H. Lundmark, "Higher-dimensional integrable Newton systems with quadratic integrals of motion". *Studies in Applied Math.* **110** (2003), 257–296.
11. V.S. Matveev and P.J. Topalov, "Trajectory equivalence and corresponding integrals". *Regular and Chaotic Dynamics* **3** (1998), 30–45.
12. R. Montgomery, "Fitting hyperbolic pants to a three-body problem". *Ergod. Th. & Dynam. Sys.* **25** (2005), 921–947.
13. J. Moser, "Integrable Hamiltonian systems and spectral theory". *Fermi Lectures*, Accademia nazionale dei Lincei, Scuola normale superiore, Pisa, 1981.
14. I. Newton, "The Principia". A New Translation preceded by "A guide to Newton's Principia", by I. Bernard Cohen, Berkeley, University of California Press, 1999.
15. M. Pedroni, "Bi-Hamiltonian aspects of the separability of the Neumann system". *Theoretical and Mathematical Physics* **133** (2002), 1722–1727.
16. S. Tabachnikov, "Ellipsoids, complete integrability and hyperbolic geometry". *Moscow Math. J.* **2** (2002), 185–198.
17. S. Wojciechowski, "Integrable one-particle potentials related to the Neumann system and the Jacobi problem of geodesic motion on an ellipsoid". *Physics Letters A* **107** (1985), 106–111.

Bifurcations of the Spatial Central Configurations in the 5-Body Problem

Martha Álvarez-Ramírez, Motserrat Corbera, and Jaume Llibre

1 Introduction

A configuration of n particles is called central when the acceleration vector of each particle is a common scalar multiple of its position vector. One of the reasons why central configurations are interesting is that they allow us to obtain explicit homographic solutions of the n-body problem, that is, motions where the configuration of the system changes size but keeps its shape. Also, they are important in the study of total collisions.

Even the finiteness of the number of central configurations is a very difficult question. This conjecture was proposed by Chazy [6] and Wintner [17] and was listed by Smale as problem number 6 on his list of problems for this century [15]. Central configurations, which appear so deeply in the dynamics of the n body problem are very difficult to count [15]. A complete enumeration of all such solutions for $n \geq 4$ represents a very difficult task for the present day methods.

For the collinear n-body problem, an exact count of the central configurations of n bodies was found by Moulton back in 1910. He showed that there are $n!/2$ equivalence classes.

Saari [13] proved that the regular $N-1$ dimensional simplex is a central configuration of N bodies for any value of the masses. In particular, case $N = 4$

M. Álvarez-Ramírez (✉)
Departamento de Matemáticas, UAM-Iztapalapa, México, D.F., Mexico
e-mail: mar@xanum.uam.mx

M. Corbera
Departament de Tecnologies Digitals i de la Informació, Universitat de Vic, Vic, Spain
e-mail: montserrat.corbera@uvic.cat

J. Llibre
Departament de Matemàtiques, Universitat Autònoma de Barcelona, Barcelona, Spain
e-mail: jllibre@mat.uab.cat

M. Corbera et al. (eds.), *Extended Abstracts Spring 2014*, Trends in Mathematics 4,
DOI 10.1007/978-3-319-22129-8_2

has been well known over a century (Lehmann–Filhés [11]). The fact that the tetrahedron is the unique spatial central configuration of four bodies was proved in 1904 by Pizzetti [12].

The number of planar central configurations of the n-body problem for an arbitrary given set of positive masses has been established only for $n = 3$, namely, Euler's three collinear configurations and Lagrange's two equilateral triangle configurations. For $n = 4$, Hampton and Moeckel [8] showed that, in addition to the tetrahedral spatial configurations, there are only finitely many equivalence classes of planar central configurations.

For $n = 5$, Hampton and Jensen [7], with computer assistance, showed the finiteness of the spatial central configurations with positive masses, with the exception of some explicit special cases of mass values, and Albouy and Kaloshin [3] have proved that the planar 5-body central configurations are finite apart from some explicitly given special cases. For $n \geq 6$, it is not known, in general, if the number of equivalence classes of central configurations is finite. The finiteness question and a number of other interesting questions on central configurations are discussed in a recent problem list given in Albouy et al. [2].

In this work we analyze the families of central configurations of the spatial 5-body problem with four masses equal to 1 and the fifth mass, m, varying from 1 to 0. In particular, we will find two bifurcation values of m. This is accomplished by using bifurcation theory and the method of analytical continuation to follow numerically the central configurations as the mass parameter m varies, and we use symbolic computation software *Mathematica*® to handle the more tedious calculations.

2 Spatial Central Configurations in the 5-Body Problem

In this section we will describe the setting of the newtonian 5-body problem in Euclidean three-space and we give the equations of central configurations of five bodies in $\mathbb{R}^3$.

We start by considering the spatial 5-body problem

$$m_i \ddot{\mathbf{q}}_i = -\sum_{\substack{j=1 \\ j\neq i}}^{5} G m_i m_j \frac{\mathbf{q}_i - \mathbf{q}_j}{|\mathbf{q}_i - \mathbf{q}_j|^3},$$

$i = 1, \ldots, 5$, where $\mathbf{q}_i \in \mathbb{R}^3$ is the position vector of the punctual mass m_i in an inertial coordinate system, and G is the gravitational constant which can be taken equal to one. The *configuration space* of the spatial 5-body problem is defined as

$$\mathcal{P} = \{(\mathbf{q}_1, \ldots, \mathbf{q}_5) \in \mathbb{R}^{15} \ : \ \mathbf{q}_i \neq \mathbf{q}_j, \text{ for } i \neq j\}.$$

Given masses $m_1, \ldots, m_5$, the corresponding configuration $(\mathbf{q}_1, \ldots, \mathbf{q}_5) \in \mathcal{P}$ is *central* if the acceleration vector for each body is a common scalar multiple of its position vector (with respect to the center of mass). That is, if there exists a positive constant λ such that

$$\ddot{\mathbf{q}}_i = -\lambda \ (\mathbf{q}_i - \mathbf{q}_m)\,, \tag{1}$$

for $i = 1, \ldots, 5$, where $\mathbf{q}_m$ is the position vector of the center of mass of the system given by

$$\mathbf{q}_m = \frac{\sum_{i=1}^{5} m_i \mathbf{q}_i}{\sum_{i=1}^{5} m_i}. \tag{2}$$

Therefore, the configuration $(\mathbf{q}_1, \ldots, \mathbf{q}_5) \in \mathcal{P}$ of the 5-body problem with positive masses $m_1, \ldots, m_5$ is central if there exists λ such that $(\lambda, \mathbf{q}_1, \ldots, \mathbf{q}_5)$ is a solution to the system

$$\lambda \ (\mathbf{q}_i - \mathbf{q}_m) = \sum_{\substack{j=1 \\ j \neq i}}^{5} m_j \frac{\mathbf{q}_i - \mathbf{q}_j}{|\mathbf{q}_i - \mathbf{q}_j|^3}, \qquad \text{for} \quad i = 1, \ldots, 5. \tag{3}$$

We choose the coordinates for the body with mass m_i as $\mathbf{q}_i = (x_i, y_i, z_i)$ for $i = 1, \ldots, 5$. Without loss of generality we assume that the body with mass m_1 is fixed at $(x_1, y_1, z_1) = (0, 0, 1)$ and that $x_3 = 0$ (this last assumption is to avoid the rotation with respect to the z-axis). By taking the center of mass at $(0, 0, 0)$, system (3) can be written as

$$\mathbf{f}_i = \sum_{\substack{j=1 \\ j \neq i}}^{5} m_j \frac{\mathbf{q}_i - \mathbf{q}_j}{|\mathbf{q}_i - \mathbf{q}_j|^3} - \lambda \mathbf{q}_i = 0, \qquad \text{for} \quad i = 1, \ldots, 5. \tag{4}$$

It is easy to check that

$$m_1 \mathbf{f}_1 + m_2 \mathbf{f}_2 + m_3 \mathbf{f}_3 + m_4 \mathbf{f}_4 + m_5 \mathbf{f}_5 = 0. \tag{5}$$

Assume now that $m_2 \neq 0$, from (5) the vectorial equation $\mathbf{f}_2$ is a linear combination of the other ones and it can be eliminated. Moreover, since the center of mass is fixed at the origin, from (2) we get

$$x_2 = -\frac{m_4 x_4 + m_5 x_5}{m_2}, \ y_2 = -\frac{m_3 y_3 + m_4 y_4 + m_5 y_5}{m_2},$$
$$z_2 = -\frac{m_1 + m_3 z_3 + m_4 z_4 + m_5 z_5}{m_2}.$$

Finally, we isolate λ from the first component of the vectorial equation $\mathbf{f}_1$ and we substitute it into the other equations. In short, system (4) has been simplified to a set of 11 equations which depend on eight unknowns, namely, the position variables y_3, z_3, x_4, y_4, z_4, x_5, y_5, z_5. Clearly these 11 equations obtained are not all independent. Then, in order to have a central configuration, we are seeking the zeros of the system of eight equations in the eight unknowns that satisfy the remaining three equations. Since the equations obtained are essentially nonlinear, their solutions must be found combining numeric and symbolic computations, which are carried out using Mathematica® (this is just a good tool for doing such calculations).

3 Some Previously Known Results

The main impulse for our study comes from previous results which are described below.

3.1 Central Configuration for the 5*-Body Problem with Equals Masses*

Kotsireas and Lazard [9] assumed that non-planar equal mass central configurations of five bodies always have several symmetries, and used linear algebra and Gröbner bases to classify symmetric spatial central configurations of five bodies with equal masses. They conjectured that there are only four three-dimensional central configurations of five bodies with equal masses (up to isometry, rescaling and permutation of the particles), namely two convex and two concave (see Fig. 1). Álvarez-Ramírez et al. [5] and Santoprete and Lee [10] succeeded in proving the conjecture to be correct.

3.2 Central Configuration in the $(4 + 1)$*-Body Problem*

The $(4 + 1)$-body problem is a particular case of the 5-body problem with four equal masses and an infinitesimal mass. Next we summarize the known results of this problem. In [14], Schmidt shows that a configuration with four equal masses located at the vertices of an equilateral tetrahedron and an infinitesimal mass at its barycenter is a central configuration. Almeida [4] proved that for the $(4 + 1)$-body problem there are 25 central configurations with the four positive equal masses forming a tetrahedron, among which 12 are non-convex. They provide six different classes of central configurations up to isometry, rescaling and permutation of the particles. Later, Tsai [16] found the same result using Gröebner bases.

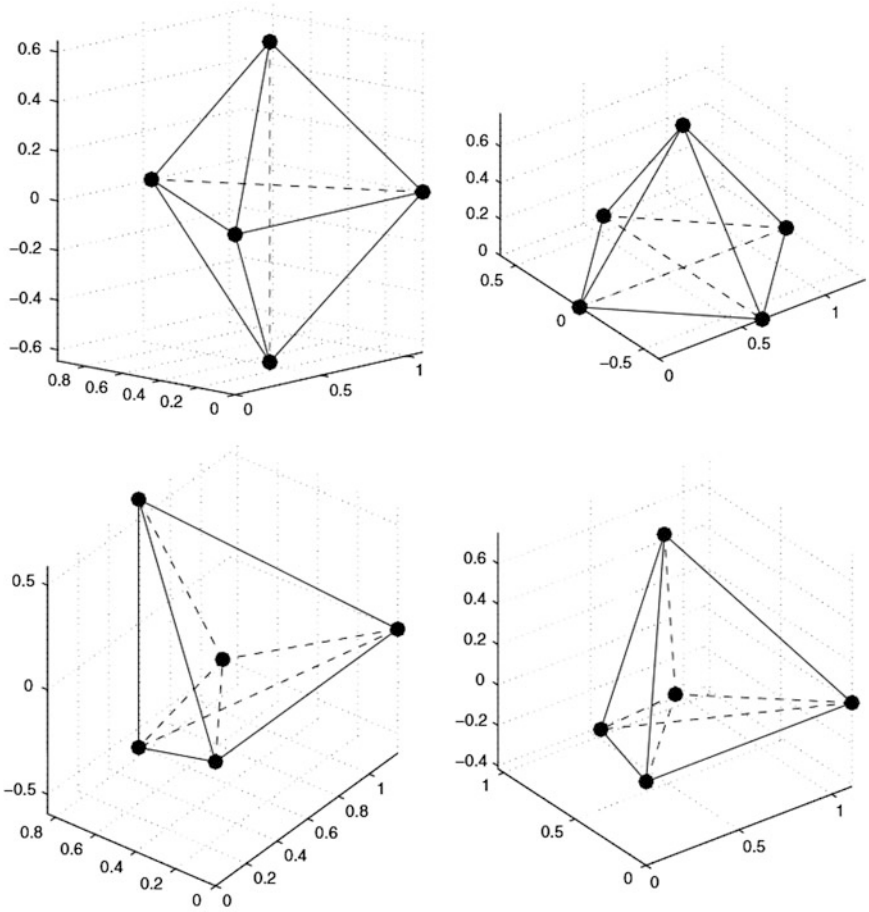

Fig. 1 Equal mass spatial 5-body central configurations. These figures were taken from [10]

It is well known that four equal masses in the plane are necessarily in non-collinear central configuration, namely, a square, an equilateral triangle with a mass at its center, and a particular isosceles triangle with another mass on its axis of symmetry, see [1]. We see that each one of these central configurations provides a central configuration of the spatial $(4 + 1)$-body problem with four equal finite masses contained in the same plane and the fifth particle with infinitesimal mass lying out of this plane.

In short, we have nine different classes of central configurations of the $(4 + 1)$-body problem.

4 Bifurcation Analysis

We continue numerically via the analytic continuation method the central configurations of the 5-body problem with equal masses to the $(4 + 1)$-body problem and viceversa. We note that the four classes of central configurations of the 5-body problem with five equal masses can be continued to nine different classes of the 5-body problem with four equal masses and the fifth mass close to 1, depending on the position of the mass that is continued to values different from 1. We find two critical values: one is the well known bifurcation mass value $m_c = (10368 + 1701\sqrt{6})/54952 \approx 0.264496\cdots$, while the second one is given by $m_f \approx 0.66\cdots$.

Our main result is summarized as follows.

Theorem 1 *There are five different families of central configurations connecting the 5-body problem with equal masses and the* $(4 + 1)$*-body problem without bifurcation.*

There are two families of central configurations starting at the 5-body problem with equal masses and ending at the bifurcation point with $m = m_c$*, and two additional families ending at the bifurcation point* m_f*.*

There are three families of central configurations starting at the $(4 + 1)$*-body problem and ending at the bifurcation point with* $m = m_c$*, and an additional family ending at the bifurcation point* m_f*.*

References

1. A. Albouy, "Symétrie des configurations centrales de quatre corps". *C. R. Acad. Sci. Paris Sér. I Math.* **320**(2) (1995), 217–220.
2. A. Albouy, H. Cabral, and H.A. Santos, "Some problems on the classical *n*-body problem". *Celest. Mech. Dyn. Astron.* **113** (2012), 369–375.
3. A. Albouy and V. Kaloshin, "Finiteness of central configurations of five bodies in the plane". *Ann. of Math.*(2) **176**(1) (2012), 535–588.
4. A. Almeida Santos, "Dziobek's configurations in restricted problems and bifurcation". *Celestial Mech. Dynam. Astronom.* **90**(3–4) (2004), 213–238.
5. M. Álvarez, J. Delgado, and J. Llibre, "On the spatial central configurations of the 5-body problem and their bifurcations". *Discrete Contin. Dyn. Syst. Ser. S* **1**(4) (2008), 505–518.
6. J. Chazy, "Sur certaines trajectoires du probleme des *n* corps". *Bull. Astron.* **35** (1916, 1918), 321–389.
7. M. Hampton and A. Jensen, "Finiteness of spatial central configurations in the five-body problem". *Celestial Mech. Dynam. Astronom.* **109**(4) (2011), 321–332.
8. M. Hampton and R. Moeckel, "Finiteness of relative equilibria of the four-body problem". *Invent. Math.* **163** (2006), 289–312.
9. I. Kotsireas and D. Lazard, "Central Configurations of the 5-body problem with equal masses in three-dimensional space", Representation theory, dynamical systems, combinatorial and algorithmic methods. Part IV, *Zap. Nauchn. Sem. POMI*, **258** (1999), 292–317; translation in *J. Math. Sci.* **108**(6) (2002), 1119–1138.

10. T.L. Lee and M. Santoprete, "Central configurations of the five-body problem with equal masses". *Celestial Mech. Dynam. Astronom.* **104**(4) (2009), 369–381.
11. R. Lehmann-Filhés, "Ueber zwei Fälle des Vielkörperproblems". *Astron. Nachr.* **127** (1891), 137–143.
12. P. Pizzetti, "Casi particolari del problema dei tre corpi". *Rendiconti* **13** (1904), 17–26.
13. D. Saari, "On the role and properties of n-body central configurations". *Celest. Mech.* **21** (1980), 9–20.
14. D.S. Schmidt, "Central configurations in $\mathbb{R}^2$ and $\mathbb{R}^3$". Hamiltonian dynamical systems (Boulder, CO, 1987), *Contemp. Math.* **81** (1988), 59–76.
15. S. Smale, "Mathematical problems for the next century". *Math. Intell.* **20** (1998), 7–15.
16. Y. Tsai, "Dziobek configurations of the restricted $(N + 1)$-body problem with equal masses". *J. Math. Phys.* **53**(7) (2012), 072902.
17. A. Wintner, "The Analytical Foundations of Celestial Mechanics". *Princeton Mathematical Series*, v. 5, Princeton Univ. Press, Princeton, NJ, 1941.

Convex Central Configurations of Two Twisted n-gons

Esther Barrabés and Josep Maria Cors

1 Introduction

The simplest motions that can be found in the Newtonian N-body problem are the ones whose configuration is constant up to rotations and scaling, and every body follows a trajectory being a keplerian orbit. Such kind of solutions are called *central configurations*.

We consider the planar $2n$-body problem, where the masses are located at the vertices of two regular n-gons, $n \geq 2$, and all the masses at the same n-gon are equal, namely m_1 and m_2. In [4], Moeckel and Simó consider the case of two *nested* regular n-gons, that is, when the vertices of the two n-gons are aligned. They prove that for all values of n and every ratio m_1/m_2, there are exactly two planar central configurations. In [2], Barrabés et al. study the case of two *twisted* n-gons, where one of the two gons is rotated an angle of π/n with respect the other. In that case, the authors prove that the number of central configurations depends on n.

Several authors have studied the convex central configurations in the four body problem. A classical result due to MacMillan and Bartky [3] states that, for any four positive masses and any assigned order, there exists a convex planar central configuration. Xia [7] gives a simple proof of that case. Albouy et al. [1] prove that in the planar four-body problem, a convex central configuration is symmetric with respect to one diagonal if and only if the masses of the two particles on the other

E. Barrabés (✉)
Departament d'Informàtica i Matemàtica Aplicada, Universitat de Girona, Girona, Spain
e-mail: barrabes@imae.udg.edu

J.M. Cors
Departament de Matemàtica Aplicada III, Universitat Politècnica de Catalunya, Barcelona, Spain
e-mail: cors@epsem.upc.edu

M. Corbera et al. (eds.), *Extended Abstracts Spring 2014*, Trends in Mathematics 4,
DOI 10.1007/978-3-319-22129-8_3

diagonal are equal. As far as we know, it is a conjecture that given four masses in a certain order, there exists only one convex central configuration.

We present here some results concerning central configurations of two twisted n-gons that are convex.

2 Equations

We consider two groups of n bodies in the same plane (x, y) at positions $\mathbf{q}_{ji} \in \mathbb{R}^2$, $i = 1, \ldots, n, j = 1, 2$. All the bodies in the same group have equal mass, m_1 and m_2, respectively. It is well known (see [6]) that a *central configuration* (CC) of the planar $2n$-body problem is a solution $\mathbf{q} = (\mathbf{q}_{11}, \mathbf{q}_{12}, \ldots, \mathbf{q}_{2n}) \in \mathbb{R}^{4n}$ of the equation

$$\nabla U(\mathbf{q}) + w^2 M\mathbf{q} = 0, \tag{1}$$

for some value of w, where U is the Newtonian potential

$$U(\mathbf{q}) = \sum_{j=1}^{2}\sum_{i=1}^{n}\left(\sum_{l=i+1}^{n}\frac{m_j^2}{||\mathbf{q}_{ji} - \mathbf{q}_{jl}||} + \sum_{l=j+1}^{n}\sum_{m=1}^{n}\frac{m_j m_l}{||\mathbf{q}_{ji} - \mathbf{q}_{lm}||}\right),$$

and M is the diagonal mass matrix with diagonal $m_1, \ldots, m_1, m_2, \ldots, m_2$ (each mass repeated n times).

We consider CC consisting in two regular n-gons rotated an angle π/n with respect to each other. Without loss of generality, we can think that the first n-gon has one vertex on the positive horizontal axis, $y = 0, x > 0$, and it is contained in a circle of radius 1.

Introducing $\mathbf{q}_{1k} = e^{i\pi 2k/n}$ and $\mathbf{q}_{2k} = ae^{i\pi(2k+1)/n}$, for $k = 0, \ldots, n-1$ and where a is the radius of the circle containing the second n-gon (that can be viewed as the size of the second n-gon), then, the system of equations (1) can be written as $4n$ real equations: $2n$ corresponding to the real parts and $2n$ to the imaginary parts. Due to the symmetries, the $2n$ equations corresponding to the imaginary parts vanish (in fact, the only two possibilities for two gons to be in a CC are being nested or twisted, see [8]), and the $2n$ equations corresponding to the real parts reduce to only 2. Finally, eliminating the variable w, the equations for the CC reduce to the following single equation

$$(C_2(a) - S_n a)m_1 + \left(\frac{S_n}{a^2} - aC_1(a)\right)m_2 = 0, \tag{2}$$

where $S_n = \frac{1}{4}\sum_{k=1}^{n-1} \frac{1}{\sin(k\pi/n)}$, and the coefficients $C_j(a)$ are

$$C_1(a) = \sum_{k=1}^{n} \frac{1 - a\cos((2k-1)\pi/n)}{(1 + a^2 - 2a\cos((2k-1)\pi/n))^{3/2}},$$

$$C_2(a) = \sum_{k=1}^{n} \frac{a - \cos((2k-1)\pi/n)}{(1 + a^2 - 2a\cos((2k-1)\pi/n))^{3/2}}.$$

We say that a value of a is admissible if there exists a solution to (2) with $m_1 > 0$ and $m_2 > 0$. In [2] the admissible values of a and the number of CC for a given mass ratio m_2/m_1 are studied.

Equation (2) was also obtained by Roberts in [5] and by Yu and Zhang in [8], and it is similar to the one obtained by Simó and Moeckel in [4] for the nested case.

3 Convex CC of Two Twisted n-gons

Given an admissible value of a, we discuss here whether the configuration is convex or not. It is not difficult to see that, given $2n$ bodies distributed uniformly in two twisted regular n-gons, the configuration is convex if and only if

$$\cos\left(\frac{\pi}{n}\right) \leq a \leq \frac{1}{\cos\left(\frac{\pi}{n}\right)}.$$

We will present the results separately for $n = 2, 3, 4$ and $n \geq 5$.

The case $n = 2$, that is two bodies in each group, can be summarized in the following result proved by MacMillan and Bartky.

Theorem 1 *For any positive value of the mass ratio m_2/m_1, there exists only one CC of two twisted segments and it is convex.*

We will present the results considering values of the mass ratio $m_2/m_1 \geq 1$. By rescaling, the number of convex central configurations for $m_2/m_1 < 1$ is obtained.

In the case $n = 3$ (two equilateral triangles rotated $\pi/3$), we prove the following result:

Theorem 2 *Consider six masses located at the vertices of two twisted equilateral triangles, such that all the masses in one triangle are equal to m_1 and the masses of the other triangle are equal to m_2. Then, there exists a value $m^* > 1$ for the mass ratio m_2/m_1 such that*

(1) *for any $m_2/m_1 \in (1, m^*)$, there exist exactly three different convex central configurations,*
(2) *for any $m_2/m_1 \in (m^*, \infty)$ there exists only one convex central configuration,*

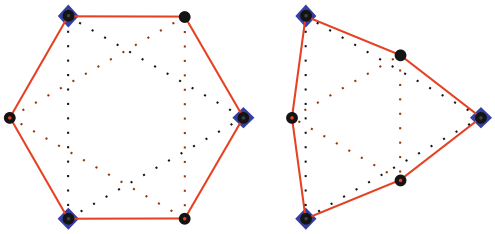

Fig. 1 Convex CC of two twisted equilateral triangles corresponding to $m_2 = m_1$ (*left*, the regular hexagon) and the limit case $m_2/m_1 = \infty$ (*right*)

(3) *for* $m_2/m_1 = 1, m^*$ *the number of different convex central configurations is exactly two.*

Approximately, $m^* = 1.0007682$. When $m_2 = m_1$, the two convex central configurations where already numerically computed by Moeckel in an unpublished report. In Fig. 1 we show three examples of convex CC in the case of two twisted equilateral triangles.

The results (for any value of n) are based on the number of solutions to Eq. (2) for a given value of the mass ratio m_2/m_1. A key point is to know the exact number of solutions to Eq. (2) corresponding to $m_2/m_1 = 0$. For $n = 3$ it can be shown that there exists exactly two of those solutions, but in the case of $n \geq 4$, it can be shown that there exists two, but as far as we know, it is not proved that they are the only ones. The results for $n \geq 4$ rely on the truthfulness of the following conjecture.

Conjecture 3 *For* $n \geq 4$ *there exists exactly two solutions of Eq.* (2) *that correspond to* $m_2 = 0$ *and* $m_1 \neq 0$.

Under that assumption, it can be shown the following results:

Theorem 4 *Consider eight masses located at the vertices of two twisted squares, such that all the masses in one square are equal to* m_1 *and the masses of the other square are equal to* m_2. *There exists a value* $\overline{m}$ *for the mass ratio* m_2/m_1 *such that*

(1) *for any* $m_2/m_1 \in [1, \overline{m}]$, *there exists exactly one convex central configuration,*
(2) *for any* $m_2/m_1 \in (\overline{m}, \infty)$ *there exists no convex central configuration.*

Approximately, this value is $\overline{m} = 16.05679941$.

Theorem 5 *Consider* $2n$ *masses, with* $n \geq 5$, *located at the vertices of two* n*-gons, such that all the masses in one* n*-gon are equal to* m_1 *and the masses of the other* n*-gon are equal to* m_2. *For any value of the mass ratio* m_2/m_1, *there exists at least one convex central configuration.*

In summary, we observe that there always exists a convex CC of twisted rings for any value of n, *except* for $n = 4$ (8-body problem). Moreover, the richer case is $n = 3$, where there are values of the mass ratio with three convex CC.

References

1. A. Albouy, Y. Fu, and S. Sun, "Symmetry of planar four-body convex central configurations". *Proc. R. Soc. A* **464**(2093) (2008), 1355–1365.
2. E. Barrabés, J.M. Cors, and G. Roberts, "Planar central configurations of twisted rings". *Preprint*.
3. W.D. MacMillan and W. Bartky, "Permanent configurations in the problem of four bodies". *Trans. Amer. Math. Soc.* **34** (1932), 838–875.
4. R. Moeckel and C. Simó, "Bifurcation of spatial central configurations from planar ones". *SIAM journal on mathematical analysis* **26** (1995), 978–998.
5. G.E. Roberts, "Existence and stability of relative equilibria in the N-body problem". PhD thesis, Boston University, 1999.
6. D.G. Saari, "Collisions, rings, and other Newtonian N-body problems", *CBMS Regional Conference Series in Mathematics* **104** (2005).
7. Z. Xia, "Convex central configurations for the n-body problem". *Journal of Differential Equations* **200**(2) (2004), 185–190.
8. X. Yu and S. Zhang, "Twisted angles for central configurations formed by two twisted regular polygons". *J. Differential Equations* **253** (2012), 2106–2122.

The Newtonian n-Body Problem in the Context of Curved Space

Florin Diacu

The idea that geometry and physics are intimately related made its way in human thought during the early part of the nineteenth century. Gauss measured the angles of a triangle formed by three mountain peaks near Göttingen, Germany, apparently hoping to learn whether the universe has positive or negative curvature, but the inevitable observational errors rendered his results inconclusive [3]. In the 1830s, Bolyai and Lobachevsky took these investigations further. They independently addressed the connection between geometry and physics by seeking a natural extension of the gravitational law from Euclidean to hyperbolic space. Their idea led to the study of the Kepler problem and the 2-body problem in spaces of nonzero constant Gaussian curvature, $\kappa \neq 0$, two fundamental problems that are not equivalent, unlike in Euclidean space. A detailed history of the results obtained in this direction since Bolyai and Lobachevsky can be found in [3, 5, 6].

It is important to emphasize the reasons why this approach provides a natural way of extending gravitation to spaces of constant Gaussian curvature, since there is no unique way of generalizing the classical equations of motion in order to recover them when the curved ambient space becomes flat. As there are no physical experiments that could test the validity of the potential, we have to rely on a mathematical approach. The potential we want to use should thus satisfy the same basic properties the Newtonian potential does in its most basic setting: the Kepler problem—the particular case when one body moves around a fixed attracting centre.

Two fundamental properties characterize the Newtonian potential of the Kepler problem: it is a harmonic function in 3D (but not in 2D), i.e., it satisfies Laplace's equation; and it generates a central field in which all bounded orbits are closed, a result proved by Joseph Louis Bertrand in 1873. In the early years of the twentieth

F. Diacu (✉)
Department of Mathematics and Statistics, Pacific Institute for the Mathematical Sciences, University of Victoria, Victoria, BC, Canada
e-mail: diacu@uvic.ca

M. Corbera et al. (eds.), *Extended Abstracts Spring 2014*, Trends in Mathematics 4,
DOI 10.1007/978-3-319-22129-8_4

century, Heinrich Liebmann proved that these properties are also satisfied by the Kepler problem in spaces of constant curvature, thus offering strong arguments for this mathematical generalization of the gravitational force.

In some recent studies, such as [1–13, 15, 16], we introduced a suitable framework for generalizing the equations of motion suggested by Bolyai and Lobachevsky to $n \geq 2$ bodies. Like the curved Kepler problem and the curved 2-body problem, our equations made sense in spaces of constant Gaussian curvature $\kappa \neq 0$, i.e., on 3-spheres of radius $R = \kappa^{-1/2}$ embedded in $\mathbb{R}^4$, for $\kappa > 0$, and on hyperbolic 3-spheres of imaginary radius $iR = \kappa^{-1/2}$ embedded in the Minkowski space $\mathbb{R}^{3,1}$, for $\kappa < 0$. But whether written in extrinsic or intrinsic coordinates, these equations contain undetermined expressions for $\kappa = 0$, although we can recover the classical Newtonian system when $\kappa \to 0$. So a study of the flat case in the context of curved space, including some understanding of the bifurcations and the stability of solutions when the parameter κ is varied through 0, is impossible to perform in that setting.

In this study we derive some equations of motion that overcome the difficulties mentioned above. Using a coordinate system in $\mathbb{R}^4$ having the origin at the North-Pole of the 3-spheres (the only point that is common to all the manifolds involved), we prove that the n-body problem in spaces of constant Gaussian curvature $\kappa \in \mathbb{R}$ can be written as

$$\ddot{\mathbf{r}}_i = \sum_{j=1, j\neq i}^{n} \frac{m_j\Big[\mathbf{r}_j - \Big(1 - \frac{\kappa r_{ij}^2}{2}\Big)\mathbf{r}_i + \frac{r_{ij}^2 \mathbf{R}}{2}\Big]}{r_{ij}^3\Big(1 - \frac{\kappa r_{ij}^2}{4}\Big)^{3/2}} - (\dot{\mathbf{r}}_i \cdot \dot{\mathbf{r}}_i)(\kappa \mathbf{r}_i + \mathbf{R}), \quad i = 1, \ldots, n, \tag{1}$$

where $m_1, m_2, \ldots, m_n > 0$ represent the masses, the dot $\cdot$ denotes the standard inner product of signature $(+,+,+,+)$ for $\kappa \geq 0$, but the Lorentz inner product of signature $(+,+,+,-)$ for $\kappa < 0$, the vectors $\mathbf{R}$ and $\mathbf{r}_i$ are given by

$$\mathbf{R} = (0, 0, 0, \sigma|\kappa|^{1/2}), \quad \mathbf{r}_i = (x_i, y_i, z_i, \omega_i), \ i = 1, \ldots, n,$$

σ is the signum function, i.e., $\sigma = +1$ for $\kappa \geq 0$ and $\sigma = -1$ for $\kappa < 0$, and

$$r_{ij} := [(x_i - x_j)^2 + (y_i - y_j)^2 + (z_i - z_j)^2 + \sigma(\omega_i - \omega_j)^2]^{1/2}$$

is the Euclidean distance for $\kappa \geq 0$ and the Minkowski distance for $\kappa < 0$.

Notice that the distances r_{ij} vary smoothly with κ. In particular, the values of the coordinates ω_i, $i = 1, \ldots, n$, and consequently the values of the expressions $(\omega_i - \omega_j)^2$, $i, j \in \{1, 2, \ldots, n\}, i \neq j$, become small when κ gets close to 0 and vanish at $\kappa = 0$.

For $\kappa \neq 0$, the initial conditions must be taken such that the bodies are restricted to 3-spheres for $\kappa > 0$ and hyperbolic 3-spheres for $\kappa < 0$. For $\kappa = 0$ and $\mathbf{r}_i =$

$(x_i, y_i, z_i, 0)$, $i = 1, \ldots, n$, we recover the Newtonian equations,

$$\ddot{\mathbf{r}}_i = \sum_{j=1, j\neq i}^{n} \frac{m_j(\mathbf{r}_j - \mathbf{r}_i)}{r_{ij}^3}, \quad i = 1, \ldots, n. \tag{2}$$

To make system (1) analytic for all values of the parameter, we can introduce the substitution $\delta = \sigma|\kappa|^{1/2}$. This slight modification of the equations of motion will be helpful in future studies of the bifurcations of solutions when the new parameter passes through the value $\delta = 0$.

A potential application of these equations is that of establishing the geometric nature of the physical space. Physicists agree that the large-scale universe has constant curvature, κ, but it is not known whether this curvature is positive, negative, or zero. All experiments, however, show that $|\kappa|$ must be very small. If the study of system (1) shows that some types of solutions exist only for one kind of curvature, but not for the other two kinds, and if the corresponding orbits prove to be stable, then we might find such motions in the universe through astronomical observations. If we do, then the physical space must necessarily have that kind of curvature.

So far we have proved that Lagrangian orbits (3-body motions for which the masses lie at the vertices of a rotating equilateral triangle) must have equal masses if $\kappa \neq 0$, [14], a fact that is not true for $\kappa = 0$. Such non-equal mass orbits have been found in the solar system, for example Sun, Jupiter, and any of the Trojan asteroids. But we cannot yet conclude that space is flat. Motions very close to Lagrangian orbits might exist for $\kappa \neq 0$; nobody, however, has proved or disproved their existence yet.

References

1. F. Diacu, "On the singularities of the curved n-body problem". *Trans. Amer. Math. Soc.* **363**(4) (2011), 2249–2264.
2. F. Diacu, "Polygonal homographic orbits of the curved 3-body problem". *Trans. Amer. Math. Soc.* **364** (2012), 2783–2802.
3. F. Diacu, "Relative equilibria of the curved n-body problem". *Atlantis Studies in Dynamical Systems* **1**, Atlantis Press, Amsterdam, 2012.
4. F. Diacu, "The non-existence of the center-of-mass and the linear-momentum integrals in the curved n-body problem". *Libertas Math.* **32**(1) (2012), 25–37.
5. F. Diacu, "Relative equilibria of the 3-dimensional curved n-body problem". *Memoirs Amer. Math. Soc.* **228** (2013), 1071.
6. F. Diacu, "The curved n-body problem: risks and rewards". *Math. Intelligencer* **35**(3) (2013), 24–33.
7. F. Diacu and S. Kordlou, "Rotopulsators of the curved n-body problem". *J. Differential Equations* **255** (2013), 2709–2750.
8. F. Diacu, R. Martínez, E. Pérez-Chavela, and C. Simó, "On the stability of tetrahedral relative equilibria in the positively curved 4-body problem". *Physica D* **256–257** (2013), 21–35.
9. F. Diacu, E. Pérez-Chavela, and M. Santoprete, "Saari's conjecture for the collinear n-body problem". *Trans. Amer. Math. Soc.* **357**(10) (2005), 4215–4223.

10. F. Diacu and E. Pérez-Chavela, "Homographic solutions of the curved 3-body problem". *J. Differential Equations* **250** (2011), 340–366.
11. F. Diacu, E. Pérez-Chavela, and J.G. Reyes Victoria, "An intrinsic approach in the curved n-body problem. The negative curvature case". *J. Differential Equations* **252** (2012), 4529–4562.
12. F. Diacu, E. Pérez-Chavela, and M. Santoprete, "The n-body problem in spaces of constant curvature. Part I: Relative equilibria". *J. Nonlinear Sci.* **22**(2) (2012), 247–266.
13. F. Diacu, E. Pérez-Chavela, and M. Santoprete, "The n-body problem in spaces of constant curvature. Part II: Singularities". *J. Nonlinear Sci.* **22**(2) (2012), 267–275.
14. F. Diacu and S. Popa, "All the Lagrangian relative equilibria of the curved 3-body problem have equal masses". *J. Math. Phys.* **55** (2014), 112701.
15. F. Diacu and B. Thorn, "Rectangular orbits of the curved 4-body problem". *Proc. Amer. Math. Soc.* **143**(4) (2015), 1583–1593.
16. E. Pérez-Chavela and J.G. Reyes Victoria, "An intrinsic approach in the curved n-body problem. The positive curvature case". *Trans. Amer. Math. Soc.* **364**(7) (2012), 3805–3827.

Poincaré Maps and Dynamics in Restricted Planar $(n+1)$-Body Problems

Antonio García

To Clark Robinson, in his 70th birthday.

1 Setting

This work deals with the motion of an infinitesimal particle, *the secondary*, in a plane subject to the gravitational attraction of n particles of mass $m = 1$, *the primaries*, which are placed in the vertices of a regular polygon on n vertices. The primaries can be fixed or rotate with an uniform velocity around their center of mass. The first case is called the n-center problem, and the second the restricted $(n+1)$-body problem. The last case has been studied in [1], in this note we will mainly study the first one.

We denote by $\mathbf{Q}_k = (A_k, B_k)$ the position of the k primary, for $k = 0, \ldots, n-1$. Without lost of generality, we assume that $\mathbf{Q}_0 = (1, 0)$ and the center of mass of the primaries is $C = -\left(0, \cot \frac{\pi}{n}\right)$.

Theorem 1 *The n-center problem has the following properties:*

(i) *It is a Hamiltonian system of two degrees of freedom. The Hamiltonian is* $H(\mathbf{q}, \mathbf{p}) = \frac{1}{2}\mathbf{p} \cdot \mathbf{p} - U(\mathbf{q})$, *where* $U(\mathbf{q}) = \sum_{k=0}^{n-1} 1/|\mathbf{q} - \mathbf{Q}_k|$.

(ii) *The singularities take place when the secondary collides with one of the primaries.*

(iii) *The energy* $h = H(\mathbf{q}, \mathbf{p})$ *is an integral.*

(iv) *Let* D_n *be the dihedral group, the group of symmetries of the n polygon, including both rotations and reflections. This group acts on the Hamiltonian, that is if* $\alpha(t) = (\mathbf{q}(t), \mathbf{p}(t))$ *is a solution and* $T \in D_n$ *then* $T\alpha(t) = (T\mathbf{q}(t), T\mathbf{p}(t))$ *is also a solution, see [2].*

(v) *The system is reversible: if* $(\mathbf{q}(t), \mathbf{p}(t))$ *is a solution, then* $(\mathbf{q}(-t), \mathbf{p}(-t))$ *is also a solution.*

A. García (✉)
Departamento de Matemáticas, UAM-Iztapalapa, Iztapalapa, México, D.F., Mexico
e-mail: agar@xanum.uam.mx

M. Corbera et al. (eds.), *Extended Abstracts Spring 2014*, Trends in Mathematics 4,
DOI 10.1007/978-3-319-22129-8_5

By (iii), we can restrict our study to a fixed level of energy h. Item (iv) gives us a partition of the orbits of the system: two orbits are equivalent if there is an element of D_n sending one to the other.

Theorem 2 *If $-h$ is a regular value of $U(\mathbf{q})$ then*

(i) The set $A = \{\mathbf{q} : h + U(\mathbf{q}) \geq 0\} \subset \mathbb{R}^2$, called the Hill region *for the level of energy h, is a manifold with boundary $\partial A = \{\mathbf{q} : h + U(\mathbf{q}) = 0\}$ and interior $A^\circ = \{\mathbf{q} : h + U(\mathbf{q}) > 0\}$.*
(ii) For certain values of $h < 0$, the Hill region has a ring shape with the center of mass of the primaries inside.
(iii) The orbit of the secondary with energy h is constrained to the Hill region; the secondary reaches ∂A at zero velocity.

2 Main Results

We choose a regular value h of $U(\mathbf{q})$ satisfying Theorem 2(ii). The intersection of the Hill region with any ray that starts in the center of masses is a segment, we call L_a the segment containing $(0, 0)$, and L_b the segment containing the primary $\mathbf{Q}_0 = (1, 0)$. Let us remark that L_a is a subset of the Y-axis.

Let S be the subset of the Hill region between L_a and L_b. This set is a fundamental region of the action of D_n on the Hamiltonian. Hence all the orbits of the Hamiltonian can be obtained as the image of the orbits contained in S by the elements of D_n. The only primary in S is $\mathbf{Q}_0 = (1, 0) \in L_b$.

Definition 3 The mechanical or Jacobi metric on S is: $\tilde{g} = 2(h + U(\mathbf{q}))\, g$, where g is the standard metric (as a subset of $\mathbb{R}^2$). The Gaussian curvature corresponding to the Jacobi metric is the mechanical curvature.

Theorem 4 *We have the following properties:*

(i) *The Jacobi metric is zero in $\partial A \cap S$ and ∞ in $\mathbf{Q}_0 = (1, 0)$.*
(ii) *The mechanical and the standard metrics are conformal.*
(iii) *The mechanical curvature is:*

$$K_h(x, y) = -\sum_{k=0}^{n-1} \frac{1}{4(h + U(\mathbf{q}))\,|\mathbf{q} - \mathbf{Q}_k|^3} + \frac{1}{8(h + U(\mathbf{q}))^2} \left[\left(\sum_{k=0}^{n-1} \frac{A_k - q_1}{|\mathbf{q} - \mathbf{Q}_k|^3} \right)^2 + \left(\sum_{k=0}^{n-1} \frac{B_k - q_2}{|\mathbf{q} - \mathbf{Q}_k|^3} \right)^2 \right],$$

with $K_h(x, y) = \infty$ in $\partial A \cap S$ and in $(1, 0)$.
(iv) *The geodesics of the mechanical metric on A are the solutions of the Hamiltonian system.*

Theorem 5 *The equivalent classes of the Hamiltonian flow by the action of D_n form a geodesic billiard.*

Proof Since the solutions of the Hamiltonian are geodesics of the mechanical metric, it is enough to study the behavior of the orbits when they cross L_a or L_b.

Let us assume that the orbit $(\mathbf{q}(t), \mathbf{p}(t))$ satisfies $\mathbf{q}(t) \in S$ if $t \leq t_0$, $\mathbf{q}(t_0) \in L_a$ and $\mathbf{q}(t) \notin S$ for $t > t_0$. Let $T_a \in D_n$ be the reflection by L_a then $(\mathbf{q}_1(t), \mathbf{p}_1(t)) = (T_a\mathbf{q}(t), T_a\mathbf{p}(t))$ is an equivalent orbit and $\mathbf{q}_1(t) \notin S$ if $t < t_0$, $\mathbf{q}_1(t_0) = \mathbf{q}(t_0) \in L_a$ and $\mathbf{q}_1(t) \in S$ for $t \geq t_0$. Therefore the broken curve formed by $(\mathbf{q}(t), \mathbf{p}(t))$ if $t \leq t_0$ and $(\mathbf{q}_1(t), \mathbf{p}_1(t))$ if $t \geq t_0$ is a representant of the orbit contained in S. It is easy to see that for this curve the angle of incidence with L_a is equal to the angle of reflection with the same line. The same argument works with L_b. □

Theorem 6 *There are three types of orbits in the fundamental region S:*

(1) Orbits starting in L_a, pointing to the interior of S and reaching L_b.
(2) Orbits starting in L_b, pointing to the interior of S and reaching L_b again.
(3) Orbits starting in L_b, pointing to the interior of S and reaching L_a.

Since $\mathbf{Q}_0 \in L_b$ then the collision orbits can be of type (1) or (2), the orbits of ejection can be of type (2) or (3), in the other hand the orbits that reaches ∂A are of type (2).

Now, since the energy is fixed, the orbits starting in $A = L_a \cup L_b$ are determinated by the point $\mathbf{p} \in A$ and the angle θ of the velocity with L_a or L_b. If we follow this orbit to the next intersection $\mathbf{p}_1 \in A$, that has an angle θ_1 with L_a or L_b. Then the map $(\mathbf{p}, \theta) \to (\mathbf{p}_1, \theta_1)$ is well defined.

Corollary 7 *The map $(\mathbf{p}, \theta) \to (\mathbf{p}_1, \theta_1)$ consists of the three Poincaré maps:*

$$
\begin{aligned}
&P_{ab}{:}L_a \times (0,\pi) \longrightarrow L_b \times (0,\pi),\\
&P_{ba}{:}D_{ba} \subset L_b \times (0,\pi) \longrightarrow L_a \times (0,\pi), \qquad (s,\theta) \longrightarrow (s_1,\theta_1)\\
&P_{bb}{:}D_{bb} \subset L_b \times (0,\pi) \longrightarrow L_b \times (0,\pi),
\end{aligned}
$$

where D_{bb} is closed, ∂D_{bb} is the set of points with orbits reaching the boundary of the Hill region, D_{ba} is open, and $D_{ba} \cup D_{bb} = L_b \times (0,\pi)$. The maps P_{ba}, P_{bb} are smooth, and P_{ab} is smooth except in the collision orbits.

By the study of these maps and the geometry of the problem, it is possible to find several kinds of periodic orbits.

Acknowledgements The author has been partially supported by Red de Cuerpos Académicos Ecuaciones Diferenciales, Proyecto Sistemas Dinámicos y Estabilización. PROMEP 2011-SEP, México.

References

1. M. Álvarez-Ramírez and A. García, "Poincaré maps and near-collision dynamics for a restricted planar $(n + 1)$-body problem". *App. Math. and Comp.* **233** (2014), 328–337.
2. P.J. Olver, "Applications of Lie group to differential equations". *Springer*, New York, Berlin, Heidelberg. 1986.

A Methodology for Obtaining Asymptotic Estimates for the Exponentially Small Splitting of Separatrices to Whiskered Tori with Quadratic Frequencies

Amadeu Delshams, Marina Gonchenko, and Pere Gutiérrez

1 Introduction

The aim of this work is to provide asymptotic estimates for the splitting of separatrices in a perturbed 3-degree-of-freedom Hamiltonian system, associated to a two-dimensional whiskered torus (invariant hyperbolic torus) whose frequency ratio is a quadratic irrational number. We show that the dependence of the asymptotic estimates on the perturbation parameter is described by some functions which satisfy a periodicity property, and whose behavior depends strongly on the arithmetic properties of the frequencies.

First, we describe the Hamiltonian system to be studied. It is also considered in [6], as a generalization of the famous Arnold's example [1], and provides a model for the behavior of a nearly-integrable Hamiltonian system in the vicinity of a single resonance (see [4] for a motivation). In canonical coordinates $(x, y, \varphi, I) \in \mathbb{T} \times \mathbb{R} \times \mathbb{T}^2 \times \mathbb{R}^2$, we consider a perturbed Hamiltonian

$$H(x, y, \varphi, I) = H_0(x, y, I) + \mu H_1(x, \varphi). \tag{1}$$

$$H_0(x, y, I) = \langle \omega_\varepsilon, I \rangle + \frac{1}{2}\langle \Lambda I, I \rangle + \frac{y^2}{2} + \cos x - 1, \tag{2}$$

$$H_1(x, \varphi) = \cos x \cdot \sum_{k_2 \geq 0} \mathrm{e}^{-\rho|k|} \cos(\langle k, \varphi \rangle - \sigma_k). \tag{3}$$

A. Delshams (✉) • P. Gutiérrez
Departament de Matemàtica Aplicada I, Universitat Politècnica de Catalunya, Barcelona, Spain
e-mail: amadeu.delshams@upc.edu; pere.gutierrez@upc.edu

M. Gonchenko
Institut für Mathematik, Technische Universität Berlin, Berlin, Germany
e-mail: gonchenk@math.tu-berlin.de

M. Corbera et al. (eds.), *Extended Abstracts Spring 2014*, Trends in Mathematics 4,
DOI 10.1007/978-3-319-22129-8_6

For the integrable Hamiltonian H_0, we consider a vector of *fast frequencies*

$$\omega_\varepsilon = \frac{\omega}{\sqrt{\varepsilon}}\,, \qquad \omega = (1, \Omega), \tag{4}$$

where the frequency ratio Ω is a *quadratic* irrational number. In this way, our system has two parameters $\varepsilon > 0$ and μ, but we assume them linked by a relation of the kind $\mu = \varepsilon^p$, $p > 0$ (the smaller p the better). Thus, if we consider ε as the unique parameter, we have a *singular* or *weakly hyperbolic* problem for $\varepsilon \to 0$ (see [4] for a discussion about singular and regular problems).

On the other hand, notice that H_0 consists of a classical pendulum and two rotors (in the coordinates x, y and φ, I respectively). Then, we see that H_0 has a family of two-dimensional whiskered tori, with coincident whiskers (invariant manifolds). Such tori can be indexed by the (constant) action I, and have frequency vectors $\omega_\varepsilon + \Lambda I$. We assume that the matrix Λ is such that the condition of *isoenergetic nondegeneracy* is satisfied (see, for instance, [6]). Among the tori, we fix our attention on the torus given by $I = 0$,

$$\mathcal{T}_0 : \quad (0, 0, \theta, 0), \quad \theta \in \mathbb{T}^2,$$

whose inner flow is given, in this parameterization, by $\dot\theta = \omega_\varepsilon$. This torus has a homoclinic whisker (i.e., coincident stable and unstable whiskers),

$$\mathcal{W}_0 : \quad (x_0(s), y_0(s), \theta, 0), \quad s \in \mathbb{R},\ \theta \in \mathbb{T}^2,$$

where $x_0(s) = 4 \arctan \mathrm{e}^s$, $y_0(s) = 2/\cosh s$ (the upper separatrix of the classical pendulum). The inner flow on $\mathcal{W}_0$ is given by $\dot s = 1$, $\dot\theta = \omega_\varepsilon$.

Concerning the perturbation H_1, it is given by a constant $\rho > 0$ (the complex width of analyticity in the angles φ), and phases σ_k that, for the purpose of this work, can be chosen arbitrarily.

Under the hypotheses described, the *hyperbolic KAM theorem* (see, for instance, [8]) can be applied to the perturbed Hamiltonian (1)–(3). We have that, for $\mu \neq 0$ small enough, the whiskered torus $\mathcal{T}_0$ persists with some shift and deformation giving rise to a perturbed torus $\mathcal{T}$, with perturbed local stable and unstable whiskers.

Such local whiskers can be extended to global whiskers $\mathcal{W}^{\mathrm{s}}$, $\mathcal{W}^{\mathrm{u}}$ but, in general, for $\mu \neq 0$ they do not coincide anymore, and one can introduce a *splitting function* giving the distance between the whiskers in the directions of the actions $I \in \mathbb{R}^2$: denoting $\mathcal{J}^{\mathrm{s,u}}(\theta)$ parameterizations of a transverse section of both whiskers, one can define $\mathcal{M}(\theta) := \mathcal{J}^{\mathrm{u}}(\theta) - \mathcal{J}^{\mathrm{s}}(\theta)$, $\theta \in \mathbb{T}^2$. In fact, this function turns out to be the gradient of the (scalar) *splitting potential*: $\mathcal{M}(\theta) = \nabla \mathcal{L}(\theta)$ (see [3, Sect. 5.2], and also [7]).

In (4), we deal with the following 24 quadratic numbers

$$[\bar 1]\,, [\bar 2]\,, \ \ldots\,, \ [\overline{13}]\,, [\overline{1,2}]\,, \ \ldots\,, \ [\overline{1,12}]\,, \tag{5}$$

where we denote a quadratic number according to its periodic part in the continued fraction, see (8).

Next, we establish the *main result* of this work, providing two types of *asymptotic estimates* for the splitting, as $\varepsilon \to 0$. On one hand, we give an estimate for the *maximal splitting distance*, i.e., for the maximum of $|\mathcal{M}(\theta)|$, $\theta \in \mathbb{T}^2$. On the other hand, we show that for most values of $\varepsilon \to 0$ there exist four transverse homoclinic orbits, associated to simple zeros θ_* of $\mathcal{M}(\theta)$ (i.e., nondegenerate critical points of $\mathcal{L}(\theta)$) and, for such homoclinic orbits, we obtain an estimate for the *transversality* of the splitting, given by the minimum eigenvalue (in modulus) of the matrices $\mathrm{D}\mathcal{M}(\theta_*)$.

We use the notation $f \sim g$ if we can bound $c_1|g| \leq |f| \leq c_2|g|$ with positive constants c_1, c_2 not depending on ε, μ.

Theorem 1 *Assume the conditions described above for the Hamiltonian* (1)–(3)*, and that* ε *is small enough and* $\mu = \varepsilon^p$*,* $p > 3$*. Then, there exist continued functions* $h_1(\varepsilon)$ *and* $h_2(\varepsilon)$ *(defined in* (17)*), periodic in* $\ln \varepsilon$ *and satisfying* $1 \leq h_1(\varepsilon) \leq h_2(\varepsilon)$*, and a positive constant* C_0 *(given in* (16)*), such that:*

(i) *for the maximal splitting distance, we have the estimate*

$$\max_{\theta \in \mathbb{T}^2} |\mathcal{M}(\theta)| \sim \frac{\mu}{\sqrt{\varepsilon}} \exp\left\{ -\frac{C_0 h_1(\varepsilon)}{\varepsilon^{1/4}} \right\};$$

(ii) *the splitting function* $\mathcal{M}(\theta)$ *has exactly four zeros* θ_**, all simple, for all* ε *except for a small neighborhood of a finite number of geometric sequences of* ε*;*

(iii) *at each zero* θ_* *of* $\mathcal{M}(\theta)$*, the minimal eigenvalue of* $\mathrm{D}\mathcal{M}(\theta_*)$ *satisfies*

$$m_* \sim \mu \varepsilon^{1/4} \exp\left\{ -\frac{C_0 h_2(\varepsilon)}{\varepsilon^{1/4}} \right\}.$$

For the proof of this theorem, we apply the *Poincaré–Melnikov method*, which provides a first order approximation

$$\mathcal{M}(\theta) = \mu \nabla L(\theta) + \mathcal{O}(\mu^2) \tag{6}$$

in terms of the *Melnikov potential*, which can be defined by integrating the perturbation H_1 along the trajectories of the unperturbed homoclinic whisker $\mathcal{W}_0$:

$$L(\theta) := -\int_{-\infty}^{\infty} H_1(x_0(t), \theta + \omega_\varepsilon t)\, \mathrm{d}t. \tag{7}$$

Since this first order approximation is exponentially small in ε, in principle the approximation (6) cannot be directly applied in our singular problem with $\mu = \varepsilon^p$. However, using suitable bounds for the error term $\mathcal{O}(\mu^2)$, given in [6], one can see that for $p > 3$ the first order approximation given by the Melnikov

potential overcomes the error term and provides the right asymptotic estimates for the splitting. Such estimates come from the size of *dominant harmonics* in the Fourier expansion of (7), and studying their dependence on ε. More precisely, to estimate the maximal splitting one dominant harmonic is enough and, to estimate the transversality of the splitting, two dominant harmonics are required (excluding the values of ε such that the second and third harmonics are of the same magnitude, which could give rise to bifurcations in the homoclinic orbits and would require a further study).

The remaining sections of this work are devoted to the definition of the functions $h_1(\varepsilon)$ and $h_2(\varepsilon)$, making emphasis on their dependence on the arithmetic properties of the quadratic number Ω.

2 Continued Fractions and Resonant Sequences

We review briefly the technique developed in [5] for studying the resonances of quadratic frequencies. Let $0 < \Omega < 1$ be a quadratic irrational number. It is well-known that it has an infinite continued fraction

$$\Omega = [a_1, a_2, a_3, \ldots] = \cfrac{1}{a_1 + \cfrac{1}{a_2 + \cfrac{1}{a_3 + \cdots}}}, \qquad a_n \in \mathbb{Z}^+,\ n \geq 1 \quad (\text{and } a_0 = 0), \tag{8}$$

which is *eventually periodic*, i.e., periodic starting at some a_l. For a purely m-periodic continued fraction $\Omega = [\overline{a_1, \ldots, a_m}]$ we introduce the matrix

$$U = (-1)^m A_1^{-1} \cdots A_m^{-1}, \text{ where } A_l = \begin{pmatrix} a_l & 1 \\ 1 & 0 \end{pmatrix}, \quad l = 1, \ldots, m.$$

It is well-known that quadratic vectors satisfy a *Diophantine condition*

$$|\langle k, \omega \rangle| \geq \frac{\gamma}{|k|}, \quad \forall k \in \mathbb{Z}^2 \setminus \{0\}.$$

With this in mind, we define the *"numerators"*

$$\gamma_k := |\langle k, \omega \rangle| \cdot |k|, \qquad k \in \mathbb{Z}^2 \setminus \{0\} \tag{9}$$

(for integer vectors, we use the norm $|\cdot| = |\cdot|_1$). Our aim is to find the integer vectors k which give the smallest values γ_k; we call such vectors the *primary resonances*.

All vectors $k \in \mathbb{Z}^2 \setminus \{0\}$ with $|\langle k, \omega \rangle| < 1/2$ are subdivided into *resonant sequences*:

$$s(j, n) := U^n k^0(j), \qquad n = 0, 1, 2, \ldots, \tag{10}$$

where the initial vector $k^0(j) = (-\operatorname{rint}(j\Omega), j), j \in \mathbb{Z}^+$, satisfies

$$\frac{1}{2\lambda} < |\langle k^0(j), \omega\rangle| < \frac{1}{2}, \tag{11}$$

λ being the eigenvalue of U with $\lambda > 1$. For each $j \in \mathbb{Z}^+$ satisfying (11), it was proved in [5, Theorem 2] (see also [2]) that, asymptotically, the resonant sequence $s(j,n)$ exhibits a geometric growth and the sequence $\gamma_{s(j,n)}$ has a limit γ_j^*:

$$|s(j,n)| = K_j\lambda^n + \mathcal{O}(\lambda^{-n}), \quad \gamma_{s(j,n)} = \gamma_j^* + \mathcal{O}(\lambda^{-2n}), \text{ as } n \to \infty, \tag{12}$$

where K_j and γ_j^* can be determined explicitly for each resonant sequence (see explicit formulas in [5]). We select the minimal of γ_j^*:

$$\gamma^* := \liminf_{|k|\to\infty} \gamma_k = \min_j \gamma_j^* = \gamma_{j_0}^* > 0. \tag{13}$$

The integer vectors of the corresponding sequence $s(j_0,n)$ are *the primary resonances*, and we call the *secondary resonances* the integer vectors belonging to any of the remaining resonant sequences $s(j,n), j \neq j_0$. We also call by *the main secondary resonances* the sequence $s(j_1,n)$ which is linearly independent with $s(j_0,n)$ and gives the smallest limit $\gamma_{j_1}^*$ among the secondary resonances.

3 The Functions $h_1(\varepsilon)$ and $h_2(\varepsilon)$

Taking into account the form of H_1 in (3), we present the Melnikov potential (7) in its Fourier expansion. Using (4) and (9), we present the coefficients in the form

$$L_k = \frac{2\pi|\langle k,\omega_\varepsilon\rangle|\,\mathrm{e}^{-\rho|k|}}{\sinh|\frac{\pi}{2}\langle k,\omega_\varepsilon\rangle|} = \alpha_k\,\mathrm{e}^{-\beta_k}, \qquad \alpha_k \approx \frac{4\pi\gamma_k}{|k|\sqrt{\varepsilon}}, \quad \beta_k = \rho|k| + \frac{\pi\gamma_k}{2|k|\sqrt{\varepsilon}}. \tag{14}$$

For any given ε, we find the dominant harmonics $L_k(\varepsilon)$ which correspond essentially to the smallest exponents $\beta_k(\varepsilon)$.

The exponents $\beta_k(\varepsilon)$ in (14) can be presented in the form

$$\beta_k(\varepsilon) = \frac{C_0}{\varepsilon^{1/4}}\,g_k(\varepsilon), \qquad g_k(\varepsilon) := \frac{\tilde\gamma_k^{1/2}}{2}\left[\left(\frac{\varepsilon}{\varepsilon_k}\right)^{1/4} + \left(\frac{\varepsilon_k}{\varepsilon}\right)^{1/4}\right], \tag{15}$$

where

$$\varepsilon_k := D_0\,\frac{\tilde\gamma_k^2}{|k|^4}, \qquad \tilde\gamma_k = \frac{\gamma_k}{\gamma^*}, \qquad C_0 = (2\pi\rho\gamma^*)^{1/2}, \qquad D_0 = \left(\frac{\pi\gamma^*}{2\rho}\right)^2. \tag{16}$$

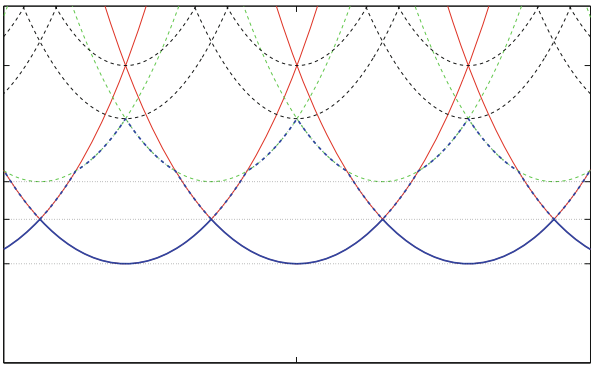

Fig. 1 Graphs of the functions $h_1(\varepsilon)$ (*solid blue*) and $h_2(\varepsilon)$ (*dash-dot blue*) for $[\overline{1,2}] = \sqrt{3}-1$. *Red lines* are the primary functions $g_{s(j_0,n)}(\varepsilon)$, and *green lines* correspond to the main secondary functions $g_{s(j_1,n)}(\varepsilon)$

Since the coefficients L_k are exponentially small in ε, it is more convenient to work with the functions g_k, whose smallest values correspond to the largest L_k. To this aim, it is useful to consider the graphs of the functions $g_k(\varepsilon)$, $k \in \mathbb{Z}^2 \setminus \{0\}$, in order to detect the minimum of them for a given value of ε.

We know from (15) that the functions $g_k(\varepsilon)$ have their minimum at $\varepsilon = \varepsilon_k$ and the corresponding minimal values are $g_k(\varepsilon_k) = \tilde{\gamma}_k^{1/2}$. For the integer vectors $k = s(j,n)$ belonging to a resonant sequence (10), using the approximations (12), we have

$$\varepsilon_{s(j,n)} \approx \frac{D_0(\tilde{\gamma}_j^*)^2}{K_j^4 \lambda^{4n}}, \quad g_{s(j,n)}(\varepsilon) \approx \frac{(\tilde{\gamma}_j^*)^{1/2}}{2}\left[\left(\frac{\varepsilon}{\varepsilon_{s(j,n)}}\right)^{1/4} + \left(\frac{\varepsilon_{s(j,n)}}{\varepsilon}\right)^{1/4}\right], \text{ as } n \to \infty.$$

Taking into account such approximations, we have a periodic behavior of the functions with respect to $\ln \varepsilon$, as we see in Fig. 1 (where a logarithmic scale for ε is used).

We define, for any given ε, the function $h_1(\varepsilon)$ and $h_2(\varepsilon)$ as

$$h_1(\varepsilon) := \min_k g_k(\varepsilon) = g_{S_1}(\varepsilon), \quad h_2(\varepsilon) := \min_{k \text{ lin.indep.of } S_1} g_k(\varepsilon) = g_{S_2}(\varepsilon), \tag{17}$$

with some integer vectors $S_1(\varepsilon)$ and $S_2(\varepsilon)$ realizing such minima. The functions are continuous and $4 \ln \lambda$-periodic in $\ln \varepsilon$. It turns out that for the 24 quadratic numbers (5), the integer vector $S_1(\varepsilon)$ providing $h_1(\varepsilon)$ always corresponds to a primary resonance, defined in (13). On the other hand, the vector $S_2(\varepsilon)$ providing $h_2(\varepsilon)$ may correspond to primary or main secondary resonances in different intervals of ε (see Fig. 1 for an illustration for the number $[\overline{1,2}] = \sqrt{3}-1$). There is a finite number of geometric sequences of ε, where a change in $S_2(\varepsilon)$ occurs. These points require a special study for the transversality and they are excluded in Theorem 1.

Acknowledgements This work has been partially supported by the Spanish MINECO-FEDER grant number MTM2012-31714 and the Catalan grant 2009SGR859. The author MG has also been supported by the DFG Collaborative Research Center TRR 109 "Discretization in Geometry and Dynamics".

References

1. V.I. Arnold, "Instability of dynamical systems with several degrees of freedom". *Soviet Math. Dokl.* **5**(3) (1964), 581–585.
2. A. Delshams, M. Gonchenko, and P. Gutiérrez, "Exponentially small asymptotic estimates for the splitting of separatrices to whiskered tori with quadratic and cubic frequencies". *Electron. Res. Ann. Math. Sci.* **21** (2014), 41–61.
3. A. Delshams and P. Gutiérrez, "Splitting potential and the Poincaré–Melnikov method for whiskered tori in Hamiltonian systems". *J. Nonlinear Sci.* **10**(4) (2000), 433–476.
4. A. Delshams and P. Gutiérrez, "Homoclinic orbits to invariant tori in Hamiltonian systems". In C.K.R.T. Jones and A.I. Khibnik, editors, "Multiple-Time-Scale Dynamical Systems" (Minneapolis, MN, 1997), **122**, pages. 1–27. Springer-Verlag, New York, 2001.
5. A. Delshams and P. Gutiérrez, "Exponentially small splitting of separatrices for whiskered tori in Hamiltonian systems". *Zap. Nauchn. Sem. S.-Peterburg. Otdel. Mat. Inst. Steklov. (POMI)* **300** (2003), 87–121; translation in *J. Math. Sci.* **128**(2) (2005), 2726–2746.
6. A. Delshams, P. Gutiérrez, and T.M. Seara, "Exponentially small splitting for whiskered tori in Hamiltonian systems: flow-box coordinates and upper bounds". *Discrete Contin. Dyn. Syst.* **11**(4) (2004), 785–826.
7. L.H. Eliasson, "Biasymptotic solutions of perturbed integrable Hamiltonian systems". *Bol. Soc. Brasil. Mat.* **25**(1) (1994), 57–76.
8. L. Niederman, "Dynamics around simple resonant tori in nearly integrable Hamiltonian systems". *J. Differential Equations* **161**(1) (2000), 1–41.

Homoclinic and Heteroclinic Orbits for a Class of Singular Planar Newtonian Systems

Joanna Janczewska

1 Introduction

The study of existence and multiplicity of solutions of differential equations possessing a variational nature is a problem of great meaning since most of them derives from mechanics and physics. In particular, this relates to Hamiltonian systems including Newtonian ones. During the past 30 years there has been a great deal of progress in the use of variational methods to find periodic, homoclinic and heteroclinic solutions of Hamiltonian systems. Hamiltonian systems with singular potentials, i.e., potentials that become infinite at a point or a larger subset of $\mathbb{R}^n$, are among those of the greatest interest. Let us remark that such potentials arise in celestial mechanics. For example, the Kepler problem with

$$V(q) = -\frac{1}{|q-\xi|}$$

has a point singularity at ξ ($q \in \mathbb{R}^n \setminus \{\xi\}$). In physics, the gradient ∇V of the gravitational potential is called a weak force.

Our presentation is based on [3, 5]. We are interested in conservative dynamical systems involving strong forces. A model potential in a neighbourhood of a singular point ξ is defined by

$$V(q) = -\frac{1}{|q-\xi|^\alpha},$$

where $\alpha \geq 2$.

J. Janczewska (✉)
Faculty of Applied Physics and Mathematics, Gdańsk University of Technology, Gdańsk, Poland
e-mail: janczewska@mif.pg.gda.pl

M. Corbera et al. (eds.), *Extended Abstracts Spring 2014*, Trends in Mathematics 4,
DOI 10.1007/978-3-319-22129-8_7

Consider an autonomous Newtonian system

$$\ddot{q} + \nabla V(q) = 0, \tag{HS}$$

where $q \in \mathbb{R}^2$. Assume that a potential V satisfies the following conditions:

(V_1) $V \in C^1(\mathbb{R}^2 \setminus \{\xi\}, \mathbb{R})$;
(V_2) $V(x) \to -\infty$ as $x \to \xi$;
(V_3) there exist a neighbourhood $\mathcal{N}$ of the point ξ and a function $U \in C^1(\mathcal{N} \setminus \{\xi\}, \mathbb{R})$ such that $|U(x)| \to \infty$ as $x \to \xi$, and $-|\nabla U(x)|^2 \geq V(x)$ for every $x \in \mathcal{N} \setminus \{\xi\}$;
(V_4) $V(x) \leq 0$ and $V(x) = 0$ iff $x \in \{a, b\}$, $a, b \in \mathbb{R}^2 \setminus \{\xi\}$;
(V_5) there is $V_0 < 0$ such that $\limsup_{|x|\to\infty} V(x) \leq V_0$.

The assumption (V_3) due to W.B. Gordon is called a strong force condition, see [2].

Let E denote the Sobolev space

$$\left\{ q \in W^{1,2}_{\mathrm{loc}}(\mathbb{R}, \mathbb{R}^2) \colon \int_{-\infty}^{\infty} |\dot{q}(t)|^2 dt < \infty \right\}$$

with the norm

$$\|q\|_E = \left(|q(0)|^2 + \int_{-\infty}^{\infty} |\dot{q}(t)|^2 dt \right)^{\frac{1}{2}}.$$

Set

$$\Lambda = \{ q \in E \colon q(t) \neq \xi \text{ for } t \in \mathbb{R} \}.$$

We can define a rotation number map

$$\{ q \in \Lambda \colon q(\pm\infty) \in \{a, b\} \} \ni q \longrightarrow \mathrm{rot}_\xi(q) \in \mathbb{Z}$$

as follows. In the polar coordinate system with the pole ξ and the polar axis $l = \{x \in \mathbb{R}^2 \colon x = \xi + s \cdot \vec{\xi a},\ s \geq 0\}$ one has $q(t) = (r(t)\cos\varphi(t), r(t)\sin\varphi(t))$. We can assume that $r(t)$ and $\varphi(t)$ are continuous. (Polar angles are measured counterclockwise from l.) If $q(-\infty) = b$ and $q(\infty) = a$ then

$$\mathrm{rot}_\xi(q) = \left[\frac{\varphi(\infty) - \varphi(-\infty)}{2\pi} \right] + 1.$$

Otherwise,

$$\mathrm{rot}_\xi(q) = \left[\frac{\varphi(\infty) - \varphi(-\infty)}{2\pi} \right],$$

where $[\tau]$ is the integral part of τ. Let us remark that if $q(-\infty) = q(\infty)$ then $\mathrm{rot}_\xi(q)$ is the winding number of the curve q about ξ. Moreover, after a reparametrization, q can be considered to be the continuous image of S^1. Therefore one can associated with q its Brouwer degree with respect to ξ. The Brouwer degree of q equals $\mathrm{rot}_\xi(q)$.

Theorem 1 (See Conclusion 1.5 in [5]) *Under the assumptions* (V_1)–(V_5)*, the Newtonian system* (HS) *has at least two solutions which wind around* ξ *and join* $\{a, b\}$ *to* $\{a, b\}$*. One of them is a heteroclinic orbit joining the point a to the point b. The second is either heteroclinic with a rotation different from the first, or homoclinic.*

Theorem 1 is a generalization of the result given by Rabinowitz in [6] on the existence of homoclinic solutions in the case $a = b$.

2 Variational Approach

Our approach to the problem of existence and multiplicity of connecting orbits of (HS) is variational. Homoclinic and heteroclinic solutions are global in time. Moreover, they are critical points of an action functional. Therefore it is reasonable to use variational (global) methods to receive them.

For $q \in \Lambda$, set

$$I(q) = \int_{-\infty}^{\infty} \left(\frac{1}{2}|\dot{q}(t)|^2 - V(q(t)) \right) dt.$$

We define the family $\mathcal{F}$ as follows. A subset $Z \subset \Lambda$ is a member of $\mathcal{F}$ iff it has the following properties:

- $I(q) < \infty$ for all $q \in Z$,
- if $p, q \in Z$ then $p(-\infty) = q(-\infty)$ and $p(\infty) = q(\infty)$,
- for each $q \in Z$ and for each $\psi \in C_0^\infty(\mathbb{R}, \mathbb{R}^2)$ there exists $\delta > 0$ such that if $s \in (-\delta, \delta)$ then $q + s\psi \in Z$.

Of course $\mathcal{F}$ is nonempty. We see at once that for example:

$$\Gamma^+ = \{q \in \Lambda : q(-\infty) = a,\ q(\infty) = b \ \wedge\ rot(q) \geq 0\},$$
$$\Gamma^- = \{q \in \Lambda : q(-\infty) = a,\ q(\infty) = b \ \wedge\ rot(q) < 0\},$$
$$\Omega_a^{\pm n} = \{q \in \Lambda : q(\pm\infty) = a \ \wedge\ \pm rot(q) \geq n\},$$
$$\Omega_b^{\pm n} = \{q \in \Lambda : q(\pm\infty) = b \ \wedge\ \pm rot(q) \geq n\},$$

where $n \in \mathbb{N}$, are members of this family. Standard arguments show that if q is a minimizer of I on $Z \in \mathcal{F}$ then q is a classical solution of (HS).

Outline of the Proof of Theorem 1 Set

$$\gamma^{\pm} = \inf\{I(q): q \in \Gamma^{\pm}\}.$$

Without loss of generality we can assume that $\gamma^- \leq \gamma^+$. Let $\{q_m\}_{m\in\mathbb{N}} \subset \Gamma^-$ and $\{\tilde{q}_m\}_{m\in\mathbb{N}} \subset \Gamma^+$ be minimizing sequences of I on Γ^- and Γ^+, respectively. There exist Q and $\tilde{Q}$ in Λ such that, going to subsequences if necessary, $q_m \rightharpoonup Q$ and $\tilde{q}_m \rightharpoonup \tilde{Q}$ in E. Both Q and $\tilde{Q}$ are connecting orbits of (HS). One can show that $Q \in \Gamma^-$. Whereas $\tilde{Q}$ may belong to Γ^-, Γ^+ or Ω_a^k for a certain $k \in \mathbb{N}$.

In the case $\tilde{Q} \in \Gamma^-$ we check that $\gamma^+ = I(\tilde{Q}) + \omega_b^n$, where $\omega_b^n = \inf\{I(q): q \in \Omega_b^n\}$ and $n = -\mathrm{rot}_\xi(\tilde{Q})$. Moreover, the Hamiltonian system (HS) possesses either a homoclinic solution $p: \mathbb{R} \to \mathbb{R}^2 \setminus \{\xi\}$ such that $p(\pm\infty) = b$ and $\mathrm{rot}_\xi(p) > 0$, or a heteroclinic solution $Q_0 \in \Gamma^-$ such that $\mathrm{rot}_\xi(Q_0) < \mathrm{rot}_\xi(\tilde{Q})$ (see [5, Theorems 1.3, 1.4]). This connecting orbit is obtained as a weak limit of a minimizing sequence of the action functional I on Ω_b^n. □

Fix $Z \in \mathcal{F}$ such that if $q, p \in Z$ then $\mathrm{rot}_\xi(q) = \mathrm{rot}_\xi(p)$. Let

$$z = \inf\{I(q): q \in Z\}$$

and $\{q_m\}_{m\in\mathbb{N}} \subset Z$ be a sequence such that

$$\lim_{m\to\infty} I(q_m) = z.$$

For each $i \in \mathbb{N}$, set

$$C_i = \overline{\bigcup_{m=i}^{\infty} q_m(\mathbb{R})}.$$

Define

$$SC = \bigcap_{i=1}^{\infty} C_i.$$

Theorem 2 (Shadowing Chain Lemma, See Lemma 3.2 in [3]) *Under the assumptions* (V_1)–(V_5)*, there are a finite number of homoclinic and heteroclinic orbits,* $Q_1, Q_2, \ldots, Q_l$*, of the Newtonian system* (HS) *such that*

$$z = I(Q_1) + I(Q_2) + \cdots + I(Q_l)$$

and

$$rot_\xi(q_m) = rot_\xi(Q_1) + rot_\xi(Q_2) + \cdots + rot_\xi(Q_l).$$

Theorem 2 is the starting point to show the existence of infinitely many homoclinic and heteroclinic orbits to the Newtonian system (HS) under certain extra conditions of Bolotin's type (see [1]) on the existence of minimal noncontractible periodic orbits around ξ.

Theorem 3 (M. Izydorek, J. Janczewska) *Let $a = b$. Suppose that $V \in C^{1,1}(\mathbb{R}^2 \setminus \{\xi\}, \mathbb{R})$ satisfies the conditions (V_2)–(V_5) and, moreover,*

(B_1) *there are $T_1 \in (0, \infty)$ and $p_1 \in W^{1,2}([0, T_1], \mathbb{R}^2 \setminus \{a, \xi\})$ such that $p_1(0) = p_1(T_1)$, $rot_a(p_1) = 0$, $rot_\xi(p_1) = 1$ and $\int_0^{T_1} \left(\frac{1}{2}|\dot{p}_1(t)|^2 - V(p_1(t))\right) dt < \lambda_1$;*

(B_2) *there are $T_2 \in (0, \infty)$ and $p_2 \in W^{1,2}([0, T_2], \mathbb{R}^2 \setminus \{a, \xi\})$ such that $p_2(0) = p_2(T_2)$, $rot_a(p_2) = rot_\xi(p_2) = 1$ and $\int_0^{T_2} \left(\frac{1}{2}|\dot{p}_2(t)|^2 - V(p_2(t))\right) dt < \lambda_1$, where*

$$\lambda_1 = \inf\{I(q) : q \in \Omega_a^1 \ \wedge \ rot_\xi(q) = 1\},$$

and $rot_a(p_i)$, $rot_\xi(p_i)$ are the winding numbers (Brouwer's degree) of the curve p_i about the point a and ξ, respectively.

Under the above assumptions, there exist infinitely many homotopy classes in $\pi_1(\mathbb{R}^2 \setminus \{\xi\})$ containing at least two geometrically distinct homoclinic (to a) solutions.

The detailed proof of Theorem 3 is contained in the paper [4].

Acknowledgements The research is supported by the Grant number 2011/03/B/ST1/04533 of National Science Centre of Poland.

References

1. S.V. Bolotin, "Variational criteria for nonintegrability and chaos in Hamiltonian systems". Hamiltonian Mechanics, *NATO Adv. Sci. Inst. Ser. B* **331** (1994), 173–179.
2. W.B. Gordon, "Conservative dynamical systems involving strong forces". *Trans. Amer. Math. Soc.* **204** (1975), 113–135.
3. M. Izydorek and J. Janczewska, "The shadowing chain lemma for singular Hamiltonian systems involving strong forces". *Cent. Eur. J. Math.* **10** (2012), 1928–1939.
4. M. Izydorek and J. Janczewska, "Two families of infinitely many homoclinics for singular strong force Hamiltonian systems". *J. Fixed Point Theory Appl.* **16**(1-2) (2014), 301–311.
5. J. Janczewska, "The existence and multiplicity of heteroclinic and homoclinic orbits for a class of singular Hamiltonian systems in $\mathbb{R}^2$". *Boll. Unione Mat. Ital. (9)* **3** (2010), 471–491.
6. P.H. Rabinowitz, "Homoclinics for a singular Hamiltonian system", in "Geometric analysis and the calculus of variations". Int. Press, Cambridge, MA, (1996), 267–296.

Transport Dynamics: From the Bicircular to the Real Solar System Problem

Mercè Ollé, Esther Barrabés, Gerard Gómez, and Josep Maria Mondelo

1 Introduction

The main goal is to give an explanation of transport in the Solar System based in dynamical systems theory. More concretely, we consider as an approximation of the Solar System, a chain of independent Bicircular problems in order to get a first insight of transport in this simplified case. Each bicircular problem (BP) consists of the Sun (S), Jupiter (J), a planet and an infinitesimal mass. For each fixed BP we consider *natural* periodic orbits which are unstable. These periodic orbits are the dynamical substitutes in the BP of the collinear equilibrium points L_1 and L_2 of the Circular Restricted Three Body Problem (CRTBP) Sun-Planet-particle. We study the behavior of their invariant manifolds, in order to look for *connections* between invariant manifolds of consecutive BP.

We are interested in transport from the external Solar System to the internal one. On one hand we start with the BP S-J-Neptune-particle and the dynamical substitute of L_1 of the CRTBP S-Neptune-particle, and its unstable invariant manifold. On the other hand we consider the BP S-J-Uranus-particle, and the dynamical substitute of

M. Ollé (✉)
Departament de Matemàtica Aplicada I, Universitat Politècnica de Catalunya, Barcelona, Spain
e-mail: merce.olle@upc.edu

E. Barrabés
Departament d'Informàtica i Matemàtica Aplicada, Universitat de Girona, Girona, Spain
e-mail: barrabes@imae.udg.edu

G. Gómez
Departament de Matemàtica Aplicada i Anàlisi, Universitat de Barcelona, Barcelona, Spain
e-mail: gerard@maia.ub.es

J.M. Mondelo
Departament de Matemàtiques, Universitat Autònoma de Barcelona, Barcelona, Spain
e-mail: jmm@mat.uab.cat

M. Corbera et al. (eds.), *Extended Abstracts Spring 2014*, Trends in Mathematics 4,
DOI 10.1007/978-3-319-22129-8_8

L_2 of the CRTBP S-Uranus-particle, and its stable invariant manifold. The key idea is to compute both manifolds up to a suitable Poincaré section in such a way that *heteroclinic* connections are found. As we deal with two independent BP, they are not really connections, but they can be viewed as seeds to be used in a more realistic model. Of course, the same kind of simulation may be carried out considering now the BP S-J-Uranus-particle and S-J-Saturn-particle problems. And so on.

Therefore, these *heteroclinic* connections provide an skeleton of dynamics that explains how to transfer from the outer part of the Solar System to the inner one.

The final goal—in progress—is concerned with a more realistic model of the Solar System where the dynamical substitutes of the previous invariant objects used (periodic orbits and their invariant manifolds) should be obtained and study their role to explain transport.

2 The Bicircular Problem

The Bicircular problem (BP) is a simplified model of the four body problem. In this model we assume that the Sun and Jupiter are revolving in circular orbits around their center of mass, and a planet (P) moves in a circular orbit around this baricenter. A remark to comment is that this model is not coherent, that is, the positions of the Sun, Jupiter and the planet do not satisfy Newton's equations.

Let m_S, m_J and m_P be the masses of S, J and P respectively. Let B be the barycenter of the S-J system and assume that the distance between S and J is equal to one. Let a_P be the distance from the planet to B. In a suitable rotating system of coordinates with origin at B (where the Sun and Jupiter remain fixed in the x-axis), being (x, y, z) the position of the particle and defining momenta $p_x = \dot{x} - y$, $p_y = \dot{y} + x$, $p_z = \dot{z}$, the equations may be written as a Hamiltonian system of differential equations with Hamiltonian function

$$\begin{aligned} H(x, y, z, p_x, p_y, p_z) \; &= \frac{1}{2}(p_x^2 + p_y^2 + p_z^2) + y p_x - x p_y \\ &\quad - \frac{1-\mu}{\rho_1} - \frac{\mu}{\rho_2} - \frac{\mu_P}{\rho_P} - \frac{\mu_P}{a_P^2}(y \sin\theta - x \cos\theta), \end{aligned} \tag{1}$$

where

$$\begin{aligned} &\rho_1 = ((x-\mu)^2 + y^2 + z^2)^{1/2}, && \theta = t(1-\omega_P), \\ &\rho_2 = ((x-\mu+1)^2 + y^2 + z^2)^{1/2}, && \mu = \tfrac{m_J}{m_J+m_S}, \\ &\rho_P = ((x - a_P\cos\theta)^2 + (y + a_P \sin\theta)^2 + z^2)^{1/2}, && \mu_P = \tfrac{m_P}{m_J+m_S}. \end{aligned}$$

We obtain a Hamiltonian system of 3 degrees of freedom, non autonomous but periodic in t with period $T_P = 2\pi/\omega_P$. For more details see [2].

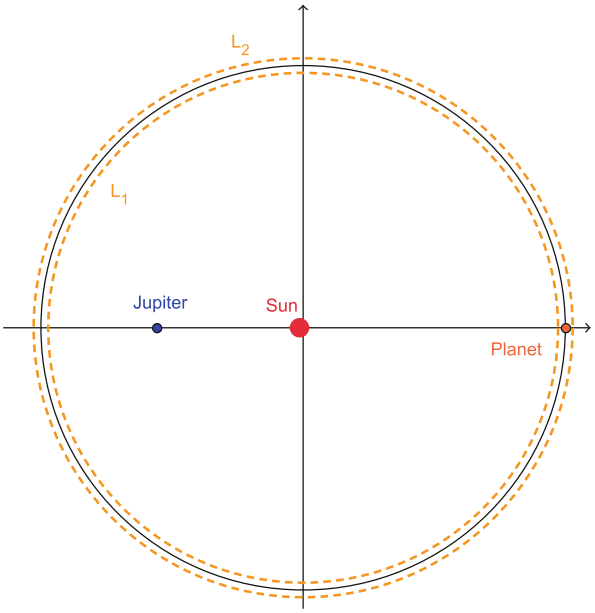

Fig. 1 Periodic orbits POL_i, $i = 1, 2$, in a BP problem in rotating coordinates (x, y)

For small values of μ, the BP can be view as a perturbation of the CRTBP Sun-Planet-particle. It is well known that the CRTBP has three collinear equilibrium points L_i, $i = 1, 2, 3$. The points L_1 and L_2 are the ones close to the planet. The dynamical substitutes of these equilibrium points are periodic orbits, with period T_P in the BP, which are denoted by POL_1 and POL_2. See Fig. 1.

The periodic orbits POL_i, $i = 1, 2$, are unstable so, there exist stable and unstable invariant manifolds associated to them. Each invariant manifold has two branches. The orbits of one branch, in mean, spiral inwards, whereas the orbits of the other branch spiral outwards.

3 Transport Between Neptune and Uranus

Let us consider the BP S-J-Neptune-particle, the periodic orbit POL_1 and the branch of its unstable manifold W^u that spirals inwards. And let us consider the BP S-J-Uranus-particle, the periodic orbit POL_2, and the branch of its stable manifold W^s such that spirals outwards. We can see that behavior considering the distance $r(t) = \sqrt{x^2 + y^2 + z^2}$ from the orbits of the invariant manifolds to the origin. We plot in Fig. 2 the distance $r(t)$ for the unstable branch $W^u(POL_1)$ of the Neptune BP (left) and for the stable branch $W^s(POL_2)$ of the Uranus BP (right).

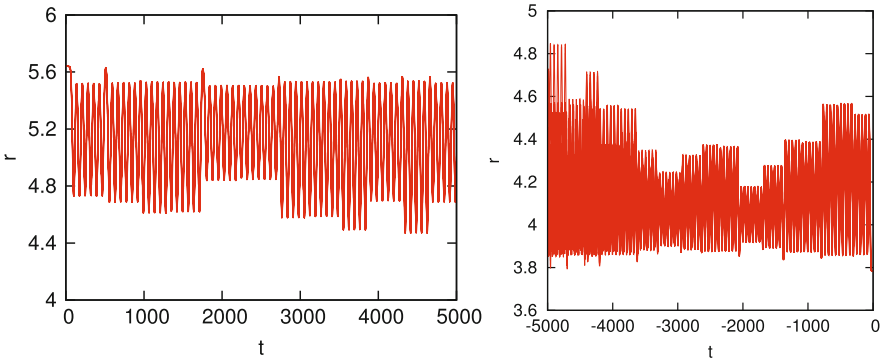

Fig. 2 Behavior of the distance $r(t)$ of some orbits of the branches of the invariant manifolds $W^u(POL_1)$ for the BP S-J-Neptune-particle (*left*) and $W^s(POL_2)$ for the BP S-J-Uranus-particle (*right*)

Next, in order to look for *heteroclinic* connections, we fix a Poincaré section $\Sigma = \{r = R\}$, where R is an intermediate constant value between the position of Uranus and Neptune. We compute both manifolds for a range of time of $t = 50{,}000$, and we keep all the intersections of the orbits with Σ. So we have a set of points S_1 of $W^u(POL_1) \cap \Sigma$ and a set of points S_2 of $W^s(POL_2) \cap \Sigma$. We compute the minimum distance between each point in S_1 to S_2. If one of these minimum distances is 0, then we should obtain a heteroclinic connection, assuming the particle goes from Σ backward/forward in time asymptotically to the periodic orbit $POL_{1/2}$ taking into account different BP, that is, S, J and Neptune/Uranus. In positions, the distances obtained are of order 10^{-7}, but in velocities the minimum obtained is of order 10^{-4}. Nevertheless, as we are matching different BP problems, and the results must be refined in a more realistic model, it seems a good enough result to support the idea that the invariant manifolds of some objects are responsible for *natural* transport in the Solar System.

Other simulations can be done taking into account other BP (see [1]) in order to study similar transport between other two consecutive planets.

Finally, the results obtained are considered as seeds to look for trajectories in a more realistic model of the Solar System, like the model of the JPL ephemerides or an N-body problem.

References

1. E. Barrabés, G. Gómez, J.M. Mondelo, and M. Ollé, "Transport in the Solar System". *Preprint*.
2. G. Gómez, J. Llibre, R. Martínez, and C. Simó, "Study on orbits near the triangular libration points in the perturbed restricted three-body problem". Report ESOC 6139/84/D/JS(SC), 1987.

Quasi-Periodic Almost-Collision Motions in the Spatial Three-Body Problem

Jesús F. Palacián, Flora Sayas, and Patricia Yanguas

1 Introduction

We deal with the spatial three-body problem in the various regimes where the Hamiltonian is split as the sum of two Keplerian systems plus a small perturbation. This is a region of the phase space $T^*\mathbb{R}^6$ where the perturbation is small [3], the so called perturbing region $\mathcal{P}_{\varepsilon,n}$. In particular, we prove the existence of quasi-periodic motions where the inner particles describe bounded near-rectilinear trajectories whereas the outer particle follows an orbit lying near the invariable plane. These motions fill in five-dimensional invariant tori. Moreover, the inner particles move in orbits either near an axis perpendicular to the invariable plane or near the invariable plane.

By averaging over the mean anomalies, truncating higher-order terms and using singular reduction theory we get a one-degree-of-freedom Hamiltonian system defined in a singular reduced space, the so called orbit space. In [3] we analyse the relative equilibria and bifurcations and in [4] we reconstruct the invariant tori corresponding to motions of non-rectilinear type. Three of the relative equilibria of the reduced Hamiltonian in the orbit space are elliptic points corresponding to near-rectilinear motions of the inner bodies, and these are the ones we carry out the reconstruction of the KAM 5-tori surrounding them. We regularise the double inner collisions following the guidelines of Zhao [6, 7]. In particular, he applies the Kustaanheimo–Stiefel regularisation. This allows us to build sets of action-angle coordinates needed to apply KAM theory. The motions we deal with admit different combinations, for instance, the outer particle may move in a near-circular orbit or the invariable plane may coincide with the horizontal plane. This leads to

J.F. Palacián (✉) • F. Sayas • P. Yanguas
Departamento de Ingeniería Matemática e Informática, Universidad Pública de Navarra, Pamplona, Spain
e-mail: palacian@unavarra.es; flora.sayas@unavarra.es; yanguas@unavarra.es

M. Corbera et al. (eds.), *Extended Abstracts Spring 2014*, Trends in Mathematics 4,
DOI 10.1007/978-3-319-22129-8_9

various situations that have to be analysed in different intermediate reduced spaces. We achieve our study by considering all possible cases, constructing an adequate set of coordinates and computing the corresponding torsion in each case. Hence, our analysis is global and we characterise properly all type of bounded motions of the three particles (excluding triple collisions). In order to achieve the existence of the quasi-periodic motions we use a theorem by Han et al. [2] allowing us to handle the high-order degeneracy of the Hamiltonians involved in the process. The application of this theorem is not straightforward as one needs to bring the Hamiltonian to normal form through successive changes of symplectic coordinates and these transformations are rather cumbersome.

2 Reconstruction of the Full System

We reconstruct the rectilinear motions of the inner particles which are represented by elliptic relative equilibria of the reduced space, establishing the existence of KAM tori in the spatial 3-body problem. We characterise properly all type of bounded motions of the three particles, excluding triple collisions. In this sense our analysis, stated in Theorem 1, extends Zhao's results [6]. The proof will appear in [5].

Deprit's elements are used in Theorem 1. These coordinates were introduced by Deprit in [1] for eliminating two nodal angles in the N-body problem. In particular, ℓ_1 and ℓ_2 denote the mean anomalies of the inner and outer ellipses respectively, L_i is the conjugate momentum to ℓ_i ($i = 1, 2$) and C is the modulus of the total angular momentum vector.

Theorem 1 *The Hamiltonian system of the spatial 3-body problem, reduced by the symmetry of translations and defined in* $\mathcal{Q}_{\varepsilon,n} \subseteq T^*\mathbb{R}^6$ *(i.e., subset of* $\mathcal{P}_{\varepsilon,n}$ *where resonances between the mean anomalies are avoided), has invariant KAM* 5*-tori densely filled with quasi-periodic trajectories of the fictitious inner and outer bodies of the following types:*

(i) *The fictitious inner body moves in orbits nearly rectilinear, bounded and perpendicular to the invariable plane, whereas the outer body moves in a non-circular orbit lying near the invariable plane, and they are provided by* $L_1 \not\approx \sqrt{3/10}C$.

(ii) *The fictitious inner body moves in orbits nearly rectilinear, bounded and perpendicular to the invariable plane, whereas the outer body moves in a near-circular orbit lying near the invariable plane, which is not the horizontal plane.*

(iii) *The fictitious inner body moves in orbits nearly rectilinear, bounded and perpendicular to the invariable plane which is near the horizontal plane. The outer body moves in a near-circular orbit lying near the invariable plane, which is the horizontal plane.*

(iv) *The fictitious inner body moves in orbits nearly rectilinear, bounded and lying near the invariable plane, whereas the outer body moves in a non-circular orbit that lies near the invariable plane.*

For a given constant $0 < \delta < 1/5$*, the excluding measure for the existence of invariant* 5*-tori is of order* $\mathcal{O}(\varepsilon^{\delta/4})$.

References

1. A. Deprit, "Elimination of the nodes in problems of *N* bodies". *Celestial Mech.* **30** (1983), 181–195.
2. Y. Han, Y. Li, and Y. Yi, "Invariant tori in Hamiltonian systems with high order proper degeneracy". *Ann. Henri Poincaré* **10** (2010), 1419–1436.
3. J.F. Palacián, F. Sayas, and P. Yanguas, "Regular and singular reductions in the spatial three-body problem". *Qual. Theory Dyn. Syst.* **12** (2013), 143–182.
4. J.F. Palacián, F. Sayas, and P. Yanguas, "Flow reconstruction and invariant tori in the spatial three-body problem". *J. Differential Equations* **258**(6) (2015), 2114–2159.
5. J.F. Palacián, F. Sayas, and P. Yanguas, "Invariant tori of the spatial three-body problem reconstructed from relative equilibria of rectilinear type". *Submitted*.
6. Z. Lei, "Quasi-periodic almost-collision orbits in the spatial three-body problem". Commun. Pure Appl. Math. (2014). doi:10.1002/cpa.21539. ISSN 1097-0312. http://dx.doi.org/10.1002/cpa.21539
7. L. Zhao, "The Kustaanheimo-Stiefel regularization and the quadrupolar conjugacy". Regular Chaotic Dyn. **20**(1) (2015), 19–36. ISSN 1560-3547.

Generalized Discrete Nonlinear Schrödinger as a Normal Form at the Thermodynamic Limit for the Klein–Gordon Chain

Simone Paleari and Tiziano Penati

1 Motivations: The Problem

A still open challenge in Hamiltonian dynamics is the development of a perturbation theory for Hamiltonian systems with an arbitrarily large number of degrees of freedom and, in particular, in the thermodynamic limit. Indeed, motivated by the problems arising in the foundations of Statistical Mechanics, it is relevant to consider large systems (e.g., for a model of a crystal the number of particles should be of the order of the Avogadro number) with non vanishing energy per particle (which corresponds to a non zero temperature in the physical model).

Being interested in the low temperature regime (aiming for example at some rigorous results of the classical mechanics description of the behavior of the specific heats in such a regime), it is foreseeable the use of perturbation theory to exploit the presence of a small parameter like the specific energy. Unfortunately, it is a well known limit of the classical results of this theory (like KAM or Nekhoroshev theorem) to suffer a bad dependence on the number of degrees of freedom, often resulting in void or non applicable statements in the thermodynamic limit.

We present here some results, which can be considered to be among the first to (at least partially) accomplish the aforementioned goals, and some ideas for future developments.

S. Paleari (✉) • T. Penati
Dipartimento di Matematica, Università degli Studi di Milano, Milano, Italy
e-mail: simone.paleari@unimi.it

M. Corbera et al. (eds.), *Extended Abstracts Spring 2014*, Trends in Mathematics 4,
DOI 10.1007/978-3-319-22129-8_10

2 Recent Results: Extensive Adiabatic Invariant

To overcome the problem illustrated above, we exploited and implemented two kind of ideas. The first one, for which we give credit to Carati (see, e.g., [2]), is to give up controlling all the orbits in the phase space. Instead, we try to measure the set of initial data for which we are able to perform our construction and our estimates.

The second idea is to formalize and exploit some physical properties of the model at hand, in particular the system being extensive and the short range of interaction. We thus developed a perturbation construction adapted to preserve such properties, and then we exploited them also in the statistical part.

We consider a Klein–Gordon model as described by the following Hamiltonian

$$H(x,y) = \frac{1}{2}\sum_{j=1}^{N}\left[y_j^2 + x_j^2 + a(x_{j+1}-x_j)^2\right] + \frac{1}{4}\sum_{j=1}^{N} x_j^4\,, \qquad x_0 = x_N,\ y_0 = y_N, \tag{1}$$

i.e., a finite chain of N degrees of freedom and periodic boundary conditions.

Our construction of an extensive adiabatic invariant in the thermodynamic limit can be described as follows. Given a fixed and sufficiently small value of the coupling constant a, the evolution of the adiabatic invariant is controlled up to times scaling as $\beta^{1/a}$ for any large enough value of the inverse temperature β. The time scale becomes a stretched exponential if the coupling constant is allowed to vanish jointly with the specific energy. The adiabatic invariance is exhibited by showing that the variance along the dynamics, i.e., calculated with respect to time averages, is much smaller than the corresponding variance over the whole phase space, i.e., calculated with the Gibbs measure, for a set of initial data of large measure. All the perturbation constructions and the subsequent estimates are consistent with the extensive nature of the system.

To give a more precise statement, let us denote by dm the Gibbs measure and by Z the corresponding partition function, namely $dm(\beta,a) := e^{-\beta H(z,a)}/Z(\beta,a)dz$, and $Z(\beta,a) := \int_{\mathcal{M}} e^{-\beta H(z,a)}dz$; for every function $X\colon \mathcal{M} \to \mathbb{R}$ we denote its phase average and its variance respectively by $\langle X\rangle := \int_{\mathcal{M}} X dm(\beta,a)$ and $\sigma^2[X] := \langle X^2\rangle - \langle X\rangle^2$. For every measurable set $A \in \mathcal{M}$, we will denote $m(A) := \int_A dm(\beta,a)$. We also need to define the time average and the time variance, evaluated along the time evolution. Denoting by ϕ^t the Hamiltonian flow, we have $\overline{X}(z,t) := \frac{1}{t}\int_0^t (X\circ\phi^s)(z)ds$ and $\sigma_t^2[X] := \overline{X^2} - \overline{X}^2$.

Theorem 1 (Giorgilli et al. [7]) *There exist positive constants a^*, β_0, β_1, C_1 and C_2 such that, for all $0 < a < a^*$, given the integer $r := \left\lfloor C_1\sqrt{(1+2a)/a}\right\rfloor$,*

there exists an extensive polynomial Φ *of degree* $2r+2$*, such that, for all* $\beta > \max\{\beta_0, \beta_1 r^6\}$ *one has*

$$m\left(z \in \mathbb{R}^{2N} : \sigma_t^2[\Phi] \geq \frac{\sigma^2[\Phi]}{\sqrt{\beta}}\right) \leq \frac{C_2}{\beta}\left(\frac{t}{\bar{t}}\right)^2, \qquad \bar{t} = \beta^{r/2}.$$

The above result can be seen as an improvement over the previous paper by Carati and Maiocchi [3], where the perturbation parameter is the sum of the coupling a and the temperature $1/\beta$. We were able to made them independent from each other, so that one can fix the model (fix a) and let the temperature vanish. We also slightly improved, in an independent way, the statistical part.

Another result worth to be quoted is [11], where several adiabatic invariants are constructed for the Fermi–Pasta–Ulam model, though for short time scales.

3 GdNLS as an Extensive Normal Form

The natural step, after the direct construction of an approximated conserved quantity, is the construction of a normal form, which is a more versatile tool to investigate the dynamics. Further exploiting the extensive nature and the short range of interaction, in the limit of small couplings, and small (total or specific) energy, we constructed a high order resonant normal form with estimates uniform in the number of degrees of freedom.

Theorem 2 (Paleari and Penati [13]) *There exist* C_1 *and* C_2*, such that for every* N*, every small enough value of the coupling constant* a*, every integer* $r < C_1/a$*, and (total or specific) energy less than* C_2/r^2*, there exists an analytic canonical transformation, under which the Hamiltonian* (1) *takes the form*

$$H^{(r)} = H_\Omega + Z_0 + \cdots + Z_r + P^{(r+1)}, \qquad \{H_\Omega, Z_s\} = 0 \quad \forall s \in \{0, \ldots, r\},$$

with H_Ω *a system of* N *identical oscillators,* Z_s *homogeneous polynomials of order* $2s+2$*, and* $P^{(r+1)}$ *a remainder of order* $2r+4$ *and higher.*

In particular, the first order normal form is a generalized discrete nonlinear Schrödinger model, characterized by all-neighbors coupling with exponentially decaying strength. Indeed, in such a normal form we have a truncated expansion in (specific or total) energy, given by the index s, and an infinite expansion in the coupling, in each term Z_s; at every given order in such an expansion we have terms with coupling between sites at the corresponding distance. Using only the first term in both Z_0 and Z_1 we have exactly the usual dNLS.

A relevant point is that, due to this particular structure, such a normal form allows to postpone the problem of the double scaling in the two small parameters: it is possible to chose afterwards the regime, possibly discarding the tails in the Z_s.

Another important comment is that, since the normal form itself is a transformation of the Hamiltonian, it does not involve the dynamics in its formulation. And this is the reason for its validity at the thermodynamic limit without the use of the statistical argument. Of course, once we try to use it to control the dynamics, either we give measure estimates, or we revert to a small total energy regime. As in the next section.

3.1 An Application: Long Time Stability for a Breather

As a first application of our normal form, we showed a long time stability result for a Breather solution in KG model (actually a slightly more general one, also with nonlinear couplings). The idea is to exploit stability of the dNLS breathers, induced by the existence of the additional conserved quantity via variational methods. In this way we reproduce, and slightly improve a classical result by Bambusi [1] which was based on a different normal form construction. The model (a mixed FPU-KG one) is the following:

$$H(x,y) = \frac{1}{2}\sum_{j=1}^{N}\left[y_j^2 + x_j^2 + a(x_{j+1}-x_j)^2\right] + \frac{1}{4}\sum_{j=1}^{N}\left[x_j^4 + b(x_{j+1}-x_j)^4\right], \qquad (2)$$

with periodic boundary conditions $x_0 = x_N$, $y_0 = y_N$, where $a > 0$ and $b \geq 0$; fix also $c := \max\{a, b\}$. Let us denote by $\Psi_{a,b}$ and $\mathsf{O}(\Psi_{a,b})$ respectively the Breather profile, i.e., an initial datum, and its orbit for our model (2). Concerning $\Psi_{a,b}$, we require it to emerge, in the anticontinuous limit, from the one-site excitation with prescribed amplitude $\|\Psi_{0,0}\| = R/6$. Using the usual Hausdorff distance[1] d_H, we have

Theorem 3 (Paleari and Penati [14]) *Fix an arbitrary integer $r \geq 1$. Then there exists $R_*(r) < 1$ such that for all $R < R_*$ and $0 < \epsilon \ll R^2$ there exist $c_*(r, R, \epsilon)$ and $\delta(\epsilon)$, such that for all $c < c_*$ the (piece of) orbit $\mathsf{O}(\phi) := \{\phi(t) : |t| \leq \frac{\epsilon^2}{r^2}R^{-2(r+2)}, \phi(0) = \phi\}$, solution of (2), satisfies*

$$\|\phi - \Psi_{a,b}\| < \delta \quad \Longrightarrow \quad d_H\left(\mathsf{O}(\phi), \mathsf{O}(\Psi_{a,b})\right) < \epsilon. \qquad (3)$$

[1] Given A and B one has $d_H(A,B) := \max\{d(A,B), d(B,A)\}$, with $d(A,B) := \sup_{a\in A}\inf_{b\in B}\|a - b\|$.

3.2 Planned Investigations

Several other possible application of the normal form result exist, and we plan to investigate in (at least some of) the following directions.

Some work has been recently devoted to the study (see, e.g., [10, 15, 16]) of multibreathers, also with holes; it is feasible to use techniques like Krein signature to study the linear stability of such object in the GdNLS, and then transport the corresponding properties to the KG chain.

Another promising direction is that of the variational approximation techniques for an effective description of breathers-like solutions in the dNLS and some generalizations (see, e.g., [4, 5, 12]). Once again, it should be interesting to try to exploit the normal form to provide this kind of results in the KG models.

A further benefit of the normal form could be in better approximation results for the Cauchy problem, opposed to more traditional multiscale approaches.

We also plan possible extension of the normal form result in order to deal with infinite chains, or with model supporting (almost-)compact solutions (like in [6, 17, 18]) or model for granular chains (like those in [8, 9]).

References

1. D. Bambusi, "Exponential stability of breathers in Hamiltonian networks of weakly coupled oscillators". *Nonlinearity* **9** (1996), 433–457.
2. A. Carati, "An averaging theorem for Hamiltonian dynamical systems in the thermodynamic limit", *J. Stat. Phys.* **128** (2007), 1057–1077.
3. A. Carati and A.M. Maiocchi, "Exponentially long stability times for a nonlinear lattice in the thermodynamic limit". *Communications in Mathematical Physics* **314** (2012), 129–161.
4. C. Chong, R. Carretero-González, B.A. Malomed, and P.G. Kevrekidis, "Variational approximations in discrete nonlinear Schrödinger equations with next-nearest-neighbor couplings". *Phys. D* **240** (2011), 1205–1212.
5. C. Chong, D.E. Pelinovsky, and G. Schneider, "On the validity of the variational approximation in discrete nonlinear Schrödinger equations". *Phys. D* **241** (2012), 115–124.
6. M. Eleftheriou, B. Dey, and G.P. Tsironis, "Compactlike breathers: Bridging the continuous with the anticontinuous limit". *Phys. Rev. E* **62** (2000), 7540–7543.
7. A. Giorgilli, S. Paleari, and T. Penati, "An extensive adiabatic invariant for the Klein–Gordon model in the thermodynamic limit". *Ann. Henri Poincaré* **16**(4) (2015), 897–959.
8. G. James, "Periodic travelling waves and compactons in granular chains". *J. Nonlinear Sci.* **22** (2012), 813–848.
9. G. James, P.G. Kevrekidis, and J. Cuevas, "Breathers in oscillator chains with Hertzian interactions". *Physica D: Nonlinear Phenomena*, **251** (2013), 39–59.
10. V. Koukouloyannis and P.G. Kevrekidis, "On the stability of multibreathers in Klein–Gordon chains". *Nonlinearity* **22** (2009), 2269–2285.
11. A.M. Maiocchi, D. Bambusi, and A. Carati, "An averaging theorem for FPU in the thermodynamic limit". *J. Statist. Phys.* **155** (2014), 300–322.
12. B. Malomed and M.I. Weinstein, "Soliton dynamics in the discrete nonlinear Schrödinger equation". *Phys. Lett. A* **220** (1996), 91–96.
13. S. Paleari and T. Penati, "An extensive resonant normal form for an arbitrary large Klein-Gordon model". Annali di Matematica Pura ed Applicata (1923), 1–33.

14. S. Paleari and T. Penati, “Long time stability of small amplitude Breathers in a mixed FPU-KG model”. *Preprint* (2014). http://arxiv.org/abs/1405.7841.
15. D.E. Pelinovsky, P.G. Kevrekidis, and D.J. Frantzeskakis, “Stability of discrete solitons in nonlinear Schrödinger lattices”. *Phys. D* **212** (2005), 1–19.
16. D. Pelinovsky and A. Sakovich, “Multi-site breathers in Klein–Gordon lattices: stability, resonances and bifurcations”. *Nonlinearity* **25** (2012), 3423.
17. P. Rosenau and S. Schochet, “Compact and almost compact breathers: a bridge between an anharmonic lattice and its continuum limit”. *Chaos* **15** (2005), 015111.
18. P. Tchofo Dinda and M. Remoissenet, “Breather compactons in nonlinear Klein–Gordon systems”. *Phys. Rev. E* **60** (1999), 6218–6221.

Stability of Euler-Type Relative Equilibria in the Curved Three Body Problem

Ernesto Pérez-Chavela and Juan Manuel Sánchez Cerritos

1 Introduction

We consider three point particles of masses m_1, m_2, m_3 moving on a two-dimensional surface of constant curvature k. It is well known that, locally, these surfaces are characterized by the sign of the curvature k. If $k > 0$, the surface is the two dimensional sphere S^2 of radius $R = 1/k$ embedded in the Euclidian space $\mathbb{R}^3$. If $k = 0$, we recover the Euclidean space $\mathbb{R}^2$. And if $k < 0$, the surface is the upper part of the hyperboloid $x^2 + y^2 - z^2 = -1/(-k)^{1/2}$, known as the pseudo-sphere S_h^2 embedded in the three dimensional Minkowski space $\mathbb{R}^{2,1}$, corresponding to the Weierstrass model of hyperbolic geometry.

Let $q_i = (x_i, y_i, z_i)$, $i = 1, 2, 3$, be the position of the ith particle. The force function which extends the Newtonian one to S^2 or S_h^2 is given by

$$U(q) = \sum_{i=1}^{3} \sum_{j=1, j\neq i}^{3} \frac{m_i m_j (\sigma)^{1/2} q_i * q_j}{\sqrt{\sigma - \sigma \left(q_i * q_j\right)^2}}, \tag{1}$$

where $(*)$ denotes the classical scalar product if the curvature is positive, or the Lorentz product in the case of negative curvature. In the same way, the symbol σ stands for $\sigma = 1$ if we consider $k > 0$, and $\sigma = -1$ for $k < 0$.

E. Pérez-Chavela (✉) • J.M.S. Cerritos
Departamento de Matemáticas, UAM-Iztapalapa, México, D.F., México
e-mail: epc@xanum.uam.mx; sanchezj01@gmail.com

M. Corbera et al. (eds.), *Extended Abstracts Spring 2014*, Trends in Mathematics 4,
DOI 10.1007/978-3-319-22129-8_11

Using a variational method with constrains to maintain the particles on the respective surface, we can write the equations of motion as follows

$$\ddot{q}_i = \sum_{j\neq i}^{3} \frac{m_j[q_j - \sigma(q_i * q_j)q_i]}{[\sigma - \sigma(q_i * q_j)^2]^{3/2}} - \sigma(\dot{q}_i * \dot{q}_i)q_i, \quad i = 1, 2, \ldots, n, \tag{2}$$

where ($\dot{}$) represents the differentiation with respect to the time t. The curved problem has energy and angular momentum as first integrals, the centre of mass is no longer an integral in contrast with the Euclidean case.

In this work we are interested in the linear spectral stability of a particular kind of periodic solutions know as relative equilibria.

Definition 1 A relative equilibrium is a solution of the curved n-body problem in which the mutual distances between particles are constant in time.

In the curved three body problem for $k \neq 0$ we have two different types of relative equilibria, the Lagrangian ones, which a difference of the Euclidean case only exist if the three masses are equal [3], the stability of this kind of equilateral relative equilibria has been wide studied by Martínez and Simó in [5]. The other type of relative equilibria are the so called *Eulerian-type relative equilibrium*, that is a relative equilibrium in which the particles are for all time t on a same geodesic of the corresponding surface. We will be focused on the linear spectral stability of an especial type of Eulerian relative equilibria, that by short we will call isosceles Eulerian relative equilibria, where the three particles are on the same geodesic, the masses at the ends are equal and the mass between them is arbitrary, the geodesic distance between the central mass and each mass at the ends is equal, by short along this work we will call them as Eulerian relative equilibria [4]. In the proofs of the main results we use the same kind of ideas than in [5].

Since we always can map a geodesic into other geodesic, we will assume without loss of generality that m_1 is the particle in the middle located at the point $(0, 0, 1)$, and the other two equal masses m_2 and m_3 are at the opposite ends of a diameter on the circle determined by z_i being constant, $i = 1, 2$.

2 The Positive Curvature Case

In [3], Diacu et al. find the value of the angular velocity ω allowing to obtain the Eulerian relative equilibrium of the three body problem on S^2. To achieve our goal we consider a time transformation and position coordinates $Q_i = (X_i, Y_i)$ in the following way

$$\begin{aligned} t &= r^{\frac{3}{2}}\tau, \\ x_i &= rX_i, \quad y_i = rY_i, \\ Q_i &= (X_i, Y_i). \end{aligned} \tag{3}$$

With these changes, the angular velocity ω found in [3] becomes

$$\Omega^2 = \frac{M + 4m(1 - r^2)}{4(1 - r^2)^{\frac{3}{2}}}, \tag{4}$$

where M is the fixed mass at the north pole and m denotes the value of the masses on the circle of radius r. With the above expressions we are able to express the system in a rotating frame, defining new variables (ξ_i, η_i), $i = 1, 2, 3$, as

$$\begin{pmatrix} X_i \\ Y_i \end{pmatrix} = R(\Omega\tau) \begin{pmatrix} \xi_i \\ \eta_i \end{pmatrix}, \tag{5}$$

where

$$R(\Omega\tau) = \begin{pmatrix} \cos\Omega\tau & -\sin\Omega\tau \\ \sin\Omega\tau & \cos\Omega\tau \end{pmatrix}. \tag{6}$$

After a straightforward computation it is possible to show that the new equations of motion are the following

$$\begin{pmatrix} \xi_i'' \\ \eta_i'' \end{pmatrix} = 2\Omega \begin{pmatrix} \eta_i' \\ -\xi_i' \end{pmatrix} + \Omega^2 \begin{pmatrix} \xi_i \\ \eta_i \end{pmatrix} - r^2 h_i \begin{pmatrix} \xi_i \\ \eta_i \end{pmatrix}$$

$$+ \sum_{j=1, j\neq i}^{3} m_j \left[\xi_i^2 + \eta_i^2 + \xi_j^2 + \eta_j^2 - 2(\xi_i\xi_j + \eta_i\eta_j)T_{i,j}\right.$$

$$\left. - r^2((\xi_i\xi_j + \eta_i\eta_j)^2 + (\xi_i^2 + \eta_i^2)(\xi_j^2 + \eta_j^2))\right]^{-3/2} \left[\begin{pmatrix} \xi_j \\ \eta_j \end{pmatrix} - \left(r^2(\xi_i\xi_j + \eta_i\eta_j)\right.\right.$$

$$\left.\left. + \sqrt{(1 - r^2(\xi_i^2 + \eta_i^2))(1 - r^2(\xi_j^2 + \eta_j^2))}\right) \begin{pmatrix} \xi_i \\ \eta_i \end{pmatrix}\right],$$

where

$$h_i = \Omega^2(\xi_i^2 + \eta_i^2) + 2\Omega(\xi_i\eta_i' - \eta_i\xi_i') + ((\xi_i'^2) + (\eta_i'^2)) + \frac{r^2}{1 - r^2(\xi_i^2 + \eta_i^2)}(\xi_i\xi_i' + \eta_i\eta_i')^2,$$

and

$$T_{i,j} = \sqrt{(1 - r^2(\xi_i^2 + \eta_i^2))(1 - r^2(\xi_j^2 + \eta_j^2))},$$

for $i = 1, 2, 3$.

The main result for the stability of the Eulerian relative equilibria is the following:

Theorem 2 *Consider Eulerian-relative equilibria of three masses moving on S^2, where m_1 is fixed at $(0, 0, 1)$, m_2 and m_3 are at opposite ends of a diameter on a circle with constant z. Then,*

(i) *if $m_1 = m_2 = m_3$ and $z \in (-1/2, 1) \setminus 0$, the generated orbits are unstable, and the motion is not possible if $z \in (-1, -1/2)$;*
(ii) *if m_1 is negligible and $m_2 = m_3$, the generated orbits are unstable for every $z \in (0, 1)$, and the motion is not possible if $z \in (-1, 0)$;*
(iii) *if m_2 and m_3 are negligible, the generated orbits are stable if $z \in (0, 1)$, and the motion is not possible if $z \in (-1, 0)$.*

Sketch of the Proof The idea is the classical one for studying stability, we must find the matrix associated to the linearization of the equations of motion at the equilibrium point in a rotating frame. The size of the corresponding matrix is 12×12, which makes the computations of the roots of the corresponding characteristic polynomial difficult. We have introduced a new change of variables and we have applied Descartes rule of signs to obtain the results. □

3 The Negative Curvature Case

Here we have three independent groups of isometries acting on the pseudo-sphere S^2_h, then a priori we can have three different kind of relative equilibria, elliptic, parabolic and hyperbolic [6]. In [1, 2] the authors prove that there are not relative equilibria of parabolic type.

For the case of elliptic relative equilibria, we analyze the motions which are invariant through the isometric group generated by the matrix

$$A(\omega\tau) = \begin{pmatrix} \cos\omega\tau & -\sin\omega\tau & 0 \\ \sin\omega\tau & \cos\omega\tau & 0 \\ 0 & 0 & 1 \end{pmatrix}.$$

The main result in this case is the following.

Theorem 3 *Consider an Eulerian relative equilibria of three masses of elliptic type on S^2_h, where m_1 is fixed at $(0, 0, 1)$ and m_2 and m_3 are located at opposite ends of a diameter on a circle with z constant. Then,*

(i) *if $m_1 = m_2 = m_3$ the generated orbits are unstable for every $z > 1$;*
(ii) *if m_1 is negligible, and $m_2 = m_3$, the generated orbits are unstable for every $z \in (1, \infty)$;*
(iii) *if m_2 and m_3 are negligible, then the generated orbits are stable if $z \in (1, \infty)$.*

For the case of hyperbolic relative equilibria we analyze the motions which are invariant through the isometric group generated by the matrix

$$H(\omega\tau) = \begin{pmatrix} 1 & 0 & 0 \\ 0 & \cosh\omega\tau & \sinh\omega\tau \\ 0 & \sinh\omega\tau & \cosh\omega\tau \end{pmatrix}.$$

The main result in this case is the following.

Theorem 4 *Consider an Eulerian-relative equilibrium of hyperbolic type for the curved three body problem on S^2_h, where the body m_i has coordinates $q_i = (x_i, y_i, z_i)$. If m_3 is negligible, and is on the geodesic passing through $(0, 0, 1)$ with $x_3 = 0$, and m_1 and m_2 are on hyperbolas of the form $x_1 = k \neq 0$, $x_2 = -x_1$, $y_1 = y_2 = r\sinh(t)$, $z_1 = z_2 = r\cosh(t)$, $t \in \mathbb{R}$, then the generated orbits are unstable for any $r > 1$.*

Acknowledgements This research in progress has been done during 1 month visit of the first author to CRM, thanks for the hospitality. The authors has been partially supported by Conacyt-México, grant 128790.

References

1. F. Diacu and E. Pérez-Chavela, "Homographic solutions of the curved 3-body problem". *J. of Differential Equations* **250** (2011), 340–366.
2. F. Diacu, E. Pérez-Chavela, and J.G. Reyes, "An intrinsic approach in the curved *n*-body problem. The negative case". *Journal of Differential Equations*, **252** (2012), 4529–4562.
3. F. Diacu, E. Pérez-Chavela, and M. Santoprete, "The *n*-body problem in spaces of constant curvature. Part I: relative equilibria". *J. Nonlinear Sci.* **22** (2012), 247–266.
4. F. Diacu, E. Pérez-Chavela, and M. Santoprete, "The *n*-body problem in spaces of constant curvature. Part II: singularities". *J. Nonlinear Sci.* **22** (2012), 267–275.
5. R. Martínez and C. Simó, "On the stability of the Lagrangian homographic solutions in a curved three-body problem on S^2". *Discrete Contin. Dyn. Syst. Ser. A* **33** (2013), 1157–1175.
6. E. Pérez-Chavela and J.G. Reyes-Victoria, "An intrinsic approach in the curved *n*-body problem. The positive curvature case". *Transactions of the American Math Society* **364** (2012), 3805–3827.

Two-Dimensional Symplectic Return Maps and Applications

Regina Martínez and Carles Simó

The goal of this extended abstract is to show how return maps, even in simple cases, can provide accurate information in some dynamical aspects.

We restrict our attention to 2D symplectic maps, despite many ideas are useful in wider contexts; see, e.g., [1, 3, 6]. Those maps can appear as discrete models of a conservative, area-preserving, systems or as Poincaré maps of some Hamiltonian system with two degrees of freedom (dof). To present the problem we describe next the setting, illustrated by the plots in Fig. 1.

Assume that a 2D symplectic map F has a hyperbolic fixed point, H, which in the 2 dof Hamiltonian case comes from a periodic hyperbolic orbit. Assume also that both branches of the unstable and stable manifolds of H ($W^{u,s,\pm}$ in Fig. 1, left) intersect transversally giving rise to homoclinic points like h_1 and h_3 whose images under F are, respectively, h_2 and h_4. A similar behaviour can be found in the case that F has two hyperbolic fixed points, $H_\pm$, with transversal heteroclinic points (Fig. 1, middle).

If the map F belongs to a family of maps, F_ε, it can happen that in the left plot $W^{u,+}$ and $W^{s,+}$ (and also $W^{u,-}$ and $W^{s,-}$) tend to coincide when $\varepsilon \to 0$. In an analogous way in the middle plot $W^{u,+}$ and $W^{s,-}$ (and also $W^{u,-}$ and $W^{s,+}$) can tend to coincide. In the homoclinic case one would obtain the integrable dynamics shown in the right plot. Under suitable conditions it turns out to be the flow time τ, φ_τ (eventually $\tau = \tau(\varepsilon)$) of a 1 dof Hamiltonian $\mathcal{H}$. The integrable limit is easy to imagine in the heteroclinic case and we skip it.

R. Martínez (✉)
Departament de Matemàtiques, Universitat Autònoma de Barcelona, Bellaterra, Barcelona, Spain
e-mail: reginamb@mat.uab.cat

C. Simó
Departament de Matemàtica Aplicada i Anàlisi, Universitat de Barcelona, Barcelona, Spain
e-mail: carles@maia.ub.es

M. Corbera et al. (eds.), *Extended Abstracts Spring 2014*, Trends in Mathematics 4,
DOI 10.1007/978-3-319-22129-8_12

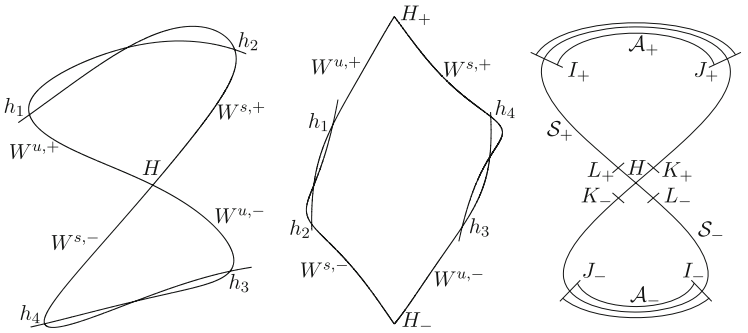

Fig. 1 Models for the homoclinic (*left*) and double heteroclinic (*middle*) connections giving rise to return maps. The *right* plot shows the integrable homoclinic case. See text for detailed explanation

In the integrable case (right plot) $W^{u,+}$ and $W^{s,+}$ (resp. $W^{u,-}$ and $W^{s,-}$) coincide and give rise to the separatrix $\mathcal{S}_+$ (resp. $\mathcal{S}_-$). One can define two domains $\mathcal{A}_\pm$ around $\mathcal{S}_\pm$, limited by levels of the energy, $\mathcal{H}$, assumed to be zero on $\mathcal{S}_\pm$, > 0 (resp. < 0) inside (resp. outside) the loops, and segments I_+ and $J_+ = \varphi_\tau(I_+)$ (resp. I_- and $J_- = \varphi_\tau(I_-)$). Taking a point in $\mathcal{A} = \mathcal{A}_+ \cup \mathcal{A}_-$ the *return map* describes the first return to $\mathcal{A}$ by iteration under φ_τ. It is clear that the upper (resp. lower) part of $\mathcal{A}_+$ (resp. of $\mathcal{A}_-$) returns to $\mathcal{A}_-$ (resp. to $\mathcal{A}_+$) and the lower part of $\mathcal{A}_+$ (resp. upper of $\mathcal{A}_-$) returns to $\mathcal{A}_+$ (resp. to $\mathcal{A}_-$). Suitable variables in $\mathcal{A}$ are some time t that we can assume to be in $[0, 2\pi)$ (it is not restrictive to assume $\tau = 2\pi$ by scaling $\mathcal{H}$) taking the value 0 at I_+ and at I_-, the energy level h and a sign $\pm$ to specify the domain $\mathcal{A}_\pm$. The return map, as associated to dynamics close to separatrices is known as *separatrix map*. In the integrable case all the points in $\mathcal{A} \setminus \mathcal{S}_\pm$ are periodic. The period T depends on the location of the initial point, either T_+, T_- or $T_\pm$ and in all cases is of the form $T(h, \varepsilon) = |\log(|h|)|/\gamma + c_0 + \mathcal{O}(h, \varepsilon)$, where γ (eventually $\gamma(\varepsilon)$) denotes the dominant eigenvalue of the map at H, c_0 is related to the passage time from L_+ to I_+ then to J_+ and return to K_+ (in the case of T_+, similar in other cases). Hence, the separatrix map is given, in the integrable case, by

$$SepM_I : \begin{pmatrix} t \\ h \end{pmatrix} \to \begin{pmatrix} \bar{t} = t - T(\bar{h}, \varepsilon) \,(\mathrm{mod}\, 2\pi) \\ \bar{h} = h \end{pmatrix}. \tag{1}$$

To define *SepM* in cases like the left plot in Fig. 1 one has to take into account that the energy is not preserved, due to the *splitting* of the separatrices. It can be measured using the energy (or suitable definitions of stable/unstable energies, see, e.g., [5, 15]). Let $a(\varepsilon)\,\xi(t)$ be the position, in energy, of W^u wrt W^s in $\mathcal{A}$ (or in $\mathcal{A}_+$ or in $\mathcal{A}_-$). The value $a(\varepsilon)$ measures the amplitude of the splitting and $\xi(t)$ is a normalized shape. Then,

$$SepM : \begin{pmatrix} t \\ h \end{pmatrix} \to \begin{pmatrix} \bar{t} = t - T(\bar{h}, \varepsilon) \,(\mathrm{mod}\, 2\pi) \\ \bar{h} = h + a(\varepsilon)\xi(t) \end{pmatrix}. \tag{2}$$

For the *classical* and very popular separatrix map (see, e.g., [4]) one takes $\xi(t) = \sin(t)$.

The maps (1) and (2) are not defined in $W^{s\pm}$. One can confine attention only to $\mathcal{A}_+$ or to $\mathcal{A}_-$. The upper and lower loops can be symmetric or not, or have additional symmetries. In the heteroclinic case (middle plot in Fig. 1), with I_+, J_+, I_-, J_- containing h_1, h_2, h_3, h_4, respectively, the separatrix map goes from $\mathcal{A}_+$ to $\mathcal{A}_-$ and from $\mathcal{A}_-$ to $\mathcal{A}_+$. It is not defined also if a point in $\mathcal{A}_+$ is to the left of $W^{s,-}$ and so on. The times of passage near H_+ or near H_- can also have different expressions. In case of symmetry just the same expression can be used for $\mathcal{A}_+ \mapsto \mathcal{A}_-$ and for $\mathcal{A}_- \mapsto \mathcal{A}_+$.

If the map family F_ε comes from a 2π periodic perturbation with size ε of a 1 dof Hamiltonian then, typically, one has $a(\varepsilon) = \mathcal{O}(\varepsilon)$. If the map family F_ε is an $\mathcal{O}(\varepsilon)$ perturbation of the identity, then the usual suspension+averaging techniques [2, 12, 13] combined with analyticity properties and suitable parametrization [5] give exponentially small upper bounds, typically of the form $a(\varepsilon) = A\varepsilon^B \exp(-c/\gamma(\varepsilon))(1 + \mathcal{O}(\varepsilon))$, $A > 0$, $c > 0$.

In turn the map in (2) can be approximated around $h = h_0 > 0$, if $h_0 \geq a(\varepsilon)/\gamma(\varepsilon)$, by a *standard* map (in the case $\xi(t) = \sin(t)$ by the classical standard map [4])

$$SM_\kappa : \begin{pmatrix} u \\ v \end{pmatrix} \to \begin{pmatrix} \bar{u} = u + \bar{v} \\ \bar{v} = v + \kappa\xi(u) \end{pmatrix}, \tag{3}$$

where $\kappa = a(\varepsilon)/(h_0\gamma(\varepsilon))$. If $\xi(t) = \sin(t)$ for $\kappa > \kappa_G \approx 0.971635406$ (Greene's value [7]) SM_κ has no rotational invariant curves and the dynamics has an important chaotic part. Hence, chaos is mainly present for values $h_0 < a(\varepsilon)/(\kappa_G\gamma(\varepsilon))$ for (3). See [14] for different applications to measure the amount of chaos. To this end, one requires to introduce a *chaotic factor*, which gives an average, wrt h, of the amount of chaos for the related values of κ; see [8] for details. In the same reference there is an analysis of the changes to be introduced, both on the equivalent to Greene's value and in the chaotic factor, in the case that $\xi(t)$ includes also the effect of a second harmonic.

It is clear that for return maps of the separatrix type both the return period and the size/shape of the splitting play a key role. For applications to several problems, specially in Celestial Mechanics, it is necessary to consider the case in which points like H or $H_\pm$ are no longer hyperbolic, but parabolic with stable and unstable manifolds (at least with one branch of each type, as shown in Fig. 1, middle plot).

In a general context, near a fixed point (q, p) at $(0, 0)$ one can consider, normalizing constants,

$$-h = p^{2l} - q^k, \quad p' = q^r, \quad l, k, r \in \mathbb{N}, \quad q \geq 0, \tag{4}$$

as dominant terms, so that on $h = 0$ the unstable (stable) manifold starts as $p = \pm q^{k/(2l)}$ (defined only for $q \geq 0$ is k is odd). The relevant parameter is $m = 2lr - k$.

It is positive in the parabolic case and the case $m = 0$ can be seen, in some sense, as hyperbolic. Furthermore, the case $m < 0$ can be named super-hyperbolic. In all these cases it is possible to produce a unified study and to derive the related separatrix maps, as a function of h and the splitting, see [8].

As an application we consider the Sitnikov problem, which describes the motion of a massless particle moving on the z-axis under the gravitational attraction of two bodies of mass 1/2 which move on the (x, y)-plane in elliptic orbits of eccentricity ε and centre of masses at $(0, 0, 0)$, see [10, 11, 16]. The motion equations are

$$\ddot{z} = -\frac{z}{(z^2 + r(t)^2/4)^{3/2}}, \quad r(t) = 1-\varepsilon\cos(E), \quad t = E-\varepsilon\sin(E) \text{ (Kepler)}, \tag{5}$$

being E the eccentric anomaly. System (5) is integrable for $\varepsilon = 0$ with energy levels $\frac{1}{2}v^2 - (z^2 + 1/4)^{-1/2}$ =constant, being $v = \dot{z}$. One can use $\Sigma = \{z = 0\}$ as Poincaré section and $(\hat{v}, E)$ as variables on it, being $\hat{v} = |v|(1-\varepsilon\cos(E))^{1/2}$, taking into account symmetries. The orbits are bounded for $\varepsilon = 0$ if they intersect Σ with $|v| < 2$.

There exist periodic orbits at infinity, which are parabolic in the Dynamical Systems sense. They have weak hyperbolicity and have invariant manifolds which can be studied in McGehee's coordinates, $z = 2/q^2$, $\dot{z} = -p$; see [10]. For $\varepsilon = 0$ the passage through $E = 0$ gives an integrable version of the middle plot in Fig. 1. For $\varepsilon \neq 0$ these manifolds intersect transversally [11]. They are of class Gevrey 1/3 around $(q, p) = (0, 0)$, $q \geq 0$; see [9]. According to [11], the splitting measured as energy variation in Σ is $\varepsilon A \sin(E) + \mathcal{O}(\varepsilon^2)$, where A is given by an explicit integral. See [8] for details. In the same reference one can find the proofs of the following results.

Lemma 1 *Sitnikov's problem fits in the setting of* (4) *with* $l = 1$, $k = 2$, $r = 4$ *and the passage time from* Σ *to* Σ *is* $T(h, \varepsilon) = \pi\sqrt{2}|h|^{-3/2} + c_0 + \mathcal{O}(h, \varepsilon)$.

Using this lemma, the related separatrix map using the splitting value, the passage to (3) and Greene's value, one has

Theorem 2 *For Sitnikov's problem and small eccentricity, there are invariant curves up to a distance of* $|v| = 2$ *given by*

$$\Delta v = \frac{1}{2}\left(\frac{6\pi A}{\kappa_G\sqrt{2}}\right)^{2/5}\varepsilon^{2/5} + \mathcal{O}(\varepsilon^{4/5}).$$

Using numerical values for the constants in the previous bound, one obtains $\Delta v \approx 0.82333\varepsilon^{2/5} + \mathcal{O}(\varepsilon^{4/5})$, in very good agreement with direct numerical estimates for $\varepsilon < \varepsilon_0 \approx 0.02$. See again [8] for details.

Acknowledgements This work has been supported by grants MTM2010-16425 (Spain) and 2009 SGR 67 (Catalonia). The second author is indebted to the Centre de Recerca Matemàtica (CRM), where he was staying during the preparation of this note.

References

1. M. Bosch and C. Simó, "Attractors in a Silnikov–Hopf scenario and a related one-dimensional map". *Physica D* **62** (1993), 217–229.
2. H. Broer, R. Roussarie, and C. Simó, "Invariant circles in the Bogdanov–Takens diffeomorphisms". *Ergodic Theory and Dynamical Systems* **16** (1996), 1147–1172.
3. H. Broer, C. Simó, and J.C. Tatjer, "Towards global models near homoclinic tangencies of dissipative diffeomorphisms". *Nonlinearity* **11** (1998), 667–770.
4. B.V. Chirikov, "A universal instability of many-dimensional oscillator systems". *Phys. Rep.* **52** (1979), 264–379.
5. E. Fontich and C. Simó, "The splitting of separatrices for analytic diffeomorphisms". *Ergod. Th. and Dynam. Sys.* **10** (1990), 295–318.
6. S.V. Gonchenko, C. Simó, and A. Vieiro, "Richness of dynamics and global bifurcations in systems with a homoclinic figure-eight". *Nonlinearity* **26** (2013), 621–678.
7. J.M. Greene, "A method for determining stochastic transition". *J. Math. Phys.* **6** (1979), 1183–1201.
8. R. Martínez and C. Simó, "Return maps, dynamical consequences and applications". *In preparation*.
9. R. Martínez and C. Simó, "Regularity of the infinity manifolds and global dynamics in the Sitnikov problem". *In preparation*.
10. R. McGehee, "A stable manifold theorem for degenerate fixed points with applications to Celestial Mechanics". *J. of Differential Equations* **14** (1973), 70–88.
11. J. Moser, "Stable and Random Motions in Dynamical Systems". *Annals of Mathematics Studies*, Princeton Univ. Press 1973.
12. A.I. Neishtadt, "The separation of motions in systems with rapidly rotating phase". *Prikladnaja Matematika i Mekhanika* **48** (1984), 133–139.
13. C. Simó, "Averaging under fast quasiperiodic forcing", in J. Seimenis, editor, "Hamiltonian Mechanics: Integrability and Chaotic Behaviour", *NATO Adv. Sci. Inst. Ser. B Phys.* **331**, 13–34.
14. C. Simó, "Measuring the total amount of chaos in some Hamiltonian systems". *Discrete and Continuous Dynamical Systems A* **34** (2014), 5135–5164.
15. C. Simó and D. Treschev, "Stability islands in the vicinity of separatrices of near-integrable symplectic maps". *Discrete and Continuous Dynamical Systems B* **10** (2008), 681–698.
16. K.A. Sitnikov, "The existence of oscillatory motions in the three-body problems". *Soviet Physics Doklady* **5**, 647–650 (1960).

Central Configurations of an Isosceles Trapezoidal Five-Body Problem

Abdulrehman Kashif, Muhammad Shoaib, and Anoop Sivasankaran

1 Introduction

The study of central configurations is very popular for producing the simplest solutions of the planar n-body problems (cf., [1, 2, 4]). In this paper, we study the central configuration of the isosceles trapezoidal five-body problem where four of the masses are placed at the vertices of the isosceles trapezoid and the fifth body can take various positions on the axis of symmetry. We identify regions in the phase space where it is possible to choose positive masses which will make the configuration central. A similar approach was adopted by Shoaib et al. in [3] for the rhomboidal five-body problem.

2 General Equations

The condition that $(m_1, m_2, \ldots, m_n)$ form a planar, non-collinear, central configuration is equivalent to

$$f_{ij} = \sum_{k=1, k\neq i,j}^{n} m_k (R_{ik} - R_{jk}) \Delta_{ijk} = 0, \tag{1}$$

A. Kashif (✉) • M. Shoaib
Department of Mathematics, University of Hail, Hail, Saudi Arabia
e-mail: kashmology@gmail.com; safridi@gmail.com

A. Sivasankaran
Department of Applied Mathematics and Sciences, Khalifa University of Science Technology and Research, Sharjah, UAE
e-mail: anooppgd@gmail.com

M. Corbera et al. (eds.), *Extended Abstracts Spring 2014*, Trends in Mathematics 4,
DOI 10.1007/978-3-319-22129-8_13

where $R_{ij} = 1/r_{ij}^3$ and $\Delta_{ijk} = (r_i - r_j) \wedge (r_i - r_k)$, see [1]. Let us consider five bodies of masses m_1, m_2, m_3, m_4 and m_5. The mass m_2 is on the line of symmetry. The remaining four bodies are placed at the vertices of an isosceles trapezoid. We choose the coordinates for the five bodies as follows:

$$\mathbf{r}_1 = (-1, 0),\ \mathbf{r}_2 = (0, -w),\ \mathbf{r}_3 = (1, 0),\ \mathbf{r}_4 = (-t, t),\ \text{and}\ \mathbf{r}_5 = (t, t). \tag{2}$$

Due to the inherent symmetries of the trapezoidal five-body model we get the following four equations from Eq. (1), which define the central configurations for the model described above:

$$f_{14} = m_1 h_{11} + m_2 h_{12} + m_4 h_{13} = 0, \qquad f_{15} = m_1 h_{21} + m_2 h_{22} + m_4 h_{23} = 0, \tag{3}$$

$$f_{12} = m_1 h_{31} + m_4 h_{33} = 0, \qquad f_{24} = m_1 h_{41} + m_4 h_{43} = 0, \tag{4}$$

where

$$\begin{aligned}
h_{11} &= (R_{13} - R_{15})\Delta_{143},\ h_{12} = (R_{24} - R_{12})\Delta_{124}, h_{13} = (R_{15} - R_{45})\Delta_{145},\\
h_{21} &= (R_{13} - R_{14})\Delta_{143},\ h_{22} = (R_{24} - R_{12})\Delta_{125}, h_{23} = (R_{45} - R_{14})\Delta_{145},\\
h_{31} &= (R_{13} - R_{12})\Delta_{123}, h_{33} = (R_{14} - R_{24})\Delta_{124} + (R_{15} - R_{24})\Delta_{125},\\
h_{41} &= (R_{12} - R_{14})\Delta_{124} + (R_{23} - R_{34})\Delta_{243},\ h_{43} = (R_{24} - R_{45})\Delta_{245},\\
R_{12} &= R_{23} = (1 + w^2)^{-\frac{3}{2}}, 8R_{13} = 1, R_{14} = R_{35} = ((1 - t)^2 + t^2)^{-\frac{3}{2}},\\
R_{15} &= R_{34} = ((1 + t)^2 + t^2)^{-\frac{3}{2}}, R_{24} = R_{25} = ((t + w)^2 + t^2)^{-\frac{3}{2}}, 8R_{45} = t^{-3},\\
\Delta_{124} &= \Delta_{235} = (t + w(1 - t)), \Delta_{125} = \Delta_{234} = (t + w(1 + t)),\\
\Delta_{145} &= \Delta_{345} = -2t^2, \Delta_{245} = -2t(t + w), \Delta_{123} = 2w.
\end{aligned}$$

After writing Eqs. (3) and (4) in matrix form, and after a number of row operations, we are left with a system of three equations which gives the following values of $\mu_1 = m_1/m_4$, and $\mu_2 = m_2/m_4$ and the geometric constraint C:

$$\mu_1 = -\frac{h_{43}}{h_{41}}; \qquad \mu_2 = \frac{h_{21}h_{43} - h_{23}h_{41}}{h_{41}h_{22}} = \frac{N_{\mu_2}}{D_{\mu_2}}, \tag{5}$$

$$C = h_{31}h_{43} - h_{41}h_{33} = 0. \tag{6}$$

3 Trapezoidal Five-Body Central Configurations

Theorem 1 *Let* $\vec{r} = (\mathbf{r}_1, \mathbf{r}_2, \mathbf{r}_3, \mathbf{r}_4, \mathbf{r}_5)$ *be a non-collinear configuration with a positive mass vector* $(m_1, m_2, m_3, m_4, m_5)$*. Then,*

(i) *there is a region* R_{μ_1} *given by* (9) *in the tw-plane, such that for any* $(t, w) \in R_{\mu_1} \exists \mu_1 > 0$ *making* $\vec{r}$ *a central configuration;*
(ii) *there is a region* R_{μ_2} *given by* (10) *in the tw-plane, such that for any* $(t, w) \in R_{\mu_2} \exists \mu_2 > 0$ *making* $\vec{r}$ *a central configuration;*
(iii) *there is a region R in the tw-plane, such that for any* $(t, w) \in R \exists \mu_1 > 0$, $\mu_2 > 0$ *making* $\vec{r}$ *a central configuration subject to the constraint* $C = 0$*.*

No central configurations are possible in the complement R_{μ_1}, R_{μ_2} *and R. Numerically,* R_{μ_1}, R_{μ_2} *and R are given in Figs. 1 and 2.*

3.1 *Proof of Theorem 1(i)*

To find the central configuration region where μ_1 is positive, we will need to find regions in the *tw*-plane where h_{43} and h_{41} have opposite signs. Note that

$$h_{43} = 2t(t+w)\left(\frac{1}{8t^3} - \frac{1}{(t^2 + (t+w)^2)^{3/2}}\right) < 0$$

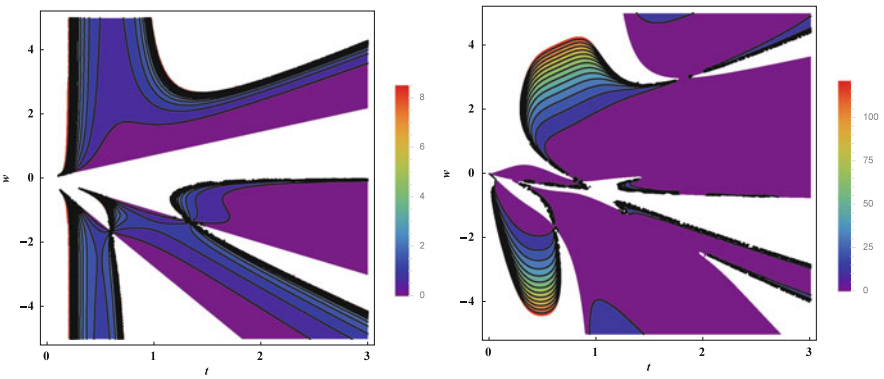

Fig. 1 Central configuration region. *Left:* for $\mu_1 > 0$; *right:* for $\mu_2 > 0$

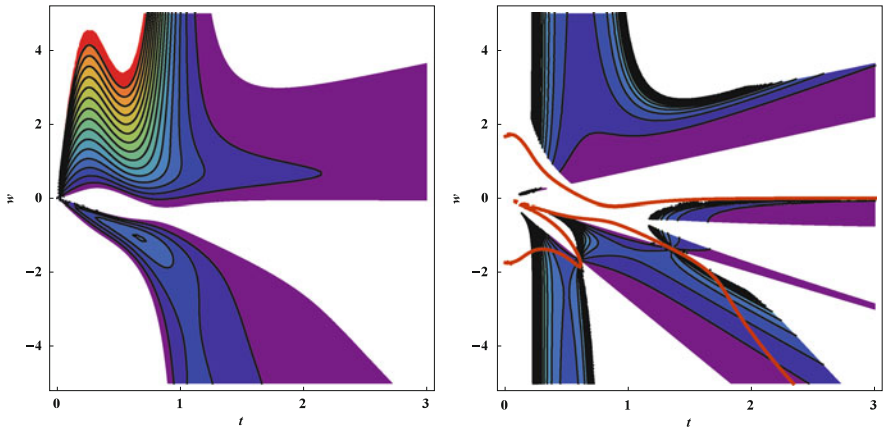

Fig. 2 *Left*: region $R_{N\mu_2}$ (*shaded*); *right*: central configuration region $R = R_{\mu_1} \cap R_{\mu 2}$ (*shaded*) where both μ_1 and μ_2 are positive. The *bold line* correspond to $C = 0$

when both of its factors have opposite sign. This is satisfied in the following region of the *tw*-plane:

$$R^{-}_{h_{43}} = \Big\{(t,w) \mid \Big(w \le 0 \wedge \Big(0 < t < 0.5(\sqrt{3}|w| + w) \vee t > -w\Big)\Big) \\ \vee \Big(w > 0 \wedge t > 0.5(\sqrt{3}|w| + w)\Big)\Big\}. \tag{7}$$

In the complement of $R^{-}_{h_{43}}$, we have $h_{43} > 0$. The denominator of μ_1 (i.e., h_{41}) can be written as

$$h_{41} = ((1-t)w + t)\left(\left(w^2+1\right)^{-3/2} - \left(t^2 + (1-t)^2\right)^{-3/2}\right) \\ + ((t+1)w + t)\left(\left(t^2 + (t+1)^2\right)^{-3/2} - \left(w^2+1\right)^{-3/2}\right).$$

As h_{41} is a sum of two non-linear functions of t and w, we have to use some approximation techniques to find the region in the *tw*-plane where $h_{41} > 0$:

$$R^{+}_{h_{41}} = \Big\{(t,w) \mid \Big(w < 0 \wedge 0 < t < \frac{w}{w-1}\Big) \vee \Big(w < 0 \wedge t > 0.5\sqrt{2w^2+3.5} + 0.1\Big) \\ \vee \Big(w > 2.81 \wedge \frac{0.75w}{w-1} < t < 0.5\sqrt{2w^2+3.} - 0.3\Big)\Big\}. \tag{8}$$

Thus the CC region where μ_1 has positive real values is given as below. Numerically, this region is given in Fig. 1:

$$R_{\mu_1} = \left(R^-_{h_{43}} \cap R^+_{h_{41}}\right) \cup \left((R^-_{h_{43}})^c \cap (R^+_{h_{41}})^c\right). \tag{9}$$

This completes the proof of Theorem 1(i).

3.2 *Proof of Theorem 1(ii)*

For μ_2 to be positive, N_{μ_2} and D_{μ_2} must have the same sign. The denominator of μ_2, i.e., D_{μ_2} is positive when its components (h_{22}, h_{41}) have the same signs. We have shown that $h_{41} > 0$ in $R^+_{h_{41}}$. Let

$$h_{22} = \Big((t+1)w + t\Big)\left((t^2 + (t+w)^2\right)^{-3/2} - \left(w^2+1\right)^{-3/2}\Big).$$

Using a simple sign analysis of the two factors of h_{22} it is found that $h_{22} > 0$ in the following region:

$$R^+_{h_{22}} = \Big\{(t,w) \mid \Big(0 < t < 1 \wedge -t(t+1)^{-1} < w < \left(1-2t^2\right)(2t)^{-1}\Big)$$
$$\vee \Big(t > 1 \wedge \left(1-2t^2\right)(2t)^{-1} < w < -t(t+1)^{-1}\Big)\Big\}.$$

Therefore, $D_{\mu_2} > 0$ in $R_{D_{\mu_2}} = (R^+_{h_{22}} \cap R^+_{h_{41}}) \cup ((R^+_{h_{22}})^c \cap (R^+_{h_{41}})^c)$.

Using the same technique as we have used for h_{22}, h_{41} and h_{43}, we show that h_{21}, h_{23} and h_{43} are positive, respectively, in the following regions:

$$R^+_{h_{21}} = \big\{(t,w) \mid 0 < t < 1.82 \wedge w \in R\big\},$$
$$R^+_{h_{23}} = \big\{(t,w) \mid \{(t,w) | t > 0.37 \wedge w \in R\big\},$$
$$R^+_{h_{43}} = \Big\{(t,w) \mid \Big(w < 0 \wedge 0.5(\sqrt{3}|w| + w) < t < -w\Big)$$
$$\vee \Big(w > 0 \wedge 0 < t < 0.5(\sqrt{3}|w| + w)\Big)\Big\}.$$

It is also possible for N_{μ_2} to be positive when at least one of $h_{21}h_{43}$ and $h_{23}h_{41}$ are positive. It is found that N_{μ_2} is positive in the following region:

$$R_{N\mu_2} = \left(R_{N_{\mu_2}a} \cap R^+_{h_{41}}\right) \cup \left(R_{N_{\mu_2}b} \cap (R^+_{h_{41}})^c\right) \cup \left(R_{N_{\mu_2}c} \cap (R^+_{h_{41}})^c\right) \cup \left(R_{N_{\mu_2}d} \cap (R^+_{h_{41}})^c\right),$$

where

$$
\begin{aligned}
R_{N_{\mu_2}a} &= \{(t,w)|-1<w\leq -0.26\wedge 0.9|w|+0.5w<t<0.35\},\\
R_{N_{\mu_2}b} &= \{(t,w)|\,(-5<w\leq -1.8\wedge 0.9|w|+0.5w<t<1.8)\\
&\quad\vee\big(-1.8<w\leq -1\wedge 0.9|w|+0.5w<t<-1w\big)\\
&\quad\vee(-1<w<-0.4\wedge 0.4<t<-w)\\
&\quad\vee\big(0.3<w<1.3\wedge 0.4<t<0.9|w|+0.5w\big)\vee(w\geq 1.3\wedge 0.4<t<1.8)\},\\
R_{N_{\mu_2}c} &= \big\{(t,w)|\big(w<-5\wedge\big(1.8<t<0.9|w|+0.5w\vee t>-w\big)\big)\\
&\quad\vee(-5\leq w\leq -1.8\wedge t>-w)\\
&\quad\vee(-1.8<w\leq 1.3\wedge t>1.8)\vee\big(w>1.3\wedge t>0.9|w|+0.5w\big)\big\},\\
R_{N_{\mu_2}d} &= \big\{(t,w)|\big(w\geq 0.27\wedge 0<t<0.37\big)\\
&\quad\vee\big(0<w<0.27\wedge 0<t<0.5(\sqrt{3}|w|+w)\big)\big\}.
\end{aligned}
$$

Thus, the central configuration where $\mu_2>0$ is given by

$$R_{\mu_2}=\big(R_{N_{\mu_2}a}\cap R_{D_{\mu_2}}\big)\cup\big(R^c_{N_{\mu_2}a}\cap R^c_{D_{\mu_2}}\big). \tag{10}$$

This completes the proof of Theorem 1(ii).

Finally, Theorem 1(iii) follows as a direct consequence of 1(i) and 1(ii). That is, the central configuration region $R=R_{\mu_1}\cap R_{\mu 2}$ where both μ_1 and μ_2 are positive can be found by taking the intersection of the regions found for μ_1 and μ_2. This region is given in Fig. 2 with the geometric constraint $C=0$.

Acknowledgements The authors thank the Deanship of Scientific research at the University of Hail, Saudi Arabia for funding this work under grant number SM14014.

References

1. A. Albouy and R. Moeckel, "The Inverse Problem for Collinear Central Configurations". *Celestial Mechanics and Dynamical Astronomy* **77** (2000), 77–91.
2. M. Gidea and J. Llbre, "Symmetric planar central configurations of five bodies: Euler plus two". *Celestial Mechanics and Dynamical Astronomy* **106** (2010), 89–107.
3. M. Shoaib, I. Faye, and A. Sivasankaran, "Some special solutions of the rhomboidal five-body problem". *ICFAS2012* **1482**(1), 496–501.
4. M. Shoaib, A. Sivasankaran, and A.R. Kashif. "Central configurations in the collinear five-body problem". *Turkish Journal of Mathematics* **36** (2014), 576–585.

The Discrete Hamiltonian–Hopf Bifurcation for 4D Symplectic Maps

Ernest Fontich, Carles Simó, and Arturo Vieiro

We consider a family of real-analytic symplectic four-dimensional maps $F_{\tilde{\nu}}$, $\tilde{\nu} \in \mathbb{R}^p$, $p \geq 1$, with respect to the standard symplectic two-form $\Omega = dx_1 \wedge dy_1 + dx_2 \wedge dy_2$, where (x_1, x_2, y_1, y_2) denote the Cartesian coordinates. We assume that:

1. $F_{\tilde{\nu}}(\mathbf{0}) = \mathbf{0}$ for all the values of $\tilde{\nu} \in \mathbb{R}^p$;
2. for $\tilde{\nu} = \tilde{\nu}_*$ the eigenvalues (multipliers) related to the fixed point $\mathbf{0} \in \mathbb{R}^4$ of $F_{\tilde{\nu}}$ undergo a Krein collision with opposite Krein signature at $e^{i\hat{\theta}_0}$ with $\hat{\theta}_0 = 2\pi\theta_0$, $\theta_0 \in (0, 1/2)$, $\theta_0 \approx q/m$, $q, m \in \mathbb{N}$, $(q, m) = 1$.

Under these hypotheses the fixed point of $F_{\tilde{\nu}}$ generically undergoes a Hamiltonian–Hopf bifurcation at $\tilde{\nu} = \tilde{\nu}_*$. At the bifurcation the two pairs of eigenvalues of $DF(\mathbf{0})$ suffer a Krein collision [9, 14] and leave the unit circle, so the point becomes complex-unstable. This is a codimension 2 bifurcation [1] and we can consider unfolding parameters δ, ϵ such that δ changes the collision angle (i.e., $\theta_0 = q/m + \delta$) and ϵ measures the relative distance (in the parameter space) to the bifurcation: $\mathbf{0}$ is a totally elliptic fixed point for $\epsilon < 0$ while it becomes a complex-saddle for $\epsilon > 0$. From now on, we shall write $F_{\delta,\epsilon}$ instead of $F_{\tilde{\nu}}$.

In this work we investigate the transition to complex instability of the origin of $F_{\delta,\epsilon}$ at $\epsilon = 0$. Several aspects are considered. We note that the 2D invariant manifolds that emanate from the complex-unstable point are of particular dynamical interest because: (1) they can destroy some invariant tori around $\mathbf{0}$; and (2) they play a role in organizing the dynamics in a neighbourhood of $\mathbf{0}$. For concreteness, below we just comment on the results concerning the geometry and the splitting of those invariant manifolds.

The normal form (NF) analysis of $F_{\delta,\epsilon}$ for $|\delta|, |\epsilon| \ll 1$ helps in clarifying the geometry of the invariant manifolds. At a Krein collision with opposite signature the

E. Fontich • C. Simó • A. Vieiro (✉)
Departament de Matemàtica Aplicada i Anàlisi, Universitat de Barcelona, Barcelona, Spain
e-mail: vieiro@maia.ub.es

M. Corbera et al. (eds.), *Extended Abstracts Spring 2014*, Trends in Mathematics 4,
DOI 10.1007/978-3-319-22129-8_14

linear part $A = DF_{0,0}(\mathbf{0})$ possesses a non-trivial Jordan block. That is, $A = S + N$ with S semi-simple and N nilpotent. The Takens NF commutes with S, that is, there is a canonical change of coordinates C_1 which (formally) transforms $F_{\delta,\epsilon}$ into the NF, that is, one has

$$C_1 \circ F \circ C_1^{-1} = \mathrm{TNF}(F_{\delta,\epsilon}) + E^{(1)}_{\delta,\epsilon} = S \circ \varphi^{H_{\delta,\epsilon}}_{t=1} + E^{(1)}_{\delta,\epsilon}, \tag{1}$$

where $H_{\delta,\epsilon}$ is the 2-dof NF interpolating Hamiltonian, $\varphi^{H_{\delta,\epsilon}}_t$ denotes its associated flow and $E^{(1)}_{\delta,\epsilon}$ denotes the error between F and the Takens NF. From the "suspension+averaging" procedure, truncating the NF averaging procedure at an optimal order r_1, see [2], it follows for $\epsilon > 0$ that $|E^{(1)}_{\delta,\epsilon}| < N_1 \exp(-C_1/\gamma_1)$ with $0 < \gamma_1 < \eta_1 \max(|\delta|, \epsilon)$ and $N_1, C_1, \eta_1 > 0$ are constants.

In particular, the local geometry of the system is reflected in the 2-dof Hamiltonian $H_{\delta,\epsilon}$. Next, we will focus on the analysis of $H_{\delta,\epsilon}$ and later we will discuss our results concerning the effect of the exponentially small error $E^{(1)}_{\delta,\epsilon}$ on the splitting of the 2D invariant manifolds.

The S-invariance of $H_{\delta,\epsilon}$ implies that its quadratic terms are given by

$$H_2 = -\sigma\Gamma_2 - 2\pi\delta\Gamma_1 + \epsilon\left(\frac{\sigma}{6}\Gamma_2 + \sigma\Gamma_3 - \frac{1}{2}\Gamma_4\right) + \mathcal{O}(\epsilon^2),$$

where $\Gamma_1 = x_2y_1 - x_1y_2$, $\Gamma_2 = (x_1^2 + x_2^2)/2$, $\Gamma_3 = (y_1^2 + y_2^2)/2$ and $\Gamma_4 = x_1y_1 + x_2y_2$. Note that $S = \varphi^{-\omega\Gamma_1}_{t=1}$, $\omega = -i\log\lambda_0 = -\hat{\theta}_0$. The quadratic part of $\hat{H}_{\delta,\epsilon} = -\omega\Gamma_1 + H_{\delta,\epsilon}$ is $\hat{H}_2 = -(\omega + 2\pi\delta)\Gamma_1 - \sigma\Gamma_2 + \mathcal{O}(\epsilon)$ and we see that $-\sigma\hat{H}_{\delta,\epsilon} = -\sigma(-\omega\Gamma_1 + H_{\delta,\epsilon})$ undergoes a Hamiltonian–Hopf bifurcation. It can be then reduced to the so-called Sokolskii NF, see [13, 16]. This can be achieved by a change of coordinates C_2 so that

$$C_2 \circ H_{\delta,\epsilon} \circ C_2^{-1} = \mathrm{SNF}(H_{\delta,\epsilon}) + E^{(2)}_{\delta,\epsilon}, \tag{2}$$

where, after some non-canonical rescalings of the coordinates and time, see details in [7, 10, 12],

$$\mathrm{SNF}(H_{\delta,\epsilon}) = -\Gamma_1 + \sqrt{\epsilon}(\Gamma_2 + a\Gamma_3 + b\Gamma_3^2) + \mathcal{O}(\epsilon), \tag{3}$$

for suitable parameters $a, b \in \mathbb{R}$ (that include the dependence on δ; this dependency is also reflected in the performed scalings). In particular, Γ_1 becomes a formal integral of $\mathrm{SNF}(H_{\delta,\epsilon})$ (i.e., any truncation of the NF of the Hamiltonian is integrable). Note that the averaging procedure up to an optimal order r_2 implies $|E^{(2)}_{\delta,\epsilon}| < N_2 \exp(-C_2/\gamma_2)$ with $0 < \gamma_2 < \eta_2 \max(|\delta|, \epsilon)$ where $N_2, C_2, \eta_2 > 0$ are constants.

From (3), see [11], it follows that the 2D invariant manifolds $W^{u/s}$ are given by the rotation by an angle $\hat{\theta}_0$ of the zero energy level of a Duffing Hamiltonian

system. We are interested in the case $a < 0$, $\eta > 0$ because the manifolds of the Duffing system are bounded. For the complete Hamiltonian system (2), the invariant manifolds do not coincide. Using a suitable Poincaré section, the complete system can be regarded as a near-the-identity family of area-preserving maps. They have the Duffing system as a limit vector field. Hence, as it follows from the general approach in [5], one has that the splitting angle α behaves as

$$\alpha \sim A\epsilon^B \exp\left(\frac{-\pi}{\sqrt{-a}\sqrt{\epsilon}}\right) \sim A|\mathrm{Re}\ \lambda|^B \exp\left(\frac{-\pi\ |\mathrm{Im}\ \lambda|}{|\mathrm{Re}\ \lambda|}\right),$$

where $\lambda \in \mathbb{C}$ is one of the eigenvalues (which form a complex quadruplet) associated to the origin of the Hamiltonian system $H_{\delta,\epsilon}$. The concrete expression of the asymptotic expansion of this splitting was obtained in [7]. Here we take further advantage of the geometry of the system to reduce it to a near-the-identity family of analytic maps.

This completes the analysis of the NF Hamiltonian $H_{\delta,\epsilon}$. It remains to clarify the role of the error $E^{(1)}_{\delta,\epsilon}$ in (1). To this end we note that, from (1)–(2), it follows that the discrete system $F_{\delta,\epsilon}$ behaves, in a neighbourhood of $W^{u/s}$, as a quasi-periodic forcing of an integrable Duffing Hamiltonian system. The two frequencies are related to the Krein collision angle $\hat{\theta}_0$ (this is given by the semi-simple part of $DF_{0,0}$ and it is related to the rotation of the $W^{u/s}$ already present in the Hamiltonian $H_{\delta,\epsilon}$) and the extra time-frequency (related to the fact that the map $F_{\delta,\epsilon}$ is the composition of a semi-simple part with a near-the-identity map which can be written, by the so-called suspension procedure, as the flow of a $2 + 1/2$ dof Hamiltonian). As a consequence, one expects that the splitting of $W^{u/s}$ for $F_{\delta,\epsilon}$ behaves as described in [3, 4, 15]. That is, the dominant harmonic of the Fourier expansion of the Melnikov potential function is expected to change as the size of the perturbation ϵ tends to 0.

Nevertheless, we can take advantage of the intrinsic geometric structure given by (1)–(2). One of the frequencies basically is responsible of the splitting shown in the Hamiltonian $H_{\delta,\epsilon}$, while the interaction between the two creates the quasi-periodic phenomena. But (1)–(2) also define a privileged direction to measure the quasi-periodic effect for the map $F_{\delta,\epsilon}$: the time along the homoclinic trajectory of the interpolating Hamiltonian $H_{\delta,\epsilon}$. In this work we introduce a splitting function ψ (instead of a Melnikov vector) to measure this effect along this direction. The function ψ measures the distance between W^u and W^s in a fundamental domain (an annulus). In this annulus we introduce coordinates $(\alpha, t) \in \mathbb{S}^1 \times [0, 1]$ and relate them to the natural parametrisation of $W^{u/s}$. This can be seen as a generalization of the ideas in [5] to 4D maps.

Recall that the role of δ is to change the collision angle $\hat{\theta}_0$. Hence, the relevant unfolding parameter is ϵ. At $\epsilon = 0$ the eigenvalues $\lambda = |\lambda|e^{i\hat{\theta}}$ of F_ϵ have a Krein collision, i.e., $|\lambda| = 1 + a\epsilon + \mathcal{O}(\epsilon^2)$, $\hat{\theta} = \hat{\theta}_0 + \mathcal{O}(\epsilon^2)$. For δ fixed, assuming that F_ϵ can be extended analytically to a neighbourhood of $\{\alpha \in \mathbb{C}/2\pi\mathbb{Z} \mid |\mathrm{Im}\ \alpha| < \rho\} \times \{\sigma(t) \mid |\mathrm{Im}\ t| < \tau\}$ for some $0 < \tau < \tau_0$ and $0 < \rho < \rho_0$, one can

bound the Fourier coefficients of ψ. If h denotes $\log(\lambda)$ one obtains $|\psi(\alpha,t)| < KS$, where $K>0$ is a constant and $S=\sum_{(k,n)\in\mathbb{Z}^2\setminus\{\mathbf{0}\}}\exp(-2\pi|n-\theta_0 k|\tau/h-|k|\rho)$.

The sum S can be decomposed into $S=S_{++}+S_{+-}+S_{-+}+S_{--}+S_{+0}+S_{0+}+S_{-0}+S_{0-}$, according to the signs of $D=2\pi(n-k\theta_0)$ and k, respectively. Then we look for $k=k_*(h)>0$ such that it gives the minimum of the dominant coefficients β_{k_*} in the exponential bound of S.

Proposition 1

(i) Let $\theta_0=p/q$, with $(p,q)=1$ (rational collision). Then, there exists $\epsilon^0>0$ such that for $\epsilon<\epsilon^0$ the following properties hold:

(a) *$k_*(h)=\beta^{-+}_{k_*(h)}=q$, where $h=\log(\lambda(\epsilon))$;*

(b) *ψ can be bounded by a function whose behaviour is determined by the value of $k=k_{**}(h)$ minimizing the coefficient β^{++}_k. One has $k_{**}(h)=\lfloor(q-1)/p\rfloor$ independently of h (provided ϵ^0 is small enough). Then, $\beta^{++}_{k_{**}(h)}\sim C/h$, where $C=C(k_{**})>0$ is a constant and, consequently, ψ is bounded by*

$$|\psi(\alpha,t)|\le K\exp(-C/h),$$

where $K>0$ is independent from α, t and ϵ.

(ii) Let $\theta_0\in\mathbb{R}\setminus\mathbb{Q}$ (irrational collision). Then, ψ is bounded by a function that is asymptotically exponentially small in a parameter γ, such that $\gamma\searrow 0$ when $h\searrow 0$. In this case, the function γ reflects the quasi-periodic properties of the splitting function: the dominant harmonic $k(h)$ of ψ changes infinitely many times as $h\to 0$.

The theoretical results have been guided by several numerical explorations using a Froeschlé like 4D map as a concrete model. In particular, we have computed the splitting of $W^{u/s}$ (measuring a volume V of a 4D parallelotope defined by two tangent vectors to each invariant manifolds at a given homoclinic point, see [8]) to check that the behaviour of V is in agreement with the behaviour of ψ given by the above Proposition.

The considered map is related to the time-$\tilde{\delta}$ stroboscopic map of the 2-dof Hamiltonian

$$H(\psi_1,\psi_2,J_1,J_2)=\frac{J_1^2}{2}+a_2J_1J_2+a_3\frac{J_2^2}{2}+\cos\psi_1+\tilde{\epsilon}\cos(\psi_2),\quad \text{where } a_2,a_3,\tilde{\epsilon}\in\mathbb{R},$$

and was obtained in [8] from the NF analysis of a generic 4D analytic map around a totally elliptic fixed point when studying the non-strong double resonance structure associated to the crossing of two resonances of different (but similar!) order. Several implications of the transition to complex-saddle in this general setting have been included in [6], where the results presented here can be found.

Acknowledgements This work has been supported by grants MTM2010-16425 (Spain) and 2009 SGR 67 (Catalonia). This manuscript was prepared during a stay of the last two authors at the Centre de Recerca Matemàtica (CRM), Catalunya. They warmly thank the CRM for the facilities and support.

References

1. T.J. Bridges and J.E. Furter, "Singularity theory and equivariant symplectic maps". *Lecture Notes in Mathematics* **1558**. Springer-Verlag, 1993.
2. H. Broer, R. Roussarie, and C. Simó, "Invariant circles in the Bogdanov–Takens diffeomorphisms". *Ergodic Theory and Dynamical Systems* **16** (1996), 1147–1172.
3. A. Delshams, V. Gelfreich, A. Jorba, and T.M. Seara, "Exponentially small splitting of separatrices under fast quasiperiodic forcing". *Comm. Math. Phys.* **189**(1) (1997), 35–71.
4. A. Delshams and P. Gutiérrez, "Exponentially small splitting of separatrices for whiskered tori in Hamiltonian systems". *Journal of Mathematical Sciences* **128**(2) (2005), 2726–2745.
5. E. Fontich and C. Simó, "The splitting of separatrices for analytic diffeomorphisms". *Ergod. Th. and Dynam. Sys.* **10** (1990), 295–318.
6. E. Fontich, C. Simó, and A. Vieiro, "Geometrical and analytical aspects of the transition to complex instability within double resonances". *Preprint*.
7. J.P. Gaivão and V. Gelfreich, "Splitting of separatrices for the Hamiltonian–Hopf bifurcation with the Swift–Hohenberg equation as an example". *Nonlinearity* **24**(3) (2011), 677–698.
8. V. Gelfreich, C. Simó, and A. Vieiro, "Dynamics of 4D symplectic maps near a double resonance". *Physica D* **243**(1) (2013), 92–110.
9. J.D. Hadjidemetriou, "The stability of resonant orbits in planetary systems". In "Resonances in the Motion of Planets, Satellites and Asteroids". Ferraz-Melo, Univ. Sao Paulo, 1985.
10. L.M. Lerman and A.P. Markova, "On stability at the Hamiltonian–Hopf Bifurcation". *Regular and Chaotic Dynamics* **14** (2009), 148–162.
11. P.D. McSwiggen and K.R. Meyer, "The evolution of invariant manifolds in Hamiltonian–Hopf bifurcations". *J. Differential Equations* **189**(2) (2003), 538–555.
12. K.M. Meyer, "The evolution of the stable and unstable manifold of an equilibrium point". *Celestial Mech. Dynam. Astronom.* **70**(3) (1998), 159–165.
13. K.R. Meyer and G. Hall, "Introduction to Hamiltonian dynamical systems and the *N*-body problem". *Applied Mathematical Sciences*, **90**. Springer-Verlag, New York, 1992.
14. D. Pfenninger, "Numerical study of complex instability". *Atron. Astrophys.* **150** (1985), 97–111.
15. C. Simó, "Averaging under Fast Quasiperiodic Forcing". In J. Seimenis, editor, "Hamiltonian Mechanics: Integrability and Chaotic Behaviour", *NATO Adv. Sci. Inst. Ser. B Phys.* **331**, 13–34.
16. A.G. Sokolskiĭ, "On the stability of an autonomous Hamiltonian system with two degrees of freedom in the case of equal frequencies". *J. Appl. Math. Mech.* **38** (1974), 741–749; translated from *Prikl. Mat. Meh.* **38** (1974), 791–799.

Moment Map of the Action of $SO(3)$ on $\mathbb{R}^3 \times \mathbb{R}^3$

José Antonio Villa Morales

The aim of this extended abstract is to expose the main results of the moment map of the action of $SO(3)$ on the cotangent bundle of $\mathbb{R}^3$. The moment map for this action has a strong motivation from the angular momentum studied in classical mechanics. Suppose we have a central force and a particle which rotates around this force with velocity v and position r, then we know that the angular momentum is given by $r \times v$. Viewing the rotation of the particle as an action of the group $SO(3)$ over the cotangent bundle of $\mathbb{R}^3$ we can find that the angular momentum is related to a map between $T^*\mathbb{R}^3$ and the dual of the Lie algebra $\mathfrak{so}(3)$ called *moment map*.

1 Lie Group Actions and Symmetric Hamiltonians

Definition 1 Let M be a differential manifold and G a Lie group. An action of G on M is a smooth map $G \times M \to M$, $(g, p) \mapsto gp$, satisfying the following conditions:

(1) if e is the null element in G then $ep = p$ for all $p \in M$;
(2) for all $g, h \in G$ and $p \in M$, $g(hp) = (gh)p$.

A symplectic manifold is an even dimensional differentiable manifold M with a non-degenerate and closed 2-form ω. Remember that $\alpha \in \Omega^k(M)$ is closed if $s\alpha = 0$.

Definition 2 Let (M, ω) a symplectic manifold and G a Lie group acting on (M, ω). We say that the action is symplectic if $L_g^* \omega = \omega$, for all $g \in G$.

J.A.V. Morales (✉)
Universidad Michoacana de San Nicolás de Hidalgo, Morelia, México and
Universidad Nacional Autónoma de México, México, México
e-mail: antvilla06@gmail.com

M. Corbera et al. (eds.), *Extended Abstracts Spring 2014*, Trends in Mathematics 4,
DOI 10.1007/978-3-319-22129-8_15

Suppose we have a Lie group G acting over a differentiable manifold M. For an arbitrary tangent vector $\xi \in \mathfrak{g}$ we construct a vector field, called the infinitely generated vector field X_ξ given by

$$X_\xi(p) = \frac{d}{dt}_{t=0} exp(t\xi)p.$$

Given the symplectic manifold (M, ω), and a vector field X on M, we denote the contraction by $i_X\omega$ and it is defined by $i_X\omega(Y) = \omega(X, Y)$ for Y a vector field in M.

Definition 3 Let (M, ω) be a symplectic manifold, and X a given vector field on M. If there is a function $H \in C^\infty(M)$ such that $i_X\omega = dH$ we say that H is the Hamiltonian associate to the vector field X. Conversely, if given a differentiable function $H \in C^\infty(M)$ there exists a vector field X such that $i_X\omega = dH$ we say that X is the vector field associated to the function H.

We will denote by X_H the vector field associated to H and, conversely, by H_X the function associated to the vector field X.

2 Symplectic Structure on the Cotangent Bundle

Given an n dimensional manifold M, it is possible to construct a 1-form on T^*M which give rise to a symplectic form on T^*M. We only expose the construction result on a coordinate chart; a free coordinate construction can be found in [1].

Proposition 4 *Let M a differentiable manifold. Then, there exists a 1-form θ on T^*M such that, for a chart (U, φ) on T^*M with coordinates $(x_1, \ldots, x_n, p_1, \ldots, p_n)$, θ is given by*

$$\theta = dx_1 \wedge dp_1 + \cdots + dx_n \wedge dp_n.$$

Definition 5 The 2-form $\omega := -d\theta$ on T^*M is called the symplectic form over the cotangent bundle.

For the next section, we will use the fact that the cotangent bundle of $\mathbb{R}^3$ is trivial, so we can express the symplectic manifold $(T^*\mathbb{R}^3, \omega)$ as $(\mathbb{R}^3 \times \mathbb{R}^3, \omega)$.

3 Rotations on $\mathbb{R}^3 \times \mathbb{R}^3$

Consider the symplectic manifold $(\mathbb{R}^3 \times \mathbb{R}^3, \omega)$, and define the action of the Lie group $SO(3)$ over it given by

$$\begin{aligned} SO(3) \times (\mathbb{R}^3 \times \mathbb{R}^3, \omega) &\to (\mathbb{R}^3 \times \mathbb{R}^3, \omega) \\ (A, (u, v)) &\mapsto (Au, Av). \end{aligned}$$

Proposition 6 *This action of* $SO(3)$ *on* $(\mathbb{R}^3 \times \mathbb{R}^3, \omega)$ *is symplectic.*

We give the idea of the proof: by definition $\omega = -d\theta$, where θ is the canonical 1-form of the cotangent bundle given in a chart (U, φ) with coordinates $(x_1, \ldots, x_n, p_1, \ldots, p_n)$ by $\omega = \sum_i^n dx_i \wedge dp_i$. With some calculations we can verify that, for all $A \in SO(3)$, $L_A^* \theta = \theta$. And, by the commutativity of the operator d with the pullback, it is possible to verify that $L_A^* \omega = \omega$.

Proposition 7 *Let* $B \in \mathfrak{so}(3)$ *and let* X_B *be the corresponding infinitely generated vector field of B. Then, the Hamiltonian associated to* X_B *is given by*

$$H_{X_B}(u, v) = \langle Au, v \rangle.$$

Proposition 8 *Let* $B \in \mathfrak{so}(3)$ *and let* X_B *be the corresponding infinitely generated vector field of B. Then, the Hamiltonian* H_{X_B} *is symmetric, i.e., for all* $A \in SO(3)$,

$$L_A^* H = H.$$

3.1 Moment Map of Rotations on $\mathbb{R}^3 \times \mathbb{R}^3$

The main goal of this section is to define the moment map of a symplectic action, and to calculate it for the specific action of $SO(3)$ over the cotangent bundle of $\mathbb{R}^3$.

Definition 9 Let (M, ω) be a symplectic manifold, and let G be a Lie group with a symplectic action over (M, ω). A *moment map* is a function $\mu: M \to \mathfrak{g}^*$ such that for all $\xi \in \mathfrak{g}$ there is a function $\mu_\xi: M \to \mathbb{R}$ such that $d\mu_\xi = i_{X_\xi}\omega$ and $\mu_\xi(p) = \mu(p)(\xi)$.

Proposition 10 *Let* (M, ω) *be a symplectic manifold, let* $H \in C^\infty(M)$ *be a symmetric Hamiltonian, and consider the vector field* X_H *associated to it. Then, its moment map is a first integral of* X_H.

We have that the Lie algebra $\mathfrak{so}(3)$ has dimension three and then, we can identify it with the Euclidean space $\mathbb{R}^3$. We define the map $\mathfrak{so}(3) \to \mathbb{R}^3$ via

$$\begin{pmatrix} 0 & \xi_3 & -\xi_2 \\ -\xi_3 & 0 & \xi_1 \\ \xi_2 & -\xi_1 & 0 \end{pmatrix} \longrightarrow (\xi_1, \xi_2, \xi_3).$$

In $A \in \mathfrak{so}(3)$, we denote the associated vectors in $\mathbb{R}^3$ as ξ_A. If we take a tangent vector $B \in \mathfrak{so}(3)$ and $u \in \mathbb{R}^3$, by calculations, we can verify that

$$Bu = \xi_B \times u.$$

Proposition 11 *There exist an inner product on the Lie algebra* $\mathfrak{so}(3)$ *given by*

$$\langle A, B\rangle_{\mathfrak{so}(3)} = \frac{tr(A^t B)}{2}.$$

Now, consider the moment map $\mu\colon \mathbb{R}^3\times\mathbb{R}^3 \to \mathfrak{so}(3)$. By definition, $d\tilde{\mu}_B = i_{X_B}\omega$. But, by definition of associated Hamiltonian, we also have $d\tilde{\mu}_B = i_{X_B}\omega = dH_B$. So, we conclude $\tilde{\mu}_B(u, v) = H_B(u, v)$ and, using this last equality, we calculate the moment map

$$(\tilde{\mu}(u, v))(B) = \langle Bu, v\rangle = \langle \xi_B \times u, v\rangle = \langle u \times v, \xi_B\rangle.$$

Hence, given a tangent vector $B \in \mathfrak{so}(3)$, we have $(\mu(u, v))(B) = \langle u \times v, \xi_B\rangle$ and, using the inner product of $\mathfrak{so}(3)$, we get $\langle u \times v, \xi_B\rangle = \langle A_{u\times v}, B\rangle_{\mathfrak{so}(3)}$. It is then possible to conclude that the moment map is $\mu(u, v) = A_{u\times v}$.

4 The Moment Map of the Action $SO(3)$ Over $T^*SU(2)$

We make the construction of the action of the group $SO(3)$ over the cotangent bundle $T^*\mathbb{R}^3$ and, via the moment map, we find a first integral of the system given by this action. Naturally, we have an action of $SO(3)$ over the Euclidean space $\mathbb{R}^3$ which is the mathematical model of the rotations in three dimensional space. But if we make a one point compactification of $\mathbb{R}^3$, we obtain the Lie group $SU(2)$, so it is natural to try to extend this action to an action over $SU(2)$. But following the theory developed above, if we see the cotangent bundle of $T^*SU(2)$ as a symplectic manifold, can we extend the action of $SU(2)$ to an action of $SO(3)$ over $T^*SU(2)$? We enumerate the steps for constructing the possible action:

1. The action of $SO(3)$ over $\mathbb{R}^3$ is given by multiplication of a matrix and a vector on $\mathbb{R}^3$. If we make the one point compactification of $\mathbb{R}^3$ at the point ∞, how can we define an action $SO(3) \times SU(2) \to SU(2)$ such that $(A, \infty) \mapsto A\infty$ makes sense?
2. $SU(2)$ is a Lie group and then its cotangent bundle is $T^*SU(2) = SU(2) \times \mathbb{R}^3$. So it is natural to define the action of $SO(3)$ by $(A, v_p) \mapsto (Ap, Av)$. Does this define a symplectic action?
3. How can we calculate the moment map for this action?

Reference

1. R. Abraham and J.E. Marsden, "Foundations of mechanics". Second edition, Addison Wesley 1978.

Part II
Virus Dynamics and Evolution

Editors

Andrei Korobeinikov

Foreword

The *Workshop on Virus Dynamics and Evolution* was held from June 23th to June 27th 2014, at the Centre de Recerca Matemàtica (CRM) in Bellaterra, Barcelona, Spain. It was the third event in the framework of CRM series on *Mathematics in Life Sciences* (the two previous events being the "Workshop on Emergence, Spread and Control of Infectious Diseases", held at the CRM in 2013, and the "Advanced Course on Mathematical Methods of Biological Evolution", which preceded the workshop). The intention of the organizers of this interdisciplinary workshop was to bring together biologists and mathematicians to exchange, in an informal and friendly atmosphere, ideas, methods and open problems. The most desirable outcome of the workshop would be developing lasting collaborations between them.

The workshop attracted more than 30 scientists, both mathematicians and biologists, affiliated in Spain, Europe and around the world, and proved to be highly successful. The invited keynote lectures were delivered by Graeme Wake (Massey University, New Zealand), Yoh Iwasa (Kyushu University, Japan), Susanna Manrubia (Centro de Astrobiología, INTA-CSIC, Spain), Esteban Domingo (Centro de Biología Molecular "Severo Ochoa", CSIC-UAM, Spain), Fernando García-Arenal Rodríguez (Centro de Biotecnología y Genómica de Plantas, UPM-INIA, Spain), Ricard Solé (Universitat Pompeu Fabra, Catalonia), Santiago F. Elena (Instituto de Biología Molecular y Celular de Plantas, CSIC-UPV, Spain), and Juana Díez (Universitat Pompeu Fabra, Catalonia). The workshop also gave an opportunity to young researchers and students to present their results and findings and to learn from more experienced colleagues.

The organizers would like to thank all participants and the authors, who contributed to the success of the workshop. We would also like to thank the CRM for financial support, and the CRM's administrative staff for wonderful organization of this event.

Barcelona, Spain Andrei Korobeinikov

Modelling Infection Dynamics and Evolution of Viruses in Plant Populations

Aurora Fraile and Fernando García-Arenal

1 Introduction

Mathematical models have been used extensively to analyse and/or predict the dynamics of pathogen infection in host populations, as well as the evolution of key pathogen traits, notably infectivity and virulence. Model analyses have been very useful in identifying factors that affect infection dynamics and pathogen evolution, and in predicting their effects under different scenarios. However, a serious shortcoming of theoretical analyses is that often there is not enough information on how realistic the underlying assumptions are, and very often there is a serious lack of information on the range of values of key model parameters. An example is the classical susceptible-infected-recovered (SIR) model, first proposed by Kermack and McKendrick [8] in 1927, and becoming the basis to predict virulence evolution. A central assumption of this model is that both virulence, defined as the effect of infection on host mortality, and the rate of transmission to new hosts, are positively correlated with the within-host multiplication rate of the pathogen, so that a trade-off between virulence and transmission is established to optimize the intrinsic reproduction value. Interestingly, a positive correlation between virulence and within-host multiplication has been demonstrated in few host-parasite systems, and seems not to be the rule for the whole classes of parasites, including plant viruses [10], which has not discouraged the use (and the utility) of SIR-based evolutionary models.

A central interest of our group has been the analysis of the evolution and infection dynamics of viruses in their host populations. We have developed simple models that explain field observations, and we have made efforts to experimentally estimate the

A. Fraile (✉) • F. García-Arenal
Centro de Biotecnología y Genómica de Plantas (UPM-INIA) and E.T.S.I. Agrónomos, Universidad Politécnica de Madrid, Madrid, Spain
e-mail: aurora.fraile@upm.es; fernando.garciaarenal@upm.es

M. Corbera et al. (eds.), *Extended Abstracts Spring 2014*, Trends in Mathematics 4,
DOI 10.1007/978-3-319-22129-8_16

values of relevant model parameters, so that realistic conditions would be simulated. We work with plant-infecting viruses and a large part of this work has involved *Cucumber mosaic virus*, an economically important virus that is a good model to address significant epidemiological and evolutionary questions.

2 Cucumber Mosaic Virus

Cucumber mosaic virus (CMV, family *Bromoviridae*), is a plant virus with a single-stranded, messenger sense, RNA genome built of three segments that are separately encapsidated in isometric particles. The CMV is a typical multi-host pathogen, with the broadest host range among plant viruses, infecting more than 1200 species in more than 100 mono- and dicotyledon families. The CMV is horizontally transmitted by more than 80 aphid (Homoptera: *Aphididae*) species. Transmission is non-persistent: the virus does not infect the insect vector but is retained in its mouth parts, and the aphid is able to transmit the virus for a short time (<6 h) after acquisition. The CMV is also transmitted vertically through the seed, with varying rates according to the plant species. Seed transmission may be epidemiologically relevant in weed reservoirs that, together with other crops, are inoculum sources for crop epidemics, see [7, 9]. CMV is the helper virus for a satellite RNA (satRNA), a small, non-coding, single-stranded RNA that is not infectious by itself but depends on CMV for its replication, encapsidation, and transmission. CMV-satRNA may modulate the pathogenicity of CMV according to the strains of CMV and satRNA and to the host plant species. While most satRNA variants do not modify, or attenuate CMV symptoms in most plant species, in tomato two main types can be distinguished, those that attenuate CMV symptoms (A-satRNAs) and those that aggravate them to a systemic necrosis (N-satRNAs). Interestingly, in most other hosts of CMV the phenotypes of these two types of satRNAs are undistinguishable, and the symptoms caused by satRNA-supporting or by satRNA-free CMV isolates are apparently the same. CMV-satRNAs occur with low frequency in the field, high satRNA prevalence has been mostly associated with epidemics of tomato necrosis. It has been shown that satRNAs spreads in the CMV population as a molecular hyperparasite [1]. Indeed, CMV-satRNA parasitizes the CMV helper isolate, as it competes with the CMV genomic RNAs for the replication complex, and depresses significantly virus accumulation in different hosts. In addition, as CMV virulence in different host plant species is genetically determined, and is modulated by the presence of satRNAs, CMV-satRNA can be considered as a fourth, non-essential, component of CMV genome.

From 1986 to 1992 an epidemic of systemic necrosis occurred in tomato crops in eastern Spain, caused by CMV plus satRNAs [4]. CMV isolates collected during this epidemic caused three different symptoms in tomato plants: a systemic necrosis (*N* isolates), a stunting of the plant and curling of the leaves (*A* isolates), or a stunting of the plant with extreme reduction of the leaf lamina (*Y* isolates). *N* and *A* isolates were associated with satRNA-variants necrogenic and non-necrogenic (i.e.,

attenuating of CMV symptoms), respectively, while Y isolates were not associated with satRNAs [5]. The symptoms caused by *N* and *A* isolates were determined solely by the presence and nature of the associated satRNA, and not by the interaction between satRNA variant and CMV variant [4].

3 Conditions for the Emergence of CMV Genotypes Necrogenic for Tomato: Single Host Populations

Since tomato necrosis was not reported previously in Spain, this epidemic gave us the opportunity to model and analyse the conditions for the emergence of highly virulent virus genotypes, i.e., the conditions under which necrogenic CMV isolates would invade the tomato-infecting CMV population. We used first SIR-like models in which plants would be single-infected by just one CMV genotype [5]. At odds with typical SIR models, an equation describing the dynamics of a recovered subclass of plants was not included because CMV, as most plant viruses, cause persistent infections. The key model parameters of virulence and transmissibility were estimated experimentally for CMV genotypes, *Y*, *A* and *N*, which ranked $N > Y > A$ for virulence and $Y > A > N$ for transmissibility. While transmissibility correlated positively with within-host multiplication, this was not so for virulence, the most virulent genotype *N* accumulating to much lower levels than the *Y* or *A* genotypes, at odds with a central assumption of SIR models. For low and intermediate aphid densities, the predictions of the single-infection model agreed well with the observed long term evolution to decreased levels of virulence in the field, but did not explain the appearance and invasion of *N* genotypes, see [1, 5].

Next, we used a co-infection model that considered competition between the CMV genotypes in double-infected plants, competition affecting transmission, and included the possibility that the most competitive genotype takes over the host, approaching super-infection as a limit of co-infection. That model was a modification of that proposed by Mosquera and Adler [9], and is fully described in Escriu et al. [5]. Parameters of the competition between the different CMV genotypes in co-infected tomato plants, and the probabilities of competitive exclusion, were also determined experimentally. This co-infection model predicted the observed long-term evolution to low levels of virulence at low aphid density and, in addition, explained the invasion of the CMV population by *N*-CMV, which occurred at higher aphid densities and in co-infection with *A*-CMV, according to field observations [5]. An important conclusion from model analyses was that the density of the aphid vector's population is a major factor in the evolution of CMV virulence, which may be relevant for the design of control strategies for CMV. Another important conclusion is that SIR-like models accurately predicted the evolution of CMV virulence, even if the central assumption of a link between virulence and virus multiplication did not hold in the analysed system.

4 Conditions for the Emergence of CMV Genotypes Necrogenic for Tomato: Heterogeneous Host Populations

Since in host plant species other than tomato all CMV genotypes cause similar symptoms, it could be that their virulence, within-host accumulation and transmissibility would differ from those in tomato. Hence, these hosts should be considered in analyses of *N*-CMV emergence. Thus, analysed CMV virulence evolution over two host species, among which *N*, *A* and *Y* genotypes will differ in within host multiplication, competition in mixed infections, virulence and transmission. In addition to tomato, the focal host in which the necrosis epidemic emerged, melon was chosen as the second host. Since satRNA variants responsible for the *N* and *A* CMV types in tomato do not differ in phenotype in melon plants [2], melon represents the large majority of CMV hosts in this respect. We extended the previous co-infection model to two hosts, allowing for inoculum flows between hosts, which is according to knowledge on CMV biology. Parameters of within-host multiplication, within-host competition, virulence and transmission, were determined experimentally for different CMV genotypes in each host. Importantly, *Y*, *A* and *N* CMV genotypes ranked differently for virulence and transmissibility in either host. The model is described in Betancourt et al. [3], and simulations were done under different scenarios that would mimic realistic field conditions. For instance, both hosts would grow synchronically, and inoculum flows between host could be symmetrical or asymmetrical, as would be the case of weeds within a crop or outside of the crop; also, hosts would overlap only part of the cycle, which would be the case of other weeds or crops. For most simulated conditions, evolution to high virulence in the more competent tomato host was little dependent of inoculum flow from melon, while in melon it depended of transmission from tomato. Virulence evolution bifurcated in each host at low, but not at high, vector densities. There was no evidence of between-host trade-offs in CMV life history traits, at odds with most theoretical assumptions. Predictions agreed with field observations and, as in the previous work, are relevant for designing control strategies for multi-host plant viruses.

5 Future Work

All the above described analyses were done using models that considered that the probability of infection of susceptible-uninfected plants (*S* plants) depends on the density of susceptible and infected plants (*I* plants). Because CMV is transmitted by aphids, it could be more realistic to consider a model in which the probability of infection depends on the density of susceptible plants and of viruliferous aphid vectors. This model should allow for introducing realistic parameters of transmission according to the transmission mechanisms, e.g., for non-persistent transmission in the case of CMV. We have recently developed such a model, which

has been used to analyse how efficient a host is as a reservoir for infection of other hosts [6].

Last, an important limitation of all models considering that the probability of infection varies according to the product of susceptible and infected plants, or plants and aphids, is that they ignore how this probability is modified by the spatial distribution of *S* and *I* plants. Extensive epidemiological analyses in crops of infection by viruses non-persistently transmitted by aphids show that the distribution of infected plants is aggregated, with the number of foci, their size and the degree of aggregation varying along the epidemics as incidence increases [1]. Our next goal is to develop spatially-explicit models that would integrate these field estimates of aggregation, for the analysis of the population dynamics and evolution of plant viruses.

References

1. J.L. Alonso-Prados, M.A. Aranda, J.M. Malpica, F. García-Arenal, and A. Fraile, "Satellite RNA of Cucumber mosaic cucumovirus spreads epidemically in natural populations of its helper virus". *Phytopathology* **88** (1998), 520–524.
2. M. Betancourt, A. Fraile, and F. García-Arenal, "Cucumber mosaic virus satellite RNAs that induce similar symptoms in melon plants show large differences in fitness". *Journal of General Virology* **92** (2011), 1930–1938.
3. M. Betancourt, F. Escriu, A. Fraile, and F. García-Arenal, "Virulence evolution of a generalist plant virus in a heterogeneous host system". *Evolutionary Applications* **6** (2013), 875–890.
4. F. Escriu, A. Fraile, and F. García-Arenal, "Evolution of virulence in natural populations of the satellite RNA of Cucumber mosaic virus". *Phytopathology* **90** (2000), 480–485.
5. F. Escriu, A. Fraile, and F. García-Arenal, "The evolution of virulence in a plant virus". *Evolution* **57** (2003), 755–765.
6. J.M. Hily, A. García, A. Moreno, et al., "The relationship between host lifespan and pathogen reservoir potential: An analysis in the system arabidopsis thaliana-cucumber mosaic virus". PLoS Pathog. **10**(11) (2014), e1004492. doi:10.1371/journal.ppat.1004492.
7. M. Jacquemond, "Cucumber mosaic virus". *Advances in Virus Research* **84** (2012), 439–504.
8. W.O. Kermack and A.G. McKendrick, "A contribution to the mathematical theory of epidemics". *Proceedings of the Royal Society London Ser. A* **115** (1927), 700–721.
9. L.J. Mosquera and F.R. Adler, "Evolution of virulence: a unified framework for coinfection and superinfection". *Journal of Theoretical Biology* **195** (1998), 293–313.
10. P. Palukaitis and F. García-Arenal, "Cucumoviruses". *Advances in Virus Research* **62** (2003), 241–323.

The Spread of Two Viral Strains on a Plant Leaf

Juan Carlos Cantero-Guardeño, Vladimir Sobolev, and Andrei Korobeinikov

1 Introduction

Our objective is to construct a mathematical model for the spread of two subtypes (a wild type and a mutant) of a virus on a plant leaf. A model that we are to construct has to take account of a number of observed facts, and in particular:

1. the presence of one type of virus in infected cells;
2. it is a system with competition between two types: the presence of one type suppresses the spread of the other;
3. co-infection is a very rare event: infection of a cell by one type prevent co-infection by the other strains; thus, in real life situation, there is a spatial separation of the two types of virus on a leaf.

Our hypothesis is that a presence of a sub-type within a cell suppresses proliferation of the competitors.

2 Model

Let $u(x,t)$ and $v(x,t)$ be the concentrations of the two sub-types of a virus, respectively, at a point $x \in [0,1]$ and at a time t. Modifying Fisher–Kolmogorov equation that satisfies hypothesis (1), in order to satisfy hypothesis (2) and (3),

J.C. Cantero-Guardeño • A. Korobeinikov (✉)
Centre de Recerca Matemàtica, Campus de Bellaterra, Barcelona, Spain
e-mail: canteroguardeno@gmail.com; akorobeinikov@crm.cat

V. Sobolev
Samara State Airspace University, Samara, Russia
e-mail: hsablem@gmail.com

M. Corbera et al. (eds.), *Extended Abstracts Spring 2014*, Trends in Mathematics 4,
DOI 10.1007/978-3-319-22129-8_17

we propose the following system of partial derivative equations as a model for the problem:

$$\begin{aligned}\frac{\partial u}{\partial t} &= \mu_1 \frac{\partial^2 u}{\partial x^2} + u(1-u-bv)(1-qv),\\ \frac{\partial v}{\partial t} &= \mu_2 \frac{\partial^2 v}{\partial x^2} + av(1-cu-hv)(1-ru),\end{aligned} \tag{1}$$

where $a, b, c, h, q, r \in \mathbb{R}^+$. Here the terms $1-qv$ and $1-ru$ reflect the suppression of proliferation of a type by the presence of the competing type. This system has to be complemented with Neumann (no-flux) boundary conditions

$$\begin{aligned}\frac{\partial u}{\partial x}(x=0,t) &= \frac{\partial u}{\partial x}(x=1,t) = 0,\\ \frac{\partial v}{\partial x}(x=0,t) &= \frac{\partial vu}{\partial x}(x=1,t) = 0.\end{aligned} \tag{2}$$

Without the "suppressing" terms $(1-qv)$ and $(1-ru)$, the system exhibits a very limited degree of the sub-types interaction. The steady-state in this case is a homogeneous distribution of the sub-types over the interval $[0,1]$.

3 Numerical Simulation

For simplicity, we assume that all parameters are the same for both sub-types:

$$\begin{aligned}\frac{\partial u}{\partial t} &= \mu \frac{\partial^2 u}{\partial x^2} + u(1-u-v)(1-qv),\\ \frac{\partial v}{\partial t} &= \mu \frac{\partial^2 v}{\partial x^2} + v(1-u-v)(1-qu),\end{aligned}$$

i.e., $\mu_1 = \mu_2 = \mu$, $q = r$ and $a = b = c = h = 1$. We also assume symmetric initial conditions

$$u(x,0) = \begin{cases} 0.9 & \text{for } x \in (0, 0.1)\\ 0 & \text{else,}\end{cases} \qquad v(x,0) = \begin{cases} 0.9 & \text{for } x \in (0.9, 1)\\ 0 & \text{else.}\end{cases}$$

Depending on a value of q, we observed the spatial separation of the two types. For comparatively small q, such as that in Figs. 1 and 2, where $q = 0.1$, both $u(x,t)$ and $v(x,t)$ tend to a homogeneous steady state $u(x,t) = v(x,t) = 0.5$. For larger values of q, for instance such as that in Figs. 3 and 4, where $q = 5$ (and for the same value of $\mu = 0.00001$ the same initial conditions), the system tends to a steady state with

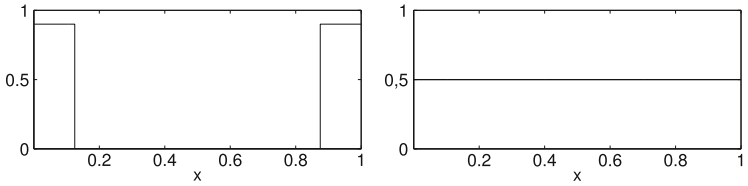

Fig. 1 Initial conditions $u(x, t = 0)$ (the left-hand column on the *left plot*) and $v(x, t = 0)$ (the right-hand column on the *left plot*), and $u(x, t = 100000) \approx v(x, t = 100000)$ on the *right plot*; for $q = 0.1$

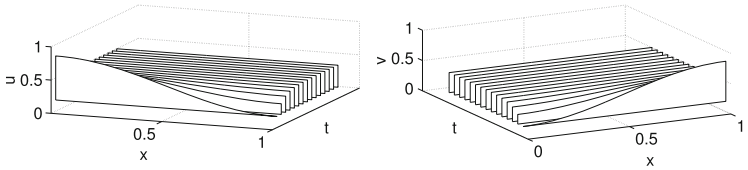

Fig. 2 Evolutions of the function $u(x, t)$ (*left*) and $v(x, t)$ (*right*) for $t \in [0, 100000]$ and $q = 0.1$

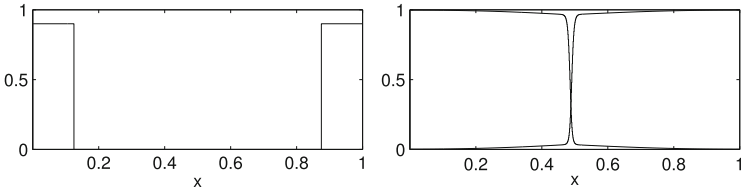

Fig. 3 Initial conditions $u(x, t = 0)$ (the left-hand column on the *left plot*) and $v(x, t = 0)$ (the right-hand column on the *left plot*), and $u(x, t = 100000) \approx v(x, t = 100000)$ on the *right plot*; for $q = 5$

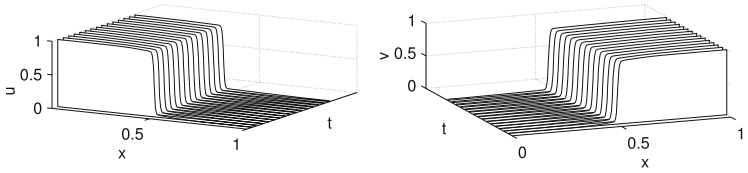

Fig. 4 Evolutions of the function $u(x, t)$ (*left*) and $v(x, t)$ (*right*) for $t \in [0, 100000]$ and $q = 5$

spatial separation of the two types. Thus, the computations clearly indicate that the separation of two viral types is possible for some q.

4 Analysis of the Stability of Homogeneous Solution

Consider the homogeneous solution $(u(x,t), v(x,t)) = (\overline{u}, \overline{v})$, $\forall\,(x,t) \in [0,1] \times \mathbb{R}^+$ of the system (1) satisfying $1 - \overline{u} - b\overline{v} = 0$ and $1 - c\overline{u} - h\overline{v} = 0$. Here, $\overline{u} = (b-h)/(bc-h)$ and $\overline{v} = (c-1)/(bc-h)$. Let us consider a perturbation of this solution in the form

$$(u(x,t), v(x,t)) = (\overline{u} + \xi(x,t), \overline{v} + \eta(x,t)).$$

Then, ξ and η must satisfy the following system of partial differential equations:

$$\xi_t = \mu_1 \xi_{xx} + A(b\eta + \xi), \quad A = \tfrac{(h-b)((bc-h)-q(1-c))}{(bc-h)^2},$$

$$\eta_t = \mu_2 \eta_{xx} + B(h\eta + c\xi), \quad B = a\tfrac{(1-c)((bc-h)-r(b-h))}{(bc-h)^2}.$$

Assuming that either $h < b$ and $1 < c$, or $h > b$ and $1 > c$, and denoting $\tau = bc - h$, we can conclude that the steady-state $\overline{u}, \overline{v}$ is unstable (A and B are both positive, and hence a small perturbation should increase), if

$$q > \frac{\tau}{b-h} \quad \text{and} \quad r > \frac{\tau}{c-1}$$

hold. Furthermore, under these same conditions, steady-state $\overline{u}, \overline{v}$ is stable (A and B are both negative, and hence a small perturbation would eventually disappear), if

$$q < \frac{\tau}{b-h} \quad \text{and} \quad r < \frac{\tau}{c-1}$$

hold.

For the simplified case with equal coefficients for both sub-types, that we numerically integrated, $\overline{u} = \overline{v} = 1/2$, and the system of partial differential equations for perturbations is

$$\xi_t = \mu \xi_{xx} + \left(\frac{q}{4} - \frac{1}{2}\right)(\eta + \xi),$$

$$\eta_t = \mu_2 \eta_{xx} + \left(\frac{q}{4} - \frac{1}{2}\right)(\eta + c\xi).$$

Hence the system asymptotic behaviour depends on the sign of $q/4 - 1/2$. That is, it depends on whether the parameter q is greater or smaller than 2: for $q < 2$ the system tends to the homogeneous steady-state $u = v = 1/2$, while for $q > 2$ the system tends to the non-homogeneous solution with a separation of $u(x,t)$ and $v(x,t)$. This result is congruent with the numerical simulation that we described above.

5 Conclusion

These computations and analysis confirm that the proposed model with the suppression of proliferation of a competing type by a type that infected a cell first is capable to describe the observed spatial separation of viral subtypes on a plant leaf.

Acknowledgements V.S. is partly supported by RFBR grants 13-01-97002-p and by the Ministry of education and science of the Russian Federation in the framework of the Program for increasing the competitiveness of SSAU for 2013–2020 years, 12-08-00069. A.K. is supported by the Ministry of Science and Innovation of Spain via Ramón y Cajal Fellowship RYC-2011-0806 and grant MTM2011-29342, by CONACYT (Mexico) via grant N 219614, and by AGAUR, Generalitat de Catalunya via grant 2014SGR1307.

Tracking the Population Dynamics of Plant Virus Escape Mutants

Santiago F. Elena

One of the most challenging problems in agronomy is to obtain plants that are resistant to the infection of pathogens. Not only this, but also that resistance must be as durable as possible. Unfortunately, most, if not all, strategies to generate such resistant plants have been overcome by the tremendous evolutionary potential of viral pathogens. In recent years, a new strategy based on the transgenic expression of artificial micro-RNAs (amiRs), designed to target viral genomes and induce their degradation, has been developed. This resistance has proven to be highly effective and sequence-specific against several plant viruses infecting *Arabidopsis thaliana* [7]. However, before these transgenic plants can be deployed in the field, it was important to evaluate the likelihood of the emergence of resistance-breaking mutants [2, 5]. Two issues were of particular interest: (1) whether such mutants can arise in non-transgenic plants that may act as reservoirs for the viral populations and (2) whether a suboptimal expression level of the transgene, resulting in sub-inhibitory concentrations of the amiR, would favor the emergence of escape mutants.

1 Evaluating the Durability of amiR-Mediated Resistance Against Evolving Virus Populations

To address the first of the above issues, we experimentally evolved independent lineages of *Turnip mosaic virus* (TuMV; genus *Potyvirus*, family Potyviridae) in fully susceptible wild-type *A. thaliana* plants and then simulated the spill over

S.F. Elena (✉)
Instituto de Biología Molecular y Celular de Plantas (CSIC-UPV), València, Spain

Santa Fe Institute, Santa Fe, NM, USA
e-mail: sfelena@ibmcp.upv.es

M. Corbera et al. (eds.), *Extended Abstracts Spring 2014*, Trends in Mathematics 4,
DOI 10.1007/978-3-319-22129-8_18

of the evolving viral populations to fully resistant *A. thaliana* transgenic plants. To address the second issue, the evolution phase took place with transgenic plants that expressed the amiR at sub-inhibitory concentrations. In both cases, 25 independent evolutionary lineages were generated and maintained until resistance was broken. Our results show that TuMV populations replicating in susceptible hosts accumulated resistance-breaking alleles that resulted in the overcoming of the resistance of fully resistant plants [3]. The rate at which resistance was broken was seven times higher for TuMV populations that experienced sub-inhibitory concentrations of the antiviral amiR [3].

A molecular characterization of escape alleles using Sanger sequencing showed that the target genomic sequence of all TuMV escape mutants contained at least one nucleotide substitution, generally a transition of the G-to-A and C-to-U types, with many instances of convergent molecular evolution. Most of these mutations were synonymous but a few changed the encoded amino acid.

Using an adaptation of the classic Luria–Delbrück fluctuation test, we also evaluated in vivo the mutation rate of TuMV on the amiR locus [1], and found that it was in the lower side of values reported for other RNA viruses [8]: 5×10^{-5} mutations per nucleotide and generation.

2 A Population Genetic Model of the Dynamical Process

To better understand the viral population dynamics taking place within each host, as well as to evaluate relevant population genetic parameters, we performed in silico simulations of the experiments [3]. The experiments were simulated using a bit string Monte Carlo model in which digital genomes were represented by binary strings, $\mathbf{S}$, of length $L = 31$ bits. The digital genomes explicitly considered the 21st of the target and added ten more bits, each corresponding to one of the ten viral cistrons. We made this distinction to disentangle the effects due to mutation in the target (evaluated at the challenging step of the experiment) from those associated to changes in other viral genes and that determine the overall fitness of the virus. Maximum string population size was set to $N_{\max} = 5000$ genomes. The simulation model considered 25 independent lineages. Each lineage started with a sample of size $N < N_{\max}$ of wild type genomes. For each lineage we let the population to experience τ replication events. At each event, two locations in the population were randomly chosen. If location i already contained a string, it was copied to site j with probability

$$P_{ij} = \frac{1}{1 + \exp\left(-\triangle f_{ij}/T\right)},$$

which depends on the fitness difference $\triangle f_{ij} = f_i - f_j$ between strings $\mathbf{S}_i$ and $\mathbf{S}_j$ (if site j is empty $f_j = 0$). Here, T is the Boltzman temperature, which is a measure of the noise tied to replication events and it was fixed to $T = 0.2$. The fitness of a given

string, S_k, is obtained from the binary composition of the 10 loci. We consider four types of deleterious fitness landscapes: additive ($\xi = 1$), antagonistic ($\xi < 1$) and synergistic ($\xi > 1$), plus one in which mutations in the bits representing the 10 viral cistrons were considered as lethal. For the three deleterious landscapes we compute the fitness as

$$f_k = 1 - d_H^{\xi}/10,$$

where d_H is the Hamming distance between sequence k and the corresponding wild type, and ξ measures the sign and strength of epistasis. During replication, each bit of the target mutated with probability μ. The other 10 loci mutated with probability $\mu_{l_i} = 3\mu v/2l_i$, where l_i is the length of locus i and the $2/3$ is introduced to consider that mutations at third codon positions are neutral. In order to differentiate between the experiments carried out in wild type and partially resistant plants, we consider that if the string chosen for replication was wild type it will be degraded with probability $\varepsilon = 0$ in wild type plants and $\varepsilon > 0$ for in partially resistant plants.

For each lineage we let the population to evolve over τ replication events according to the previous rules. Then, we took two random samples of size N. The first sample was used to initiate the next population (simulating the next passage in the experimental evolutionary lineages) until resistance was broken. The second sample was used to evaluate the likelihood of resistance-breaking as follows. For each string $\mathbf{S}_i$ in the second sample we evaluated its pathogenicity as

$$\theta(\mathbf{S}_i) = 1 - \Pi_{k=1}^{2l}[1 - \lambda(S_{ik})],$$

where $\lambda(S_{ik})$ is the empirical probability that a change in position k of the 21st target will be an escape mutation [5]. Next, we evaluated the likelihood of resistance breaking for this second sample, after 20 trials (the number of plants inoculated during the challenging experiments), as $P_b = 1 - (1 - \langle p \rangle)^{20}$, where $\langle p \rangle = \frac{1}{N}\sum_{i=l}^{N} \theta(\mathbf{S}_i)$ is the average pathogenicity of all the strains contained in the sample. If $P_b \geq 0.05$ we assumed that resistance was broken. For a sample of 20 plants this threshold means at least one plant becoming symptomatic.

The most robust estimates of model parameters were obtained for an additive fitness landscape with parameters. In the case of viruses evolved in wild type plants: $\langle \tau \rangle = 13{,}918$ replications between passages, $\langle \mu \rangle = 4.1 \times 10^{-5}$ mutations per site and generation and $\langle N_e \rangle \sim 19\,\%$ of the total population. Likewise, the parameters estimated for the viruses evolved in the partially resistant plants were $\langle \tau \rangle = 5629$, $\langle \mu \rangle = 7.7 \times 10^{-5}$, $\langle N_e \rangle \sim 1.4\,\%$ of the total population size, and $\langle \varepsilon \rangle = 0.22$ per genome. The estimated mutation rates are in excellent agreement with the empirical observations shown in the previous paragraph (Fig. 1). This data also suggests a major role of genetic drift.

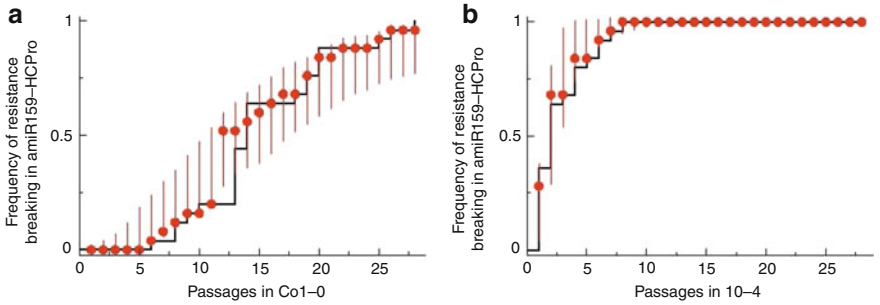

Fig. 1 Results of the simulation studies for the set of parameters that showed the best fit to empirical data (*solid lines*). *Left:* simulation results for the WT *A. thaliana*-evolved TuMV lineages. *Right:* simulation results for the TuMV lineages evolved in partially resistant 10–4 plants. The *red dots* correspond to the best-fitting trajectory obtained from the most optimized parameter set. *Red bars* denote the SD among 1000 runs of the simulation model using the best-fitting parameters. For details, see [4]

3 Molecular Characterization of the Evolutionary Dynamics of TuMV Populations

Next, to gain deeper insights into the population dynamics of these viral population, we used Illumina ultra deep sequencing to identify virus sequence variants at frequencies as low as 2×10^{-6} and to track their variation in time before and after the viral population was able of successfully infecting plants fully resistant to the ancestral virus [6]. We found that every site in the amiR-target sequence of the viral genome presented variation and that the variant that eventually broke resistance was sampled among the many coexisting ones. In this system, viral evolution in fully susceptible plants results from an equilibrium between mutation and genetic drift, whereas evolution in partially resistant plants originates from more complex dynamics involving mutation, selection, and drift. In both cases, genetic drift associated to the transmission events played an important role.

4 Development of More Durable Strategies

As we showed in the previous sections, a drawback of amiRs-based antiviral therapies in plants was the ease with which viruses generate escape mutations. In an attempt to increase the durability of transgenic resistance, we explored two alternative strategies for improving the effectiveness of resistance in plants [4]. First, we expressed two amiRs complementary to independent targets in the viral genome (the HC-Pro and the CP cistrons), and second, we designed amiRs complementary to a strictly conserved 29 nucleotides long RNA motif present at the 3′ end of the CP cistron. We found that both strategies reduced the probability of generating an

escape mutant more than 30-fold. Together, these results show that better and more rational ways of improving ami-based antiviral resistance in plants are possible.

Acknowledgements I thank N.H. Chua, J.M. Cuevas, J.A. Daròs, F. de la Iglesia, P.J. Gerrish, F. González-Candelas, J. Hillung, G. Lafforgue, S.S. Lin, F. Martínez, M. Morelli, Q.W. Niu, J. Sardanyés, and R.V. Solé for their contributions to different aspects of this project. Research was supported by grants RGP12/2008 from the Human Frontier Science Program Organization, PROMETEO2010/019 from the Generalitat Valenciana, and 2010TW0015 from CSIC.

References

1. F. de la Iglesia *et al.*, "Luria–Delbrück estimation of Turnip mosaic virus mutation rate in vivo". *J. Virol.* **86** (2012), 3386–3388.
2. J.A. García and C. Simón-Mateo, "A micropunch against plant viruses". *Nat. Biotechnol.* **24** (2006), 1358–1359.
3. G. Lafforgue *et al.*, "Tempo and mode of plant RNA virus escape from RNA interference-mediated resistance". *J. Virol.* **85** (2011), 9686–9695.
4. G. Lafforgue *et al.*, "Improving the effectiveness of artificial microRNA (amiR)-mediated resistance against Turnip mosaic virus by combining two amiRs or by targeting highly conserved viral genomic regions". J. Virol. **87** (2013), 8254–8256.
5. S.S. Lin *et al.*, "Molecular evolution of a viral non-coding sequence under the selective pressure of amiRNA-mediated silencing". PLoS Pathog. **5** (2009), e1000312.
6. F. Martínez *et al.*, "Ultradeep sequencing analysis of population dynamics of virus escape mutants in RNAi-mediated resistant plants". *Mol. Biol. Evol.* **29** (2012), 3297–3307.
7. Q.W. Niu *et al.*, "Expression of artificial microRNAs in transgenic Arabidopsis thaliana confers virus resistance". *Nat. Biotechnol.* **24** (2006), 1420–8.
8. R. Sanjuán *et al.*, "Viral mutation rates". *J. Virol.* **84** (2010), 9733–48.

Evolutionary Escape in Populations with Genotype-Phenotype Structure

Esther Ibáñez-Marcelo and Tomás Alarcón

1 Introduction

Evolutionary escape is the process whereby a population under sudden changes in the selective pressures acting upon it try to evade extinction by evolving from previously well-adapted phenotypes to those that are favoured by the new selective pressure. This evolutionary process is driven by gene mutations. Some examples are: (1) viruses evading anti-microbial therapy, (2) cancer cells escaping from chemotherapy, (3) parasite infecting a new host, and also (4) species trying to invade a new ecological niche.

Previous models of evolutionary escape have been developed by Iwasa et al. [5], and analysed in more detail by Sagitov and Serra [6] and Serra [7]. An alternative escape mechanism have been proposed in [1] whereby escape is achieved by means of a growth-restricted (quiescent) phenotype that is insensitive to the selective pressure (e.g., a drug).

Since selective pressures act on phenotypes rather than genotypes, evolutionary escape would be best described in terms of a population dynamics that accounts for the genotype-phenotype map. This modification alters the approach proposed by Iwasa and co-workers in two significant ways. First, due to evolved robustness in populations with genotype-phenotype map [3, 8–10], not every gene mutation necessarily generates a new phenotype. As a consequence, many gene mutations are neutral as far as the evolutionary escape process is concerned. Furthermore, it has been shown that the topology of genotype-phenotype networks is far from that of the hypercube lattice assumed by Iwasa et al. [2, 4]. In fact, we have recently shown that the corresponding phenotype network exhibits the small-world phenomenon

E. Ibáñez-Marcelo • T. Alarcón (✉)
Centre de Recerca Matemàtica, Campus de Bellaterra, Barcelona, Spain
e-mail: eibanez@crm.cat; talarcon@crm.cat

M. Corbera et al. (eds.), *Extended Abstracts Spring 2014*, Trends in Mathematics 4,
DOI 10.1007/978-3-319-22129-8_19

and that, as a consequence, accelerated evolvability (relative to that of a system with no genotype-phenotype map) may emerge.

Our aim is to extend the theory of evolutionary escape by analysing the effects on the probability of escape and the escape rate of considering that the evolutionary dynamics occurs on a genotype-phenotype network rather than on a regular hypercube. We apply a general theory, based on multi-type branching processes, to compute the evolutionary dynamics and probabilities of escape which takes into account the structure of the genotype-phenotype space and that only few species with a certain phenotype have a reproductive ratio R, (quotient between reproduction probability and death probability), greater than 1, which means that one of these individuals.

We consider two classes of graphs: B class comes from genotype-phenotype networks as modelled in [4] and H, an *artificial* genotype-phenotype graph where the genotype space is given by a hypercube.

2 Connectivity Structure of Genotype-Phenotype Networks

In order to estimate the time needed to hit the escape phenotype starting from another in B class graphs we consider the average shortest path length between phenotypes. Once we have that, we can know more about the structure of B graphs and use this information. Different structures appear in B genotype-phenotype networks. Some are clustered in big communities, others are in a unique community and also there are examples with a big community with some small communities.

On the other hand, we are going to introduce in a more detailed way how we obtain H genotype-phenotype networks. The process consists of given a graph B, we start with a hypercube with approximately same number of nodes than B graph and then we add phenotypes nodes with same phenotype degree distribution than in graph B. The obtained H networks, as we can expect, do not have community structure.

3 Mutation and Extinction Process

To explore networks we are going to use a Galton–Watson multi-type process. The escape phenotype has associated its corresponding genotypes (escape genotypes) and the process starts with an individual of certain genotype (with their corresponding phenotype). In the process main parameters that take part are: λ, reproduction probability of an individual and μ, mutation rate. Other parameters are defined from them, such as, probability of die $\sigma = 1 - \lambda$ and reproduction ratio $R = \lambda/\sigma$. Note that these parameters are independent of the parameters used to generate phenotype-genotype networks, B.

In order to characterize the process, we will look what can happen at each time step to each individual. This is, if an individual has a genotype of non escape:

- reproduction of the individual, with probability λ, producing depending on mutation rate μ: two new individuals identical to the ancestor, with probability $(1-\mu)^2$, mutated individual and a identical to the ancestor, with probability $2\mu(1-\mu)$ or two mutated individuals, with probability μ^2;
- die, with probability $\sigma = 1 - \lambda$.

On the other hand, if an individual has an escape genotype, this individual can not die. We refer to an escape genotype with rate $R = \lambda/\sigma > 1$, $(R = \infty)$.

Using the general Galton–Watson theory and defining $N_i(t)$ as the number of individuals of type i at time t, we consider the generating function of probability for type i,

$$f_i(s_1, \ldots, s_n; t) = \mathbb{E}(s_1^{N_1(t)} \cdot s_2^{N_2(t)} \cdots s_n^{N_n(t)} | N_i(0) = 1, N_j(0) = 0, \quad \forall j \neq i),$$

imposing that we start with one individual of type i (and zero, otherwise) at time 0. Here, n will be the number of different genotypes and $\vec{s} = (s_1, s_2, \ldots, s_n)$ is a parameter satisfying $0 \leq s_i \leq 1 \quad \forall i$. We define $A = (a_{ij})$ as the adjacency matrix of genotype network. Using Galton–Watson properties (like forward and backward equations) we can obtain the generating function $f_i(s_1, \ldots, s_n; t)$ from $f_i(s_1, \ldots, s_n; 1)$. This last, is defined as,

$$\begin{aligned} f_i(\vec{s}, 1) &= \mathbb{E}\big(s_1^{N_1(1)} \cdot s_2^{N_2(1)} \cdots s_n^{N_n(1)} | N_i(0) = 1, N_j(0) = 0, \quad \forall j \neq i\big) = \\ &= \sigma + s_i^2 \cdot \lambda \cdot (1-\mu)^2 + \sum_j 2a_{ij} s_i s_j \lambda \mu (1-\mu)/d_i + \sum_j a_{ij} s_j s_k \lambda \mu^2 / d_i^2. \end{aligned} \tag{1}$$

On the other hand, if we are in a escape genotype i, as it is immortal, the associated probability generating function is,

$$f_i(\vec{s}, 1) = \mathbb{E}\big(s_1^{N_1(1)} \cdot \cdots \cdot s_n^{N_n(1)} | N_i(0) = 1, N_j(0) = 0, \forall i \neq j\big) = s_i. \tag{2}$$

After defining the multi-type branching process, we are going to compute escape probabilities.

4 Computing Escape Probabilities

Let $N_e(t)$ be the number of individuals in escape genotype at time t, where $t \in \mathbb{N}$, and consider as initial condition:

$$(\vec{\theta}_0)_i := \begin{cases} 0 \text{ if } i \text{ is an escape genotype,} \\ 1 \text{ otherwise.} \end{cases} \qquad \text{and} \qquad \vec{\theta}_t := f(\vec{\theta}_0, t). \tag{3}$$

Then, $(\vec{\theta}_t)_i = P(N_e(t) = 0 | N_i(0) = 1, N_j(0) = 0, \quad \forall i \neq j)$, is the probability to not having any individual in escape genotypes, assuming that we have started with one individual of type i at time 0. Clearly,

$$P(N_e(\infty) > 0) = 1 - \theta_\infty = \sum_t P(N_e(t) > 0 \wedge N_e(t-1) = 0). \tag{4}$$

And it can also be checked that

$$P(N_e(t-1) = 0 \wedge N_e(t) > 0) | N_i(0) = 1, N_j(0) = 0, \forall i \neq j) = (\vec{\theta}_{t-1} - \vec{\theta}_t)_i. \tag{5}$$

Taken a graph of set B and another of H class, we compute the escape probabilities above described.

5 Results and Conclusions

We have been able to compute the probability of escape at time t [Eq. (5)] and the probability of escape (4) based on branching processes. These probabilities have been computed for two different kind of graphs: B and H genotype-phenotype networks.

The results obtained, for different mutation rates at H and B graphs, show that the probability to escape, $P(N_e(\infty) > 0)$, is higher in B graphs than in the hypercube graphs H. This fact is produced by the topological structure of B graphs, specially their local topology and small-world properties; see [4]. Moreover, if we compute the probability to escape in exactly each time t, $P(N_e(t) > 0 \wedge N_e(t-1) = 0 | N_i(0) = 1, N_j(0) = 0, \forall i \neq j)$ we obtain that these probability distributions follow an exponential distribution in both cases with the same tails. Also, we can note that a bigger variability of results is observed in the B genotype-phenotype graph, while in the hypercube case probabilities are less variable independently of the pair of genotypes chosen. This fact is given by a higher richness of structure in B graphs than in H graphs.

Finally, after obtaining an exponential distribution in the probability to escape at time t, we ask about the conditioned probability. This means, we compute the probability conditioned to escape, $P(N_e(t) > 0 \wedge N_e(t-1) = 0 | N_e(\infty) > 0, N_i(0) = 1, N_j(0) = 0 \quad \forall j \neq i)$, and compare results between H and B classes. Now, results seems very different for each genotype-phenotype structure: probability distribution of graph H is sharper and with smaller variance than in B class graph, where the probability is spread along a broad range of time. Here, the diameter of the graph turns out to be a crucial parameter of this conditioned distribution. Diameter in H graphs are smaller than in B graphs, and the probability to escape in a time greater than the diameter, assuming we are going to escape, is zero. Probabilities in B graphs are spread in all range of possible times shorter than the diameter. So, it does not

matter if we escape at time 8 or 50, because we know that we are going to escape. Remind that the diameter is defined as $\max_{(u,v)} d(u,v) \quad \forall (u,v)$ pair of nodes. This fact produces the spread through a wide range of time distribution in B graphs, and on the other hand, H probability distributions are sharped and concentrated in a small range of time to escape.

Another interesting result (not presented here) is that the decay of the probability escape distribution depending on time is 2λ, independently from the graph topology.

References

1. T. Alarcón and H.J. Jensen, "Quiescence: a mechanism for escaping the effects of drug on cell populations". *J. R. Soc. Interface* **8** (2010), 99–106.
2. J. Aguirre, J.M. Buldú, M. Stich, and S.C. Manrubia, "Topological sturcture of the space of phenotypes: The case of RNA neutral networks". *PLoS One* **6** (2011), e26324.
3. S. Ciliberti, O.C. Martin, and A. Wagner, "Robustness can evolve gradually in complex regulatory gene networks with varying topology". *PLoS Comput. Biol.* **3**(2) (2007), e15.
4. E. Ibáñez-Marcelo and T. Alarcón, "The topology of robustness and evolvability in evolutionary systems with genotype-phenotype map". *J. Theor. Biol.* **356** (2014), 144–162.
5. Y. Iwasa, F. Michor, and M.A. Nowak, "Evolutionary dynamics of invasion and escape". *J. Theor. Biol.* **226** (2004), 205–214.
6. S. Sagitov and M.C. Serra, "Multitype Bienayme–Galton–Watson processes escaping extinction". *Adv. Appl. Prob.* **41** (2009), 225–246.
7. M.C. Serra, "On the waiting time to escape". *J. Appl. Prob.* **43** (2006), 296–302.
8. A. Wagner, "Does evolutionary plasticity evolve?". *Evolution* **50** (1996), 1008–1023.
9. A. Wagner, "Robustness and evolvability in living systems". Princeton University Press, Princeton, NJ, U.S.A, 2007.
10. A. Wagner, "Neutralism and selectionism: A network-based reconciliation". *Nature Reviews Genetics* **9** (2008), 965–974.

Evolution of Stalk/Spore Ratio in a Social Amoeba: Cell-to-Cell Interaction via a Signaling Chemical Shaped by Cheating Risk

Yoh Iwasa

1 Introduction

The cellular slime mold, or social amoeba, exists as a unicellular form that divides and multiplies rapidly. When food is depleted, cells aggregate to form a fruiting body within which cells differentiate into spores and stalks. Some spores succeed in dispersing to a new micro-habitat with plenty of food and in resuming a unicellular phase with fast population growth. In contrast, stalk cells lift spores to aid in their dispersal and then die, see Fig. 1 (left). Becoming a stalk cell is an altruistic behavior, see [2]. This system provides an ideal system for studying the maintenance of altruism.

The developmental fate of a cell in a social amoeba is not fixed, but is decided based on interactions with other cells in the aggregation. A cell aggregation including both pre-spore cells and pre-stalk cells may be divided experimentally into two: one consisting mostly of pre-spore cells and the second consisting mostly of pre-stalk cells. In both of these groups, the relative abundance of the two cell types changes, resulting in an intermediate ratio of the two cell types.

Differentiation inducing factor-1 (DIF-1) controls stalk versus spore cells [1, 3]. It is produced by pres-pore cells and decomposed by pre-stalk cells [1]. It induces the differentiation of pres-pore cells into pre-stalk cells and suppresses differentiation of pre-stalk cells into pre-spore cells. Negative feedback results in a stable ratio of prestalk/prespore cells that will later differentiate into stalks and spores.

In [4], we modeled the mechanism of cell differentiation in *D. discoideum* controlled by a signaling chemical within cell aggregation, and discuss how the number of different cell types may be adjusted. When two strains are mixed in a fruiting body, one strain may predominantly become pre-spore cells, while the other

Y. Iwasa (✉)
Faculty of Sciences, Department of Biology, Kyushu University, Fukuoka, Japan
e-mail: yohiwasa@kyudai.jp

M. Corbera et al. (eds.), *Extended Abstracts Spring 2014*, Trends in Mathematics 4,
DOI 10.1007/978-3-319-22129-8_20

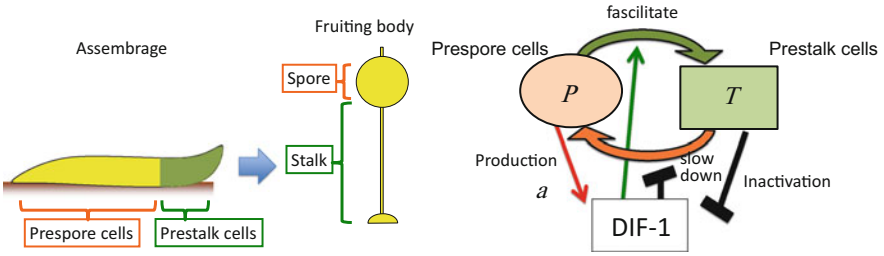

Fig. 1 *Left*: cells in an assemblage are differentiated to spore and stalk. *Right*: the cells between pre-spore (P) and pre-stalk (T) are controlled by chemical signal DIF-1

contributes more to pre-stalk cells, despite the fruiting body being formed by cells of single strains with the same stalk/spore ratio. We then considered the evolution of the rates of production of the signaling chemical, and cell sensitivity to the signaling chemical concentration.

2 The Model

We begin with the control of the stalk/spore cell ratio within an aggregation consisting of a single strain by the signaling chemical. Within the aggregation, cells change state between pres-pore cells and pre-stalk cells. After the proportion of cells in these states reaches equilibrium, pre-stalk cells and pre-spore cells develop into spores and stalks, respectively. Here, we consider the dynamics of the cell state change illustrated in Fig. 1 (right). We denote the number of pre-spore cells by P and that of pre-stalk cells by T. Cells change their states at the rates controlled by the amount of the signaling chemical, which is denoted by C,

$$\frac{dT}{dt} = f(C)P - g(C)T. \tag{1}$$

Here, the total number of cells $N = P + T$ is a constant. In (1), $f(C)$ is the rate of switching from pre-spore cells to pre-stalk cells, and is an increasing function of C. Since the signaling chemical promotes conversion from pre-spore cells to pre-stalk cells. $g(C)$ is the rate of switching from pre-stalk cells to pre-spore cells, and is a decreasing function of C. In the numerical analyses, we assumed $f(C) = f_0(C)$, and $g(C) = g_0/C$, where f_0 and g_0 are constants indicating the rate of conversion. The concentration of the signaling chemical follows:

$$\frac{dC}{dt} = aP - bCT. \tag{2}$$

The first term on the right hand side indicates that the signaling chemical is secreted by pres-pore cells at a rate of a per cell. The second term indicates that pre-stalk cells have an enzyme called DIF dechlorinase, which inactivates the signaling chemical.

Dynamics of (1) and (2) show that the ratio of pre-stalk cells to pre-spore cells converges to a globally stable ratio of T to P:

$$\hat{T}/\hat{P} = (f_0/g_0)^{1/3}(a/b)^{2/3}. \tag{3}$$

The ratio depends on f_0/g_0, the relative sensitivity to the signaling chemical between two reactions. It also depends on a/b, the ratio of the secretory capacity of signaling chemical and the inactivating capacity of signaling chemical. Since the equilibrium ratio of pre-spore cells and pre-stalk cells given by (3) is independent of the total number of cells N, the final proportion is independent of the total number of cells N, as observed in experiments; see [1].

Next, we consider the case in which multiple strains are mixed in the same fruiting body. We assume that there are two strains indicated by suffix $i\,(=1,2)$, and that both strains secrete and inactivate the same chemical, signaling chemical. Further, cells of the two strains switch between the two states according to the concentration of signaling chemical. T_i and P_i are the numbers of pre-stalk cells and pre-spore cells of strain i, respectively. The dynamics are as follows:

$$\frac{dT_i}{dt} = f_i(C)P_i - g_i(C)T_i, \qquad i = 1,2. \tag{4a}$$

Each strain shares 50 % of the total cell number N, and we have $T_i + P_i = N/2$ for $i = 1$ and 2. $f_i(C) = f_{0i}C$ is the rate of switching from a pre-spore cell to a pre-stalk cell of strain i, and $g_i(C) = g_{0i}/C$ is the rate of switching from a pre-stalk cell to a pre-spore cell of strain i. Cells of different strains may switch their states, but their sensitivity to the signaling chemical may differ. The production rate and inactivation rate of strain i are a_i and b_i, respectively. The dynamics of the chemical signal is given by

$$\frac{dC}{dt} = \sum_{i=1}^{2}\left(a_iP_i - b_iCT_i\right). \tag{4b}$$

Consider a case in which each fruiting body consists of a single strain. Here, two strains form a fruiting body of the same ratio of T to P when each fruiting body consists of cells from the same strain. However, when the strains are mixed in a fruiting body with 1 : 1 ratio, one strain develops more pre-spore cells and the other strain develops more pre-stalk cells. These values are calculated by Eq. (4). The strain that contributes less to stalk development may be called a cheater; see [2].

For the equilibrium condition of Eq. (4a), we have the following expression for the stalk/spore ratio:

$$\hat{T}_i/\hat{P}_i = \hat{C}^2 f_{0i}/g_{0i}, \quad (i = 1, 2), \qquad \text{and} \qquad \hat{C} = \sum_j a_j \hat{P}_j \Big/ \sum_j b_j \hat{T}_j. \tag{5}$$

Equation (5) indicates that the stalk/spore ratio at equilibrium is proportional to the ratio f_{0i}/g_{0i}. Hence, if there are two aggregated strains that differ in this ratio, the one with the smaller ratio can be regarded as a cheater because it contributes less to stalk formation. On the other hand, the cheater stain may have the same stalk/spore ratio when it forms a fruiting body consisting of cells from the same strain. This ratio is given by (3), which depends not only on f_0/g_0, but also on a/b. Thus, this simple model explains opponent-dependent cheating often observed in experiments; see [2].

3 Evolution

The cycle of unicellular life with asexual proliferation and fruiting body formation with dispersal occurs repeatedly. If the whole population is composed of multiple strains that differ in the number of surviving spore cells, the strain with the highest expected number of surviving spore cells increases in proportion, and eventually dominates the population after many cycles of proliferation and dispersal phases. In this section, we model this process of natural selection and discuss the evolutionary outcome.

3.1 No Mixing of Strains in a Fruiting Body

We begin with the case in which each fruiting body consists of a single strain. We consider a population composed of two strains: ξ and $1-\xi$ are the fractions of strain 1 and strain 2 in the beginning of a cycle, respectively. The success of dispersal and settlement to a new micro-habitat with a sufficient amount of food is an increasing function of the number of stalk cells:

$$S(\hat{T}) = S_0 \hat{T}^l/(\alpha' + \hat{T}^l). \tag{6}$$

Here, $\hat{T}$ is the total number of pre-stalk cells. Dispersal success increases with the number of stalk cells, but the rate of increase becomes lower for a large stalk cell number. Equation (6) saturates for a very large T. In addition, we consider the cost of signaling chemical secretion, which is expressed as a factor $e^{-ka_i}k$ is the magnitude of the cost to produce each unit amount of signaling chemical. For a fruiting body

composed only of strain i cells, the number of surviving spores of strain i is $W_i = \hat{P}_i S(\hat{T}_i) e^{-ka_i}$, where $i = 1, 2$ and W_i is proportional to the fitness of strain i. The fraction of strain 1 at the beginning of the next cycle can be expressed in terms of the fraction of strain 1 in the current cycle,

$$\xi^{\text{next}} = W_l \xi / (W_1 \xi + W_2 (1 - \xi)). \tag{7}$$

If this process of natural selection repeats over many generations, one strain may outcompete the other. If mutation introduces a new genotype into the population, it may go extinct or replace the old type. Mutation and replacement occur many times over the course of evolution, and the traits of the organism change slowly.

The evolutionary changes in the production rate (a) and the sensitivity to the chemical (f_0) caused by recurrent invasion of mutants and subsequent replacement are as follows: because the mutants are assumed to be close to the parent in phenotype, evolution appears as a continuous change in the traits. The traits quickly converge onto a curve in which the optimal ratio of stalk cells to spore cells is realized. After the convergence to this curve, changes along the curve occur slowly, where the production rate a decreases and the sensitivity f_0 increases.

3.2 When a Fruiting Body Consists of Multiple Strains

We next consider the case in which some fruiting bodies are a mixture of two strains. Specifically, we consider the following scenario. Let m be the fraction of fruiting bodies consisting of cells originating from the two initial cells, and $1 - m$ be the fraction of fruiting bodies consisting of cells originating from a single cell. If mutations occur recurrently and if the mutants are close to the parent in phenotype, the evolutionary trajectory of traits can be modeled. Unlike in the case without mixing, now the evolutionary equilibrium has a positive rate of chemical production $\bar{a}$ and an intermediate level of sensitivity to the chemical $\bar{f}_0$. When the degree of mixing m is positive, evolution would produce the equilibrium state with a faster production rate and lower sensitivity.

References

1. R.R. Kay and C.R.L. Thompson, "Cross induction of cell types in Dictyostelium: evidence that DIF-1 is made by prespore cells". *Development* **128** (2001), 4959–4966.
2. J.E. Strassmann, Y. Zhu, and D.C. Queller, "Altruism and social cheating in the social amoeba Dictyostelium discoideum". *Nature* **408** (2000), 965–967.
3. C.D. Town, J.D. Gross, and R.R. Kay, "Cell differentiation without morphogenesis in Dictyostelium discoideum". *Nature* **262** (1976), 717–719.
4. K. Uchinomiya and Y. Iwasa, "Evolution of stalk/spore ratio in social amoeba: cell-to-cell interaction via a singling chemical shaped by cheating risk". *Journal of Theoretical Biology* **336** (2013), 110–118.

Within-Host Viral Evolution Model with Cross-Immunity

Narani van Laarhoven and Andrei Korobeinikov

1 Introduction

In the last 20 years, a considerable amount of research has been done in order to mathematically study the dynamics of viruses and immunity, and HIV in particular. A mathematical model of within-host dynamics of HIV, which incorporates random mutations modelled by diffusion in a continuous one dimensional strain space and postulates that immune response is phenotype specific, shows that for a fast evolving virus the phenotype specific immune response is not able to clear HIV from its host. In this contribution, we develop the model further by including a cross-immunity, rather than specific immunity, modelled by a weight function which represents the broadness of cross-immunity. Numerical simulations show that if the cross-immunity is sufficiently broad, cell mediated immune response is able to clear a virus from its host.

2 The Model

The model of virus dynamics due to Wodarz et al. [6],

$$\begin{aligned} \frac{du(t)}{dt} &= b - \beta u(t)v(t) - cu(t), \\ \frac{dv(t)}{dt} &= \beta u(t)v(t) - mv(t), \end{aligned} \tag{1}$$

N. van Laarhoven • A. Korobeinikov (✉)
Centre de Recerca Matemàtica, Campus de Bellaterra, Barcelona, Spain
e-mail: nvlaarhoven@crm.cat; akorobeinikov@crm.cat

M. Corbera et al. (eds.), *Extended Abstracts Spring 2014*, Trends in Mathematics 4,
DOI 10.1007/978-3-319-22129-8_21

will be the basis for the model developed in the present extended abstract. Here, $u(t)$ and $v(t)$ are the population of uninfected and infected target cells, respectively. This model implicitly assumes that the population of free virus particles, which are produced by infected cells and infect target cells, have a life cycle which is much faster than that of the host cells. This assumption reduces the three-dimensional Nowak and Bangham [3] and Nowak and May [4] models to the two-dimensional model (1). In this model, uninfected cells are postulated to be produced at constant rate b and have natural death rate proportional to its population size $cu(t)$. Uninfected cells become infected at rate $\beta u(t)v(t)$, and infected cells die with a rate $mv(t)$.

Let us assume that several viral strains simultaneously coexist. Each strain can be described by a set of parameters, and all possible values of these parameters form a phenotype space, which we assume to be continuous. Since a viral strain is characterized by its basic reproduction number $R_0 = b\beta/cm$ (see [1, 2]), it suffices to consider a one-dimensional phenotype space $M = \{s \in [0, \infty)\}$, where s is proportional to R_0 and can serve as a measure of the viral fitness. Then $v(t, s)$ is the distribution of the infected population in the strain space, and $V(t) = \int_0^\infty v(t, s)ds$ is the total infected population. For simplicity, we assume $\beta(s) = as$, and new strains to emerge as a result of random mutations, which in a continuous strain space can be modelled by the diffusion. These assumptions lead to the following model, which is due to Korobeinikov and Dempsey [1]:

$$\begin{aligned} \frac{du(t)}{dt} &= b - u(t)\int_0^\infty \beta(s)v(t, s)ds - cu(t), \\ \frac{\partial v(t, s)}{\partial t} &= \beta(s)u(t)v(t, s) - mv(t, s) + \mu\frac{\partial^2 v(t, s)}{\partial s^2}. \end{aligned} \tag{2}$$

This model can be further developed by introducing $z(t, s)$ as the number of CTL cells at time t, able to recognize and kill infected cells of phenotype s. Llensa and Korobeinikov [2] modelled phenotype-specific immune response by describing the killing of infected cells by CTL by a term proportional to the product of the population of infected cells and the population of killer T-cells, thus adding to the second equation of model (2) a term $-\xi v(t, s)z(t, s)$. The dynamics of CTL cells were described by adding a third equation,

$$\frac{\partial z(t, s)}{\partial t} = qv(t, s) + \gamma z(t, s)\big(1 - \frac{z(t, s)}{p}\big),$$

such that the activation term of CTL response is proportional to the infected cell population and after activation of CTL response, the activated cells multiply according to the logistical term. By a numerical simulation of this model, Llensa–Korobeinikov showed that phenotype specific immune response is not able to clear HIV from the host.

In reality, immune cells that arise in response to a specific viral genotype can also be partly effective against mutant genotypes, which are sufficiently close to

the original one. This so-called cross-immunity can be modelled by replacing term $\xi v(t,s)z(t,s)$ by $\xi v(t,s)\int_0^\infty \eta(s,r)z(t,r)dr$; thus, we obtain the following model of study:

$$\begin{aligned}
\frac{du(t)}{dt} &= b - u(t)\int_0^\infty \beta(s)v(t,s)ds - cu(t),\\
\frac{\partial v(t,s)}{\partial t} &= \beta(s)u(t)v(t,s) - mv(t,s) + \mu\frac{\partial^2 v(t,s)}{\partial s^2}\\
&\quad - \xi v(t,s)\int_0^\infty \eta(s,r)z(t,r)dr,\\
\frac{\partial z(t,s)}{\partial t} &= qv(t,s) + \gamma z(t,s)\Big(1 - \frac{z(t,s)}{p}\Big).
\end{aligned} \tag{3}$$

A natural choice for the weight function $\eta(s,r)$ is the normal distribution

$$\eta(s,r) = \frac{1}{\sigma\sqrt{2\pi}}e^{-\frac{(s-r)^2}{2\sigma^2}},$$

since we want immune cells that arise in response to a specific genotype s to be most affective against viral strains of the same genotype and partly affective to viral strains of genotype $r \in M$, which are close to s. The closer r is to s, the more affective CTL response should be. Furthermore, we want $\int_0^\infty \eta(s,r)dr$ to be equal to one. The standard deviation σ of the normal distribution represents the broadness of cross-immunity in this case.

To complement the system, we need some boundary and initial conditions. Since $v(t,s)$ is a distribution, it is natural to assume that $v(t,s) = 0$ at $s = +\infty$. The choice for the boundary condition at $s = 0$ is not that obvious, and we will assume the no-flux condition $\partial v(t,s)/\partial s = 0$ at $s = 0$ for convenience. Furthermore, we need non-negative initial conditions $u(0) = u_0$ and $v(0,s) = v_0(s)$ and $z(0,s) = z_0(s)$ at $t = 0$.

3 Results

Figure 1 show the total concentrations of the uninfected and infected cells, respectively, for model (3). These results are obtained numerically using a semi-explicit method on a time interval from $t = 3650$ to $t = 3850$, and s is considered in the interval $[6, 9.5]$. In order to answer the main question (namely *if cross-immunity is sufficiently broad, is CTL response able to clear a virus from its host?*), in these simulations we vary variance σ, while keeping all other parameters of the model fixed. In the computations we use the same parameters as those in [1] that correspond to a certain patient with HIV: $b = 20$ cells/(mm$^3\cdot$ day), $c = 0.02$

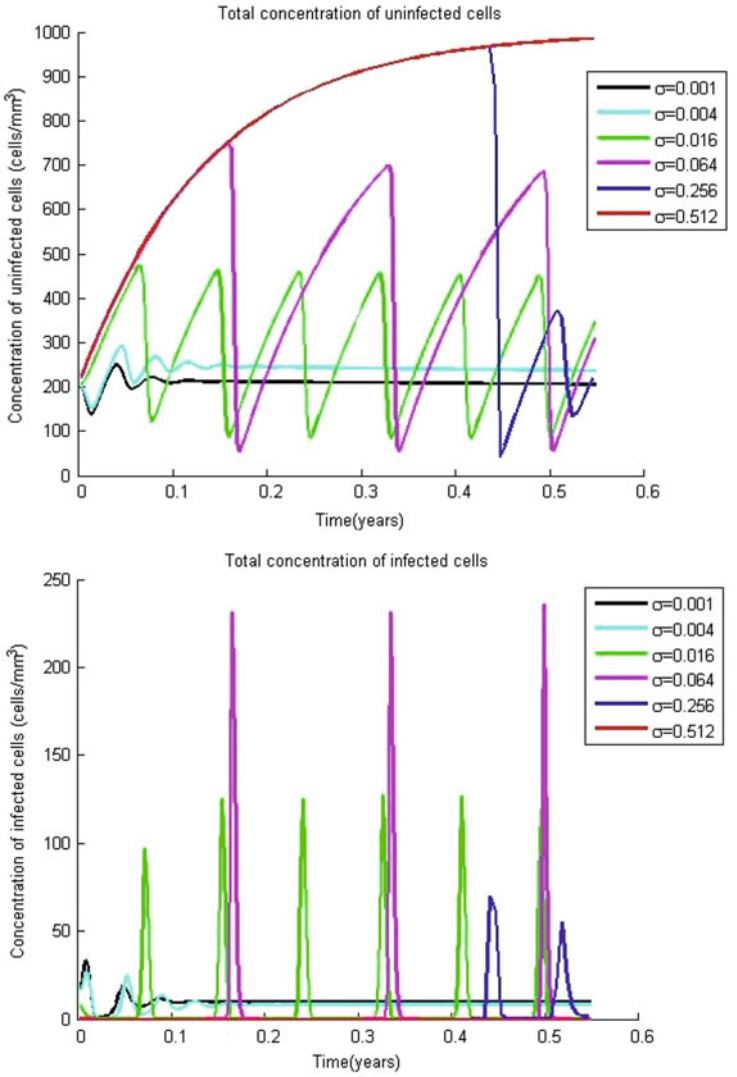

Fig. 1 Dynamics of the total population of the uninfected (*top*) and infected (*bottom*) cells in time for 200 days, for $\sigma = 0.001 \cdot 2^k$, $k \in \{0, 2, 4, 6, 8, 9\}$

day^{-1} and $m = 0.8$ day^{-1}. Furthermore, we choose $a = 10^{-3}$ mm^3/(cells·day). The immunity parameters are due to [2]: $\xi = 0.01$ mm^3/(cells·day), $q = 2 \cdot 10^{-3}$ days^{-1}, $\gamma = 1$ days^{-1} and $p = 2000$ cells/mm^3.

Note that for a comparatively narrow cross-immunity, when $\sigma = 0.001$ and $\sigma = 0.004$, the number of infected and uninfected cells quickly reach a quasi-equilibrium state, while the number of uninfected cells increase and the number of infected cells

decrease as σ increases. For $0.016 \leq \sigma \leq 0.256$, oscillations of both the uninfected cell and the infected cell levels occur. However, there appears to be a value for σ, namely $\sigma = 0.512$, such that these oscillations do not persist. We can conclude, therefore, that there indeed is a critical value σ_{CR}, which guarantees elimination of an infection.

Let us consider why oscillations occur for certain values of σ. Since mutations are modelled by diffusion, $v(t, s) > 0 \forall s \in M$. Therefore, there are values of σ, such that cross-immunity is sufficiently broad to apparently kill a virus on a broad interval of s. However, it is still not broad enough to kill the virus for all $s > 0$. A new peak in the distribution of infected cells can arise for strains that have not yet been recognized by the immune system. This increase in $v(t, s)$ triggers $z(t, s)$ such that the new peak in the distribution of infected cells is immediately suppressed again by CTL, and the same process starts over again. However, for $\sigma = 0.512$, cross-immunity is sufficiently broad to keep the infected cell population at zero level.

4 Discussion

The aim of this contribution was to further develop the model of within-host viral evolution with specific immunity, proposed by Korobeinikov and Llensa [2], by incorporating cross-immunity instead of specific immunity. Numerical simulations show that if cross-immunity is sufficiently broad, then CTL response is able to clear a virus from its host. We have seen that, for a certain broadness of cross-immunity, oscillations in the uninfected and infected cell populations arise. Whether or not these oscillations were clinically observed, is a question which lies beyond the scope of this research, due to time limitations. However, it is noteworthy that the outbreaks of the viral load closely resemble the phenomenon of the so-called viral blips [5].

An interesting topic of further research would be to find the relationship between the critical broadness of cross-immunity needed to clear a virus from its host, and the other parameters discussed in the model; especially after developing the model further by incorporating drug therapy.

References

1. A. Korobeinikov and C. Dempsey, “A continuous strain-space model of viral evolution within a host”. *Math. Biosci. Eng.* **11**(4) (2014), 919–927.
2. C. Llensa and A. Korobeinikov, “HIV evolution with random mutations and immune response”. Research report, CRM, 12 pages, (2013).
3. M.A. Nowak and C.R.M. Bangham, “Population dynamics of immune responses to persistent viruses”. *Science* **272** (1996), 74–79.
4. M.A. Nowak and R.M. May, “Virus Dynamics: Mathematical principles of immunology and virology”. Oxford University Press (2000).

5. D. Sánchez and T. Alarcón, “Are viral blips in HIV-1-infected patients clinically relevant?” Abstract for Workshop on Virus dynamics and evolution, CRM, (2014).
6. D. Wodarz, J.P. Christensen, and A.R. Thomsen, “The importance of lytic and nonlytic immune responses in viral infections”. *Trends in Immunology* **23**(4) (2002), 194–200.

Modelling Viral Evolution and Adaptation

Susanna Manrubia

1 Introduction

Viral populations are extremely plastic [5]. They maintain and steadily generate high levels of genotypic and phenotypic diversity that result in the coexistence of several different viral types in quasi-species, and eventually constitute a powerful tool to deploy different adaptive strategies. The interest in understanding and formally describing viral populations has steadily increased. At present, there are major unknown factors that difficult the construction of realistic models of viral evolution, as the way in which mutations affect fitness [19] or, in a broader scenario, which is the statistical nature of viral fitness landscapes. Our understanding of viral complexity is however improving thanks to new techniques as deep sequencing [17] or massive computation, and to systematic laboratory assays that reveal that, as other complex biological systems (e.g., cancer or ecosystems) the term *virus* embraces a dissimilar collection of populations with a remarkable ensemble of evolutionary strategies. New empirical data and improved models of viral dynamics are clearing up the role played by neutral networks of genotypes [21], by defective and cooperative interactions among viral mutants [13], by co-evolution with immune systems [22], or by changes in host populations [10], to cite but a few examples. Models of viral evolution are steadily improving their accuracy and becoming more competent from a conceptual and a predictive viewpoint [11, 12]. Here, we review some examples were well-motivated models of viral evolution succeed at capturing experimentally described features of those populations. Such are the relationship between intra-species competition and the geometry of the propagating substrate of a viral infection [3], the origin of bipartite viral genomes [8], and the adaptation to multi-drug therapies [9, 16].

S. Manrubia (✉)
Centro Nacional de Biotecnología (CSIC), Madrid, Spain
e-mail: smanrubia@cnb.csic.es

M. Corbera et al. (eds.), *Extended Abstracts Spring 2014*, Trends in Mathematics 4,
DOI 10.1007/978-3-319-22129-8_22

2 Infection Propagation in Space

The geometry of the physical space where the propagation of viral infections occurs affects quantities such as the probability of transmission from an infected to a susceptible host, the pace of accumulation of mutations, or the diversity that a viral population can sustain [1], but also to design effective contention strategies. There are two other features of infection propagation often disregarded in quasi-species models. First, the appearance of compensatory or beneficial mutations is non-negligible, especially for sub-optimally adapted viruses; second, viruses often encounter host resistance to infection. These two features were implemented in a model that studied the propagation of a viral population in 2D space, and showed that the dynamical behaviour and fate of those populations qualitatively differs from their mean-field counterpart. A first important difference between spatial and mean-field models with otherwise identical rules for viral dynamics is the appearance of clustering (of similar viral types) induced by spatial proximity, which fades as mobility increases [1] or as mutations rates augment [2]. This clustering causes a local advantage of less fit viral types, and hinders the advantage of high-fitness types, which are locally forced to compete with their equals. A second important fact regards the effect of host resistance. When spatial restrictions are absent, viruses can overcome host resistance by increasing its progeny production; however, if the number of available hosts is limited, augmenting progeny does not confer any additional advantage beyond a certain limit threshold. As a result, infection clearance may occur at a finite value of host resistance, a situation that maps the spatial model to a multi-component generalization of the Domany–Kinzel probabilistic cellular automaton [4], and thus classifies viral extinction within the directed percolation (DP) universality class.

3 On the Origin of Multipartite Viral Genomes

Multipartite viruses, characterized by fragmented genomes encapsidated in different virions (from two to eight fragments), represent about 50 % of all viruses infecting plants. Infection by such viruses is successful if at least one representative of each fragment is present in the cell—usually requiring a high multiplicity of infection (MOI). For viral multi-partition to be an evolutionary stable strategy, those viruses must compensate the cost of high MOI with an advantage originating from their fragmented nature. It was experimentally shown that such an advantage may arise from the higher stability of particles enclosing smaller genomes [14]. Inspired by those observations, a simple model of competition between a complete, wild-type virus encapsidated in a single particle and its bipartite counterpart was developed [8]. The model was successful at recovering the observations cited, assuming that bipartition appeared, as in the experiment, through segment deletion of the wild-type genome followed by competition between the two strategies. The

cooperating, smaller and fragmented solution, was able to displace the wild-type if MOI was above a threshold that could be analytically calculated. Since both fragments are symmetrically treated in the model (there were no experimental evidences indicating that they were different in any way), the stable solutions corresponded to equal amounts of each of the fragmented forms present in the population. In this scenario, the model made two predictions regarding the emergence and fixation of multipartite viruses with any number of fragments. First, it turned out that the values of MOI needed to compensate for the disadvantage of fragmentation appeared unrealistically high for viruses with four and more fragments; second, all stable solutions should present an equal amount of each of the fragmented types, any deviation from equal abundances resulting in even higher MOI values. However, it is known that the MOI of multipartite viruses is not as high as predicted by this simple model, and recent observations have come to challenge the second prediction, identifying significant imbalances in the frequencies of genomic fragments of two common plant viruses [18, 20]. The nature of the adaptive advantages enjoyed by these and likely many other multipartite viruses, and their evolutionary origin, are at this moment unsolved questions worth pursuing.

4 Viral Escape from Multidrug Therapies

Designers of antiviral therapies have to cope with the astonishing ability of viruses to escape medical treatments. The question is not whether a virus will develop resistance to an antiviral drug, but when will it occur. The simultaneous administration of two or more drugs has been used to delay the appearance of resistant mutants [6]. Searching for efficient therapeutic protocols, modelling may aid in three aspects: to characterize the response of viral populations to antiviral drugs through a more realistic implementation of their evolutionary strategies, to optimize drug administration protocols such that viral load is minimized, and to identify strategies that delay as much as possible the appearance of resistant forms [11]. A key issue to consider in multi-drug treatments is the possible interaction between the drugs involved. Combination therapies, where the drugs are simultaneously administered, are in general more efficient if the two drugs have a similar behaviour (e.g., both act as inhibitors of viral replication). However, in cases where a non-linear interaction between the effects caused by the two drugs is possible, a sequential administration might be preferred.

In experiments with foot-and-mouth disease virus, it was demonstrated that for a wide range of doses of an inhibitor of the viral replication and a mutagenic drug, their sequential administration ushered in a lower viral yield compared to their simultaneous use [15]. This fact motivated the design of a mathematical model that described viral dynamics and the response of the population to both drugs subjected to different modes of administration [9]. The model considered two types of viruses in the population, one susceptible to the inhibitor and another resistant. As indicated by experimental results, it was assumed that no resistance to the mutagen

could emerge. Viral properties (type of genome, replication mechanism, and basal mutation rate) were translated into model parameters, yielding a phase diagram where the preference of a sequential or combined administration of the drugs was quantified by means of the administered doses. The sequential treatment is preferred at high doses of both drugs, while for low doses a combination treatment is better suited. The precise dose value can be analytically calculated with the model. Further, it was also predicted that an intermediate region, where the combination treatment caused a lower viral load, but an increased likelihood of appearance of resistant forms (and vice versa for the sequential treatment), separated both phases at low doses of the inhibitor [16]. The disadvantage of a combination therapy at high doses of the mutagen (in particular) is due to the twofold effect of a mutagenic drug. On the one hand, it properly acts as an antiviral agent by augmenting the number of lethal and deleterious mutations in the population, increasing the number of defective (occasionally interfering) viral mutants. The latter are known to affect quasi-species fitness and may even cause the complete extinction of the population at doses below the error threshold [7]. On the other hand, it has been demonstrated that increases in the mutation rate may improve adaptation of suboptimal populations [12], since it produces higher diversity within the quasi-species and promotes the appearance of rare beneficial mutations. In the case of combination therapy, possible resistant forms that may get lost in absence of the inhibitor rapidly come to fixation due to the selection pressure it exerts.

5 Prospects

There are many unknowns regarding the adaptive potential of RNA viruses and their adaptive strategies. Current efforts are devoted to better understand and quantify the effect of mutational mechanisms, interactions within the mutant spectrum, and the role of the selective pressures at play. The fast increase in empirical knowledge and steady improvements in quasi-species models, together with technologies that are becoming easily accessible (as next generation sequencing or super-computation) are essential to acquire a better understanding of the general features involved in viral evolution and adaptation. Our hope for a meaningful theory of viral quasi-species depends on the existence of a reduced set of universal mechanisms, which should make possible the development of evolutionary theories of broad applicability. Advances in that direction are highly encouraging.

References

1. J. Aguirre and S.C. Manrubia, “Effects of spatial competition on the diversity of a quasis-pecies”. *Phys. Rev. Lett.* **100** (2008), 038106.
2. J.A. Capitán, J.A. Cuesta, S.C. Manrubia, and J. Aguirre, “Severe hindrance of viral infection propagation in spatially extended hosts”. *PLoS ONE* **6** (2011), e23358.

3. J.A. Cuesta, J. Aguirre, J.A. Capitán, and S.C. Manrubia, "The struggle for space: Viral extinction through competition for cells". *Physical Review Letters* **106** (2011), 028104.
4. E. Domany and W. Kinzel, "Equivalence of cellular automata to Ising models and directed percolation". *Phys. Rev. Lett.* **53** (1984), 311–314.
5. E. Domingo and J.J. Holland, "RNA virus mutations and fitness for survival". *Annu. Rev. Microbiol.* **51** (1997), 151–178.
6. J.B. Fitzgerald, B. Schoeberl, U.B. Nielsen, and P.K. Sorger, "Systems biology and combination therapy in the quest for clinical efficacy". *Nat. Chem. Biol.* **2** (2006), 458–466.
7. A. Grande-Pérez, E. Lázaro, E. Domingo, and S.C. Manrubia, "Suppression of viral infectivity through lethal defection". *Proc. Natl. Acad. Sci. U.S.A.*, **102** (2005), 4448–4452.
8. J. Iranzo and S.C. Manrubia, "Evolutionary dynamics of genome segmentation in multipartite viruses". *Proceedings of the Royal Society of London B* **279** (2012), 3812–3819.
9. J. Iranzo, C. Perales, E. Domingo, and S.C Manrubia, "Tempo and mode of inhibitor-mutagen antiviral therapies: A multidisciplinary approach". *Proc. Natl. Acad. Sci. U.S.A.* **108** (2011), 16008–16013.
10. K. Koelle, S. Cobey, B. Grenfell, and M. Pascual, "Epochal evolution shapes the phylodynamics of influenza A (H3N2) in humans". *Science* **314** (2006), 1898–1903.
11. S.C. Manrubia, "Modelling viral evolution and adaptation: challenges and rewards". *Current Opinion in Virology* **2** (2012), 531–537.
12. S. Manrubia and E. Lázaro, "Getting to Know Viral Evolutionary Strategies: Towards the Next Generation of Quasispecies Models". *Current Topics in Microbiology and Immunology*, pp. 1–17. Springer, Berlin/Heidelberg, 2015.
13. S. Ojosnegros, N. Beerenwinkel, T. Antal, M.A. Nowak, C. Escarmís, and E. Domingo, "Competition-colonization dynamics in an RNA virus". *Proc. Natl. Acad. Sci. U.S.A.* **107** (2010), 2108–2112.
14. S. Ojosnegros, J. García-Arriaza, C. Escarmís, S.C. Manrubia, C. Perales, A. Arias, M.G. Mateu, and E. Domingo, "Particle stability, a non-replicative trait in the transition towards viral genome segmentation". *PLoS Genetics* **7** (2011), e1001344.
15. C. Perales, R. Agudo, H. Tejero, S.C. Manrubia, and E. Domingo, "Potential benefits of sequential inhibitor-mutagen treatments of RNA virus infections". *PLoS Pathog* **5** (2009), e1000658.
16. C. Perales, J. Iranzo, S.C. Manrubia, and E. Domingo, "The impact of quasispecies dynamics on the use of therapeutics". *Trends Microbiol.* **20** (2012), 595–603.
17. A.D. Radford, D. Chapman, L. Dixon, J. Chantrey, A.C. Darby, and N. Hall, "Application of next-generation sequencing technologies in virology". *J. Gen. Virol.* **93** (2012), 1853–1868.
18. J.A. Sánchez-Navarro, M.P. Zwart, and S.F. Elena, "Effects of the number of genome segments on primary and systemic infections with a multipartite plant RNA virus". *J. Virol.* **87** (2013), 10805–10815.
19. R. Sanjuan, "Mutational fitness effects in RNA and single-stranded DNA viruses: common patterns revealed by site-directed mutagenesis studies". *Phil. Trans. R. Soc. Lond. B* **365** (2010), 1975–1982.
20. A. Sicard, M. Yvon, T. Timchenko, B. Gronenborn, Y. Michalakis, *et al.*, "Gene copy number is differentially regulated in a multipartite virus". *Nat. Comm.* **4** (2013), 2248.
21. A. Wagner, "The Origins of Evolutionary Innovations". Oxford University Press, 2011.
22. H.J. Woo and J. Reifman, "A quantitative quasispecies theory-based model of virus escape mutation under immune selection". *Proc. Natl. Acad. Sci. U.S.A.* **109** (2012), 12980–12985.

Changes in Codon-Pair Bias of Human Immunodeficiency Virus Type 1 Affect Virus Replication

Miguel Ángel Martínez

The standard genetic code consists of 64 codons for a set of 20 amino acids and the stop signal, showing its redundancy (except for tryptophan and methionine) and implying that several synonymous triplets encode for the same amino acid. Usually, the position of such synonymous codons is not constant along the protein coding sequences and therefore, their properties are not entirely comparable. Relative amounts of tRNAs iso-acceptors have been associated to codon usage patterns in different organisms. Codon usage bias, the frequency of occurrence of synonymous codons in coding DNA, in human cells is limited by amino acids needed for protein structure/function and by genome signatures (dinucleotide relative abundances). In contrast, translational and transcriptional influences appear to play a minor role in human codon usage [5].

The remarkable nucleotide composition of human immunodeficiency virus type 1 (HIV-1) genome, containing an above average percentage of A nucleotides, results in a codon composition different from the human one [17]. Specifically, the more flexible third codon positions are preferentially occupied by A nucleotides that usually induce ribosome pausing and inefficient translation [18]. Still, it is unclear whether HIV-1 codon composition is an adaptive trait or has neutrally evolved through genome drift. In both cases, it may influence HIV-1 evolution as well as drug resistance development. The frequent *G*-to-*A* mutations observed in HIV-1 genome might be associated to the action of APOBEC3 family host enzymes. Changes in codon composition may have a significant impact on different aspects of HIV-1. For instance, a codon-optimized gag HIV-1 showed a significant increase in protein expression (up to a 60 %) compared to wild type gag in an in vitro study [11]. However, it is unknown whether this codon optimization would increase viral fitness or virulence. Another study showed that recoding with a

M.Á. Martínez (✉)
Fundació irsiCaixa, Hospital Universitari Germans Trias i Pujol, Badalona, Spain
e-mail: mmartinez@irsicaixa.es

M. Corbera et al. (eds.), *Extended Abstracts Spring 2014*, Trends in Mathematics 4,
DOI 10.1007/978-3-319-22129-8_23

high level of preferred human codon usage may provoke the disruption of some unknown HIV-1 RNA properties deleterious for other reasons, e.g., disturbing the secondary structure of HIV-1 RNA genome [12]. Recent data have identified a novel antiviral mechanism within the innate immune response, in which human SLFN11 selectively inhibits viral protein synthesis in HIV-infected cells by means of codon-bias discrimination [7]. Synonymous substitutions optimizing for human cell expression reduces the antiviral activity of SLFN11. Synonymous mutation is thought to be selectively neutral. However, previous work demonstrated that synonymous substitutions can negatively affect the replication capacity of several RNA viruses [3], including HIV-1 [10].

While the non-random usage of synonymous codons for the same amino acids is defined as codon bias, the codon-pair bias means the non-random juxtaposition of codons in an open reading frame (ORF). Codon-pairs occur at irregular levels [4]. The observed juxtaposition frequency of two codons is different to that expected if those codons were randomly located next to each other. This codon-pair usage of two codon-pairs can be quantified as a codon-pair score (CPS) as well as the mean codon-pair bias score (CPB) through an ORF. Codon-pairs were found to be highly over-represented or under-represented independently from codon usage [4], and this was associated with increased or decreased levels of protein expression [13]. During translation in the ribosome, the formation of the peptide bond demands the adjustment of two codons and the accommodation of two tRNAs in the ribose [16]. It has been suggested that, for steric causes, not all the combinations of tRNAs and codons might be equally fitting on the ribosome surface, even though ribosomes are only occupied briefly by two tRNAs [16]. Therefore, some codon-pairs might have a translational benefit over others.

Independent groups have described that most under-represented codon-pairs possessed a central *CG* dinucleotide (e.g., the codon-pair Leu–Glu: *CTC-GAA*). CpG islands are methodically under-represented in mammals and viruses [1]. Probably, evolution lowered CpG content to avoid mammal innate immune system and elude to trigger an immune response induction. In a multiple ORFeome (a set of ORFs cloned from different species) analysis, translation was suggested to exert a more powerful impact on codon-pair bias than molecular mechanisms [15]. By analyzing in an ORFeome context the evolutionary conservation of codon usage compared to codon-pair usage, the trees topologies showed that, in eukaryotes, the resemblance of codon-pair usage is higher than codon usage. Those trees differ both in branch lengths and positions, suggesting that codon usage and codon-pair usage are independent, due to different molecular mechanisms [15]. Finally, a co-evolution between the translational machinery used and a given organism has been suggested. The consequence of that co-evolution is the non-randomness in codon-pair usage, probably explaining that, not only codon-pair bias, but also codon bias and tRNA iso-acceptors are species-specific. Despite the observed evidence of an actual CPB, as well as a means to accurately quantify CPB, it is not evident why this bias exists and what selective pressures are governing the preference of codons to be adjacent or apart from one another.

Recently, a new approach was used to rationally design live attenuated poliovirus and influenza virus vaccines [2, 9]. This approach works by recoding and synthesizing the viral genome. The wild type amino acid sequence is preserved while the existing synonymous codons are rearranged to create a suboptimal arrangement of codon-pairs [2]. For instance, eight different codon-pairs can encode the amino acid pair Ala–Glu. Thus, the expected frequency of each eight encodings can be calculated by multiplying the individual frequencies of codon usage of the two individual codons. In order to calculate the individual frequency of each codon, the consensus coding DNA sequence database dating from March 2005 and containing a total of 14,795 human genes was used [2]. If the ratio observed/expected is lower than one, this codon-pair is considered as under-represented and vice-versa. The natural logarithm of the ratio between observed/expected frequencies of each human codon-pair was used to calculate the CPS. A positive CPS implies that the codon-pair is statistically over-represented while a negative CPS implies that the pair is statistically under-represented. For an entire ORF, the CPB is calculated as a mean: the sum of all individual CPS in an ORF divided by the number of pairs present. If the CPB resulting is positive, the gene contains over-represented codon-pairs and vice-versa.

Poliovirus and influenza virus genomes were recoded in order to include infrequently used codon-pairs [2, 9]. When de-optimized, poliovirus and influenza virus displayed a much lower replication capacity in tissue culture. Moreover, mice previously immunized with deoptimized viruses, displayed a protective immunity when challenged with wild type virus. Thus, recoded viruses were efficiently used in mice as vaccines. The mechanism of attenuation remains unclear, though it has been suggested that translation might be affected [2, 9]. Since codon-pair de-optimization is the result of tens, hundreds, or even thousands of nucleotide substitutions, reversion to virulence is unlikely to occur. Attenuation may be fine-tuned by adjusting the extent of codon-pair de-optimization.

Using synonymous codon pairs, we recently rationally recoded and codon pair-optimized and de-optimized different moieties of the HIV-1 gag and pol genes [8]. De-optimized viruses had significantly lower viral replication capacity in MT-4 and peripheral blood mononuclear cells (PBMCs). Varying degrees of ex vivo attenuation were obtained, depending upon both the specific de-optimized region and the number of de-optimized codons. Importantly, a protease optimized virus carrying 38 synonymous mutations was not attenuated and displayed a replication capacity similar to that of the wild-type virus in MT-4 cells and PBMCs. Although attenuation was based on several tens of nucleotide changes, in our hands, de-optimized HIV-1 reverted to wild-type virulence after serial passages in MT-4 cells. Sequence clonal analysis of phenotypically reverted viral populations showed that phenotype reversion was due not only to the reversion of initially introduced synonymous mutations but also to the presence of new synonymous and non-synonymous mutations. Remarkably, no reversion was observed in the optimized virus. This result suggests that certain neutral genetic drift is operating in protease synonymous nucleotide residues and that, in addition to explore virus attenuation,

synonymous codon pair recoding can be used to explore other aspects of the HIV-1 biology.

Our data demonstrated that SAVE is a useful strategy to phenotypically affect the replicative properties of HIV-1. However, many questions remain to be answered. First, stability of de-optimized HIV-1 variants should be improved. We propose to generate de-optimized viruses with a lager number of substitutions but with lower CPSs to avoid lethality. We generated gag variants carrying more than 300 substitutions but only those carrying less than a hundred substitutions were viable [8], suggesting that CPSs above a threshold may be lethal. Second, it has been suggested that CPB may have an effect on translation [2]. Nevertheless, RNA sequences may be also targeted by factors other than those of the translation machinery (e.g., aberrant splicing, RNA decay process or miRNA targeting). In contrast to poliovirus and other RNA viruses HIV-1 DNA is permanently integrated into the host cell genome and transcribed by the host RNA polymerase II. Moreover, HIV-1 can initiate translation either by the classical cap-dependent mechanism or by internal recruitment of the ribosome through RNA domains called IRESs (internal ribosome entry sites). HIV-1 can be a very useful tool to know how CPB affects translation. Third, the fact that HIV-1 CPB optimized variants may have a replication capacity similar to that observed in wild type viruses opens the possibility of use these variants as tools to explore the presence of unknown functionally redundant RNA elements in the HIV-1 genome [14] or to explore the effect of the virus genome base content in the virus replication capacity [18]. Finally, to use optimized neutral virus variants may help to better define how HIV-1 deal with its high mutation rate in the real world and to define the mutation distribution of a viral population in order to establish the proportion of neutral mutations [6]. Previously, it was found that a codon pair base de-optimized poliovirus variant containing 224 synonymous substitutions did not revert its phenotype after 19 passages in HeLaR19 cells [2]. In contrast, we showed that highly attenuated HIV-1 variants carrying more or near 100 synonymous substitutions reverted their phenotype after 15 passages in MT-4 cells [8]. Differences in the life cycle between poliovirus and HIV-1 may account for the above discrepancies. Alternatively, differences in virus protein or genome mutational robustness and evolvability can not be discarded. The different codon usage between poliovirus and HIV-1 may determine differences in their mutational robustness and evolutionary capacity.

Acknowledgements This study was supported by the Spanish Ministry of Science and Innovation through grant SAF2013-41421-R.

References

1. J.R. Buchan, L.S. Aucott, and I. Stansfield, "tRNA properties help shape codon pair preferences in open reading frames". *Nucleic Acids Res* **34**(3) (2006), 1015–1027.
2. J.R. Coleman, D. Papamichail, S. Skiena, B. Futcher, E. Wimmer, and S. Mueller, "Virus attenuation by genome-scale changes in codon pair bias". *Science* **320**(5884) (2008), 1784–1787.
3. J.M. Cuevas, P. Domingo-Calap, and R. Sanjuan, "The fitness effects of synonymous mutations in DNA and RNA viruses". *Mol. Biol. Evol.* **29**(1) (2012), 17–20.
4. G.A. Gutman and G.W. Hatfield, "Nonrandom utilization of codon pairs in Escherichia coli". *Proc. Natl. Acad. Sci. U.S.A.* **86**(10) (1989), 3699–3703.
5. S. Karlin and J. Mrazek, "What drives codon choices in human genes?". *J. Mol. Biol.* **262**(4) (1996), 459–472.
6. A.S. Lauring, A. Acevedo, S.B. Cooper, and R. Andino, "Codon usage determines the mutational robustness, evolutionary capacity, and virulence of an RNA virus". *Cell Host Microbe* **12**(5) (2012), 623–632.
7. M. Li, E. Kao, X. Gao, H. Sandig, K. Limmer, M. Pavon-Eternod, T.E. Jones, S. Landry, T. Pan, M.D. Weitzman, and M. David, "Codon-usage-based inhibition of HIV protein synthesis by human schlafen 11". *Nature* **491**(7422) (2012), 125–128.
8. G. Martrus, M. Nevot, C. Andres, B. Clotet, and M.A. Martínez, "Changes in codon-pair bias of human immunodeficiency virus type 1 have profound effects on virus replication in cell culture". *Retrovirology* **10** (2013), 78.
9. S. Mueller, J.R. Coleman, D. Papamichail, C.B. Ward, A. Nimnual, B. Futcher, S. Skiena, and E. Wimmer, "Live attenuated influenza virus vaccines by computer-aided rational design". *Nat. Biotechnol.* **28**(7) (2010), 723–726.
10. M. Nevot, G. Martrus, B. Clotet, and M.A. Martínez, "RNA interference as a tool for exploring HIV-1 robustness". *J. Mol. Biol.* **413**(1) (2011), 84–96.
11. K.C. Ngumbela, K.P. Ryan, R. Sivamurthy, M.A. Brockman, R.T. Gandhi, N. Bhardwaj, and D.G. Kavanagh, "Quantitative effect of suboptimal codon usage on translational efficiency of mRNA encoding HIV-1 gag in intact T cells". *PLoS One* **3**(6) (2008), e2356.
12. R. Sanjuan and A.V. Borderia, "Interplay between RNA structure and protein evolution in HIV-1". *Mol. Biol. Evol.* **28**(4) (2011), 1333–1338.
13. Z.Q. Shao, Y.M. Zhang, X.Y. Feng, B. Wang, and J.Q. Chen, "Synonymous codon ordering: a subtle but prevalent strategy of bacteria to improve translational efficiency". *PLoS One* **7**(3) (2012), e33547.
14. Y. Song, Y. Liu, C.B. Ward, S. Mueller, B. Futcher, S. Skiena, A.V. Paul, and E. Wimmer, "Identification of two functionally redundant RNA elements in the coding sequence of poliovirus using computer-generated design". *Proc. Natl. Acad. Sci. U.S.A.* **109**(36) (2012), 14301–14307.
15. A. Tats, T. Tenson, and M. Remm, "Preferred and avoided codon pairs in three domains of life". *BMC Genomics* **9** (2008), 463.
16. S. Uemura, C.E. Aitken, J. Korlach, B.A. Flusberg, S.W. Turner, and J.D. Puglisi, "Real-time tRNA transit on single translating ribosomes at codon resolution". *Nature* **464**(7291) (2010), 1012–1017.
17. A.C. van der Kuyl and B. Berkhout, "The biased nucleotide composition of the HIV genome: a constant factor in a highly variable virus". *Retrovirology* **9** (2012), 92.
18. F.J. van Hemert, A.C. van der Kuyl, and B. Berkhout, "The A-nucleotide preference of HIV-1 in the context of its structured RNA genome". *RNA Biol.* **10**(2) (2013), 211–215.

Competing Neutral Populations of Different Diffusivity

Simone Pigolotti

1 Introduction

The possibility of moving in space is fundamental for the survival of many biological organisms. While movement patterns can sometimes be complex, reflecting evolutionary strategies to search for food, in many settings movement can be mathematically described as Brownian motion. Macroscopically, this leads to a description in terms of a diffusion equation, or a Fisher equation [2, 3] if birth-death dynamics is also taken into account.

In this work, I discuss a model of two competing species [6]. They are assumed to be neutral, i.e., characterized by the same birth and death/competition rates, except for having a different diffusion coefficient. While the outcome of a deterministic analysis is that the two species can coexist at any relative fraction, I will show that the fastest species tends to dominate when demographic stochasticity due to finite number of individuals is properly taken into account.

2 Results

We consider a particle model described by the following macroscopic equations:

$$\begin{aligned} \partial_t\, c_A(x,t) &= (D+\delta D)\nabla^2 c_A + \mu c_A(1-c_A-c_B) + \sigma_A\, \xi_A(x,t), \\ \partial_t\, c_B(x,t) &= D\nabla^2 c_B + \mu c_B(1-c_A-c_B) + \sigma_B\, \xi_B(x,t), \end{aligned} \tag{1}$$

S. Pigolotti (✉)
Departament de Física i Enginyeria Nuclear, Universitat Politècnica de Catalunya, Terrassa, Spain
e-mail: simone.pigolotti@upc.edu

M. Corbera et al. (eds.), *Extended Abstracts Spring 2014*, Trends in Mathematics 4,
DOI 10.1007/978-3-319-22129-8_24

where $\sigma_A = \sqrt{\mu c_A(1 + c_A + c_B)/N}$ and symmetrically for σ_B. The parameter N, typical of a Van Kampen expansion, tunes the noise amplitude and can be interpreted as the number density that corresponds to a macroscopic concentration $c = 1$. Now, $\xi_A(x, t)$ and $\xi_B(x, t)$ are independent noise sources, delta-correlated in space and time, $\langle \xi_i(x, t)\xi_j(x', t')\rangle = \delta_{ij}\delta(x - x')\delta(t - t')$. An equation for the relative concentration of species A, $f = c_A/(c_A + c_B)$, is readily obtained from Eq. (1), by means of Ito's formula [7, 8]. Upon neglecting fluctuations of the total particle density by imposing $c_A + c_B = 1$ at the end of the procedure, the equation reads:

$$\partial_t f = D\nabla^2 f + \delta D(1 - f)\nabla^2 f + \sigma\xi, \tag{2}$$

where $\sigma = \sqrt{2\mu f(1 - f)/N}$. Equation (2) is the starting point of our analysis. Setting $\delta D = 0$ in (2) yields the equation for spatial neutral dynamics of an allele having concentration f, see [4, 8]. Deterministically (i.e., in the limit $N \to \infty$) any state f equal to constant is a meta-stable solution of (2), meaning that one can expect coexistence. In the stochastic case of finite N, the net average effect of the difference in diffusivity can be understood by studying the time evolution of the integrated mean concentration $F(t) = \langle f\rangle$, where $\langle\cdot\rangle$ denotes an average over space and noise. Assuming periodic boundary conditions and averaging Eq. (2) we obtain

$$\frac{dF}{dt} = \frac{\delta D}{L}\int_0^L dx\, (\nabla f)^2 > 0. \tag{3}$$

The above equation shows that $F(t)$ grows with time for any $\delta D > 0$, meaning that a larger diffusion confers an average advantage, as shown in Fig. 1.

A simple calculation shows that $dF(t)/dt = (D/2)\nabla^2 H(x, t)|_{x=0}$, where we introduced the *heterozygosity* function $H(x = x_1 - x_2, t) = \langle f(x_1)[1 - f(x_2)] + f(x_2)[1 - f(x_1)]\rangle$, which depends only on $x_1 - x_2$ and t due to translational invariance. In one spatial dimension and for $\delta D = 0$, the function $H(x, t)$ is explicitly known (see e.g., [4]). For $\delta D/D \ll 1$, we estimate the average growth in perturbation theory, i.e., by replacing the average $\langle\cdot\rangle$ with the average over the solvable case of $\delta D = 0$. The result is

$$\frac{dF(t)}{dt} = \frac{\delta D}{4D\sqrt{\pi\epsilon t_f}} H(0)G(t/t_f), \tag{4}$$

where $G(x) = \exp(x)\mathrm{erfc}(\sqrt{x})$, $t_f = 2DN^2$ and ϵ is an ultraviolet cutoff that can be assumed to be of order 1. Expression (4) can be used to write the growth of $\delta F(t) = F(t) - F(0)$ in a scaling form

$$\delta F(t) = H(0)\sqrt{t_f}\frac{\delta D}{D}\phi(t/t_f), \tag{5}$$

where the scaling function ϕ is independent from parameters, and $\phi(x) \sim x$ for small x. The growth of $F(t)$ and the scaling form are numerically confirmed in Fig. 2.

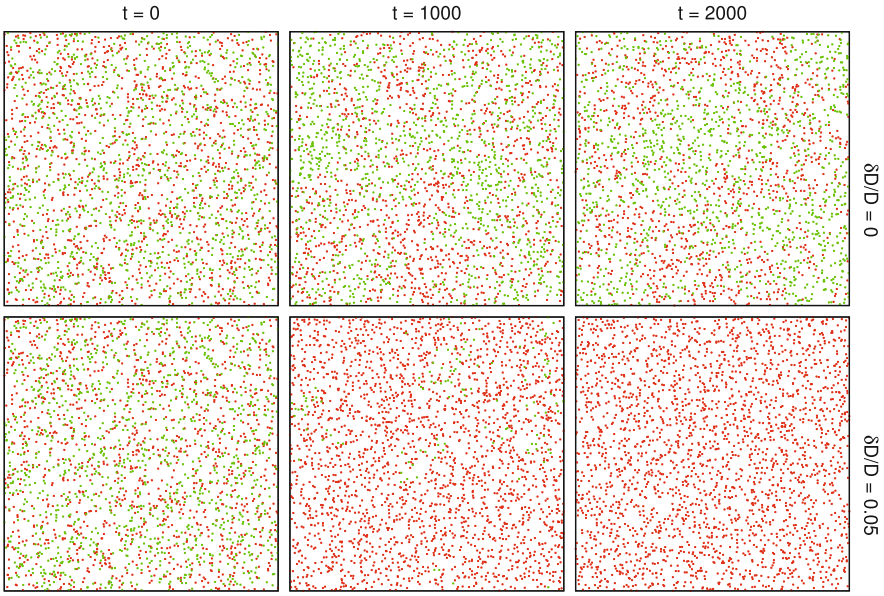

Fig. 1 Snapshots of $2D$ configurations, a particle-based simulation of model (1). In all panels, parameters are $N = 10^4$ and $D = 10^{-4}$. *Upper row*: the two species have the same diffusivity. *Lower row*: the *red species* have diffusivity $D + \delta D$ with $\delta D/D = 0.05$. To help the viewer, configurations has been down-sampled (adapted from [6])

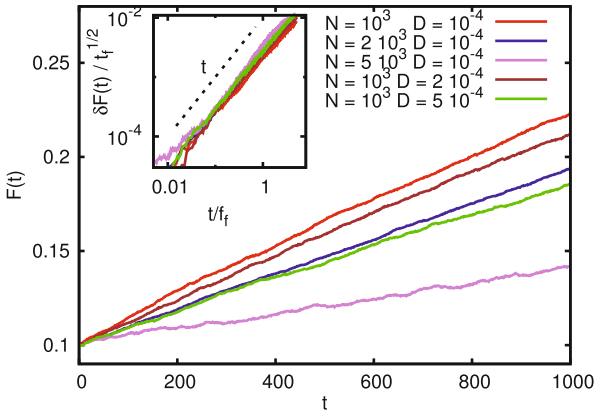

Fig. 2 Average concentration of the fast species $F(t)$ varying the number density N and the diffusion constant of the slowest species D in one dimension. In all simulations, we fixed $\delta D/D = 0.1$, the initial fraction of the fast species is $F(0) = 0.1$ and the system size is $L = 10$. Curves are average over 10^3 realizations. The *inset* shows a data collapse according to Eq. (5). Linear scaling (*black dashed line*) is shown for comparison (adapted from [6])

Notice that, at this order, perturbation theory does not predict absorbing states. This means that the perturbable approach can properly describe the dynamics only on times shorter than the global fixation time, which is of the order of L^2/D.

We now compare the selective advantage caused by a difference in diffusivity with that provoked by a difference s in reproduction rates. Assuming $s \ll 1$ and averaging directly such term, one obtains $dF/dt = sH(0)G(t/t_f)/2$. Comparing the latter expression with Eq. (4), one can define an *effective* advantage given by

$$s_{eff} = \frac{\delta D}{2D\sqrt{\epsilon \pi t_f}}. \tag{6}$$

In higher dimensions, the problem can be described starting from the general evolution equation for the heterozygosity, as obtained from Eq. (2) for $\delta D = 0$:

$$\partial_t H(x,t) = 2D\nabla^2 H - \frac{2\mu}{N} H(0,t)\delta(x). \tag{7}$$

Due to the spatial regularization [1], the delta function resulting from Ito's Lemma must be interpreted as $\delta(x) \sim 1/a^d$, where $a \sim \sqrt{2D\epsilon}$ is the lattice mesh. In an adiabatic approximation, $\nabla^2 H|_{x=0}$ can then be estimated as

$$\nabla^2 H|_{x=0} \sim \frac{\mu H(0,t)}{DN(D\epsilon)^{d/2}}, \tag{8}$$

which is consistent with Eq. (5) for $d = 1$. Evaluating Eq. (8) in $d = 2$ yields $\nabla^2 H|_{x=0} \sim \mu H(0,t)/(ND^2\epsilon)$, i.e., the effective advantage becomes a factor larger $1/\sqrt{D\epsilon}$ compared to the one dimensional case.

Finally, the effective selective advantage introduced in Eq. (6) can be used to study the probability of fixation P_{fix}, defined as the probability of reaching the absorbing state $f = 1$ from Eq. (2). In presence of a reproductive advantage, P_{fix} is given by Doering et al. [1] and Pigolotti et al. [8]:

$$P_{fix}(s) = \frac{1 - \exp(-2sNF(0))}{1 - \exp(-2sN)}. \tag{9}$$

Assuming the same formula to hold in our case with s_{eff} replacing s, leads us to an interesting prediction: P_{fix} should not depend on N as $s_{eff} \propto N^{-1}$. This prediction is confirmed in simulations shown in Fig. 3.

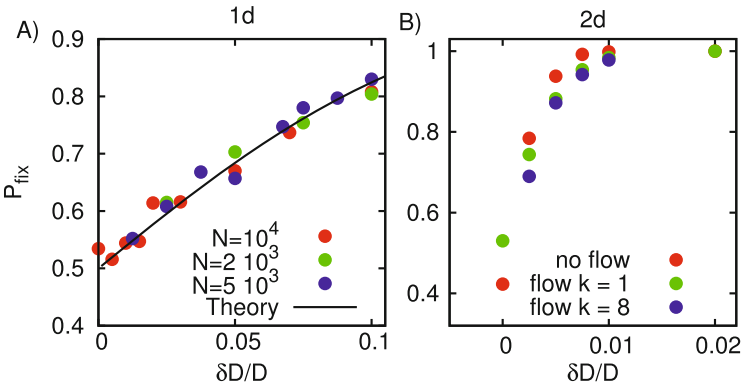

Fig. 3 Fixation probabilities. *Left*: 1D; the *black line* is the theoretical prediction of Eq. (9). *Right*: 2D; including simulations with a fluid flow. In both panels we set $D = 10^{-4}$ (adapted from [6])

3 Conclusions

An analysis of the problem of competition of species with two different diffusivities shows how taking into account stochastic fluctuation is crucial to understand the dynamics. Analytical results are quantitative consistent with particle simulations in continuous space [6]. Similar models considered on the lattice and studied with discrete equations lead to similar qualitative conclusions [5].

Acknowledgements I thank Roberto Benzi, David Nelson, Prasad Perlekar, Mogens H. Jensen and Federico Toschi for a fruitful collaboration.

References

1. C.R. Doering, C. Mueller, and P. Smereka. *Physica A* **325**(1–2) (2003), 243–259.
2. R.A. Fisher, "The wave of advance of advantageous genes". *Ann. Eugenics* **7** (1937), 353–369.
3. A. Kolmogorov, N. Petrovsky, and N. Piscounov, "Étude de l'équation de la diffusion avec croissance". *Moscow Univ. Math. Bull.* **1** (1937), 1–25.
4. K.S. Korolev, M. Avlund, O. Hallatschek, and D.R. Nelson, "Genetic demixing and evolution in linear stepping stone models". *Rev. Mod. Phys.* **82** (2010), 1691–1718.
5. Y.T. Lin, H. Kim, and C.R. Doering, "Demographic stochasticity and evolution of dispersion I. Homogeneous environments". *J. Math. Biol.* **70** (2015), 647.
6. S. Pigolotti and R. Benzi, "Selective advantage of diffusing faster". *Phys. Rev. Lett.* **112** (2014), 188102.
7. S. Pigolotti, R. Benzi, M. Jensen, and D.R. Nelson, "Population genetics in compressible flows". *Phys. Rev. Lett.* **108** (2012), 128102.
8. S. Pigolotti, R. Benzi, P. Perlekar, M.H. Jensen, F. Toschi, and D.R. Nelson, "Growth, competition and cooperation in spatial population genetics". *Theo. Pop. Biol.* **84** (2013), 72–86.

Density-Dependent Diffusion and Epidemics on Heterogeneous Metapopulations

Albert Avinyó, Marta Pellicer, Jordi Ripoll, and Joan Saldaña

1 The Model

Systems with many components (individuals or local populations as cities, or metropolitan areas, or regions, . . .) connected by non-trivial associations or relationships can be statistically described by means of the formalism of complex networks which is based on descriptors like degree distributions, degree-degree correlations, etc. In the last years, many researchers from different fields have been using different approaches to model processes taking place on complex networks.

Here we take the approach of heterogeneous mean-field models for modelling epidemic spread on a heterogeneous meta-population, which is a set of local populations with a non-trivial pattern of migratory flows amongst them. This type of approach was first introduced in [1] and extended in [2]. In [4, 6] the authors use the new formulation introduced in [5] and compare analytical results with stochastic simulations obtaining a good agreement between them. We extend our previous works [3–6] to a non-linear diffusion term and demographic turnover. For instance, the model can tackle the human mobility from rural areas to big cities to look for job opportunities, or the other way round, from crowded areas to small villages to get rid of stress.

We deal with the following mean-field type model as a system of ode's which combines (random, memoryless) movement of individuals among patches (nodes) with SIS-epidemics within each patch, with infection transmission rate β, recovery

A. Avinyó (✉) • M. Pellicer • J. Ripoll • J. Saldaña
Departament d'Informàtica, Matemàtica Aplicada i Estadística, Universitat de Girona, Girona, Spain
e-mail: albert.avinyo@udg.edu; marta.pellicer@udg.edu; jripoll@imae.udg.edu; joan.saldana@udg.edu

M. Corbera et al. (eds.), *Extended Abstracts Spring 2014*, Trends in Mathematics 4,
DOI 10.1007/978-3-319-22129-8_25

rate μ, and equal birth and death rates δ. The evolution of the average number of susceptible individuals $\rho_{S,k}(t)$ and infected individuals $\rho_{I,k}(t)$, in patches of connectivity k, $k = 1, \ldots, k_{\max}$, at time t, is governed by

$$\begin{aligned}\rho'_{S,k}(t) &= \left(\mu - \beta c(\rho_k)\tfrac{\rho_{S,k}}{\rho_k}\right)\rho_{I,k} + \delta(\rho_k - \rho_{S,k}) - D_S(\rho_k)\rho_{S,k} + k\sum_{k'} D_S(\rho_{k'})P(k'|k)\tfrac{\rho_{S,k'}}{k'},\\ \rho'_{I,k}(t) &= \left(\beta c(\rho_k)\tfrac{\rho_{S,k}}{\rho_k} - \mu\right)\rho_{I,k} - \delta\rho_{I,k} - D_I(\rho_k)\rho_{I,k} + k\sum_{k'} D_I(\rho_{k'})P(k'|k)\tfrac{\rho_{I,k'}}{k'}.\end{aligned} \tag{1}$$

Here, $P(k'|k)$ is the conditional probability that a patch of degree k has a connection to a patch of degree k'. Each local population size is denoted by $\rho_k(t) = \rho_{S,k}(t) + \rho_{I,k}(t)$ and we are assuming a density-dependent number of contacts $c(\rho_k)$, and also density-dependent diffusion rates $D_S(\rho_k)$ and $D_I(\rho_k)$ of susceptible and infected individuals respectively, in order to deal with demographic effects on the migration process. The latter is the main novelty of the present work.

The first term in each equation corresponds to the infection and recovery processes, the second one is the neutral demographic turnover, and the last ones are the migration process which can be split into the negative terms counting the number of individuals leaving the patch and the positive ones counting those arriving at it.

Once we know the solution of system (1), the total number of susceptible and infected individuals is $S(t) = N\sum_k p(k)\,\rho_{S,k}(t)$ and $I(t) = N\sum_k p(k)\,\rho_{I,k}(t)$, respectively, where $p(k)$ is the degree distribution and N is the number of nodes of the network. From (1) and assuming the consistency condition $kP(k'|k)p(k) = k'P(k|k')p(k')$ which means that the number of links from k to k' must be equal to the number of links from k' to k, it follows that the total number of individuals is conserved in the meta-population, i.e., $S(t) + I(t) = N\rho^0$, with ρ^0 being the average number of individuals per patch.

1.1 Density Dependent Rates

The number of contacts c is assumed to be a non-decreasing, density dependent function, generalizing the two cases considered in [4, 5]: $c(\rho) = \rho$ (fully-mixed population) and $c(\rho) = 1$ (limited homogeneous mixing).

The diffusion rates D_S and D_I are also density dependent and will be assumed to be of the form $D_i^0\rho^{\alpha_i}$, with exponent α_i for $i = I, S$. For $\alpha_i < 0$ we have the scenario in which the probability of emigration is higher in patches with low population (rural emigration). On the other hand, $\alpha_i > 0$ models the scenario in which the probability of emigration is higher in patches with high population (urban emigration). Finally, $\alpha_i = 0$ recovers the constant diffusion rate considered in [4, 5]. Moreover, we will assume that the total outflow of individuals in any patch, $D_i(\rho)\rho$ with $i = I, S$, is a strictly increasing function of its population ρ. This implies the assumption $\alpha_i > -1$.

2 Migration Process Without Epidemics

Denoting by $\vec{\rho}_S$ and $\vec{\rho}_I$ the vectors of the population distribution of each type in the metapopulation, system (1) can be written as

$$\begin{cases} \vec{\rho}\,'_S = \operatorname{diag}\big(\tilde{\mu} - \beta\, c(\rho_k)\dfrac{\rho_{S,k}}{\rho_k}\big)\,\vec{\rho}_I + (\mathcal{C} - Id)\operatorname{diag}(D_S(\rho_k))\,\vec{\rho}_S\,, \\ \vec{\rho}\,'_I = \Big(\operatorname{diag}\big(\beta\, c(\rho_k)\dfrac{\rho_{S,k}}{\rho_k} - \tilde{\mu}\big) + (\mathcal{C} - Id)\operatorname{diag}(D_I(\rho_k))\Big)\,\vec{\rho}_I\,, \end{cases} \tag{2}$$

where $\tilde{\mu} = \mu + \delta$ and $\mathcal{C}$, which is non-negative and assumed to be irreducible, denotes the connectivity matrix with $\mathcal{C}_{kk'} = kP(k'|k)/k'$. For uncorrelated networks, $P(k'|k) = k'p(k')/\langle k\rangle$ and, hence, $\mathcal{C}_{kk'} = kp(k')/\langle k\rangle$, where the brackets stands for the mean value. In (2) we use the notation $\operatorname{diag}(x_k)$ for a diagonal matrix whose diagonal elements are $x_1, \ldots, x_{k_{\max}}$.

To study the impact of the different diffusion rates on the population distribution ρ_k, we consider the model in the absence of epidemic, that is, with $\vec{\rho}_I = \vec{0}$, and study the disease-free equilibrium $\vec{\rho}^{\,*} = \vec{\rho}_S^{\,*}$. As $\mathcal{C}$ is irreducible, $v_k = k$, $k = 1, \ldots, k_{\max}$, is the only positive eigenvector of $\mathcal{C} - Id$ associated to the dominant eigenvalue $\lambda = 0$. So, from (2) at the disease-free equilibrium, ρ_k^* satisfies $D_S(\rho_k^*)\rho_k^* = M\,k$, with M being a suitable constant. Assuming that $F(\rho) := D_S(\rho)\rho$ is continuous and strictly increasing, with $F(0) = 0$, the existence and uniqueness of

$$\rho_k^* = F^{-1}(M\,k) \tag{3}$$

is guaranteed and, hence, M is computed from the normalizing condition $\sum_k p(k)\rho_k^* = \rho^0$.

According to the hypotheses on $F(\rho)$, the disease-free equilibrium ρ_k^* is increasing in the degree k. In particular, for $D_S(\rho_k) = D_S^0\rho_k^\alpha$, $\alpha > -1$, (3) is explicitly given by

$$\rho_k^* = \frac{k^{1/(1+\alpha)}}{\langle k^{1/(1+\alpha)}\rangle}\rho^0. \tag{4}$$

Note the linear dependence of ρ_k^* on k when the diffusion rate is constant, i.e., $\alpha = 0$ (Fig. 1).

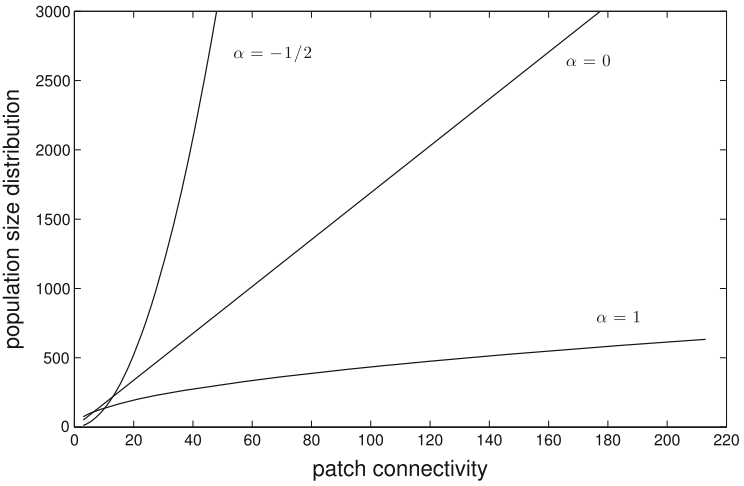

Fig. 1 Profile of ρ_k^* given by (4) with $\alpha = -1/2$ (superlinear), $\alpha = 0$ (linear), and $\alpha = 1$ (sublinear) for scale-free networks with $p(k) \sim k^{-3}$, $k_{\min} = 3$, and $k_{\max} = 213$. The average population per patch is $\rho^0 = 100$

3 Early Stage of the Epidemics

The initial growth of the epidemic is governed by the dominant eigenvalue λ_1 of the Jacobian matrix of (2) at the disease-free equilibrium, which can be written as:

$$\begin{pmatrix} (\mathcal{C} - Id) \cdot \operatorname{diag}\left(F'(\rho_k^*)\right) & -\operatorname{diag}\left(\beta c(\rho_k^*) - \tilde{\mu}\right) \\ 0 & (\mathcal{C} - Id) \cdot \operatorname{diag}\left(D_I(\rho_k^*)\right) + \operatorname{diag}\left(\beta c(\rho_k^*) - \tilde{\mu}\right) \end{pmatrix}. \tag{5}$$

An exponential initial growth of the infectious population occurs when the disease-free becomes unstable, that is, when $\lambda_1 > 0$. The block structure of the Jacobian and the fact that the dominant eigenvalue of the first block is 0 imply that $\lambda_1 > 0$ if and only if the dominant eigenvalue of the fourth block is strictly positive. A sufficient condition for this to be fulfilled is

$$\max_k \frac{\beta c(\rho_k^*)}{\tilde{\mu} + (1 - P(k|k)) D_I(\rho_k^*)} > 1, \tag{6}$$

which follows after grouping all the diagonal terms in the fourth block.

For a given k, the previous ratio can be interpreted as an estimation of the basic reproduction number of the populations living in patches with connectivity k, R_k^0, neglecting the immigration process from patches with connectivities $k' \neq k$. Note that the factor $1 - P(k|k)$ in the denominator accounts for individuals who emigrate to patches with a different connectivity.

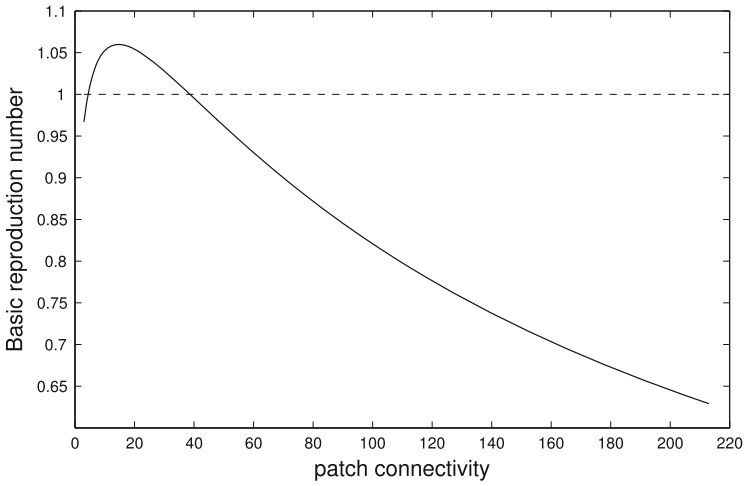

Fig. 2 Estimation of R_k^0 given by the ratio in (6) for uncorrelated scale-free networks with $\gamma = -3$. Parameters: $\beta = 1.1$, $\tilde{\mu} = 1$, $c(\rho) = \rho$, and $D_S(\rho) = D_I(\rho) = 0.1\,\rho^{\alpha}$ with $\alpha = 5$ (urban emigration)

In contrast to the case of constant diffusion in scale-free networks [4], the maximum in (6) is not necessarily attained at populations with the largest connectivities. In some cases, the maximum is attained at the minimum degree $k_{\min}$. In other cases, as the one in Fig. 2, this maximum occurs at intermediate values of k. Since the ratio in (6) is a lower bound of R_k^0, this means that local epidemic outbreaks will take place for sure in patches with intermediate connectivities. So, the early stage of an epidemic may not be triggered by infectious individuals living in large populations, as it could be expected from the fact that ρ_k^* increases with k. Hence, the role of migration becomes crucial since it determines which patches act as sources or sinks of infectious individuals.

Acknowledgements This work has been partially supported by the research grant MTM2011-27739-C04-03 of the Spanish government and the project 2009-SGR-345 of the Generalitat de Catalunya.

References

1. V. Colizza, R. Pastor-Satorras, and A. Vespignani, "Reaction-diffusion processes and metapopulation models in heterogeneous networks". *Nat. Phys.* **3** (2007), 276–282.
2. V. Colizza and A. Vespignani, "Epidemic modeling in metapopulation systems with heterogeneous coupling pattern: Theory and simulations". *J. Theor. Biol.* **251** (2008), 450–467.
3. D. Juher and V. Mañosa, "Spectral properties of the connectivity matrix and the SIS-epidemic threshold for mid-size metapopulations". *Math. Model. Nat. Phenom.* **9** (2014), 108–120.

4. D. Juher, J. Ripoll, and J. Saldaña, “Analysis and Monte-Carlo simulations of a model for the spread of infectious diseases in heterogeneous metapopulations”. *Phys. Rev. E* **80** (2009), 041920.
5. J. Saldaña, “Continuous-time formulation of reaction-diffusion processes on heterogeneous metapopulations”. *Phys. Rev. E* **78** (2008), 01290.
6. J. Saldaña, “Modelling the spread of infectious diseases in complex metapopulations”. *Math. Model. Nat. Phenom.* **5** (2010), 22–37.

Are Viral Blips in HIV-1-Infected Patients Clinically Relevant?

Daniel Sánchez-Taltavull and Tomás Alarcón

1 Introduction

HIV infection has a disturbing feature, after being treated by administration of *highly active anti-retroviral therapy* (HAART), plasma viral load decays below the detection threshold of standard clinical assays ($\sim$50 copies RNA/mL) but appears to fail to completely eradicate the infection, a residual viral load (detectable only by supersensitive assays) persists in plasma. An evidence that the virus is not completely suppressed is the observation of the so-called vira blips, transient episodes of viremia where the viral load raises above the standard test detection limit for a brief period of time. The origin and clinical relevance of these blips remains unclear. There are several studies that have compiled evidence against viral blips being correlated with virological failure.

In order to explain the origin of these blips, Rong and Perelson [3] have formulated a model in which stochastic activation of latently infected cells can maintain viral blips without completely depleting the latent reservoir, thus maintaining long-term, low-level viremia. Conway and Coombs [1] have proposed a model to analyse the stochastic viral dynamics in treated patients. This model treats viral blips as random events occurring every time the viral load reaches the standard detection limit, however, there are several properties of the statistics of viral blips in which [1] appears to depart from experimental observation, for example the duration and frequency of the viral blips.

The models discussed assume that the system is well-mixed, the number of species are uniformly distributed. For this modelling assumption to hold, the numbers of each species must be large. The system we are dealing with in this paper has at least two species, virus and infected cells, which are present in very

D. Sánchez-Taltavull • T. Alarcón (✉)
Centre de Recerca Matemàtica, Campus de Bellaterra, Barcelona, Spain
e-mail: dsanchez@crm.cat; talarcon@crm.cat

M. Corbera et al. (eds.), *Extended Abstracts Spring 2014*, Trends in Mathematics 4,
DOI 10.1007/978-3-319-22129-8_26

small numbers and we can observer large fluctuations in the local numbers of the species. The effect of this inhomogeneity can be rather sizeable, specially since measurements of viral load are performed by extracting small samples of blood which are then analysed. The aim of this paper is to ascertain whether density fluctuations affect the stochastic dynamics of the viral load in HAART-treated patients beyond the predictions of [1] and investigate if an stochastic model which includes density fluctuations is capable of reproduction of the experimental results.

2 Stochastic Inhomogeneous Model

We consider a compartmental model in which we assume that compartments are arranged on a one dimensional, closed (i.e., with periodic boundary conditions) lattice. In each compartment, we consider three types of interacting species, namely, active infected cells, latently infected cells, and virus. The number of each of these species in compartment i is referred to as T_i^*, L_i, and V_i, respectively, where $i = 1, \ldots, N_c$ with N_c is the number of compartments. We further introduce the vector $X(t) = (T_1^*(t), L_1(t), V_1(t), \ldots, T_{N_c}^*(t), L_{N_c}(t), V_{N_c}(t))$.

The stochastic dynamics of our system is described by the corresponding Master Equation:

$$\frac{\partial P_X}{\partial t}(t) = \sum_r \big(W(X-r,r,t)P(X-r,t)\big) - W(X,r,t)P(X,t). \tag{1}$$

The transition rates are defined in Table 1.

In order to facilitate later formulation of our in silico blood extraction protocol and its comparison with [2], we will consider compartments of volume $V_c = 8.5\,\mathrm{mL}$ each, which is the volume of blood sampled extracted for analysis in the study reported in [2]. We will consider that an average individual has 5 L of blood so we need to consider $N_c = 588$ compartments.

2.1 In Silico Blood Sample Analysis Model

Nettles et al. [2] designed an experimental protocol in which ten HIV-1 infected patients under HAART were intensively sampled (every 2 or 3 days) for a period of 3–4 months. Each time blood was extracted, two samples per patient were taken and sent to two different laboratories for analysis.

Our procedure is as follows. After running the compartmental dynamics until time t_c, which is chosen to be long enough so that the average properties of the system reach an steady state, we choose two compartments at random i and j among the N_c compartments that compose our system. We then record the corresponding

Table 1 Transition rates corresponding to the stochastic model of viral blip generation

Transition rate	$r_{j+(i-1)R_L} = \Delta X_i$	Description
$W_{1+(i-1)R_L} = \eta(1-\epsilon)kV_iT_i$	$(1,0,-1)$	Latent infection, $T_i + V_i \rightarrow L_i$
$W_{2+(i-1)R_L} = (1-\eta)(1-\epsilon)kV_iT_i$	$(0,1,-1)$	Active infection, $T_i + V_i \rightarrow T_i^*$
$W_{3+(i-1)R_L} = rL_i$	$(1,0,0)$	Latent cell proliferation, $L_i \rightarrow 2L_i$
$W_{4+(i-1)R_L} = \frac{r}{L_{max}} \frac{L_i(L_i-1)}{2} V_c^{-1}$	$(-2,0,0)$	Latent cell binary annihilation, $L_i + L_i \rightarrow \emptyset$
$W_{5+(i-1)R_L} = d_0L_i$	$(-1,0,0)$	Latent cell death, $L_i \rightarrow \emptyset$
$W_{6+(i-1)R_L} = a_LL_i$	$(-1,1,0)$	L_i Activation, $L_i \rightarrow T_i^*$
$W_{7+(i-1)R_L} = \delta T_i^*$	$(0,-1,0)$	Active cell death, $T_i^* \rightarrow \emptyset$
$W_{8+(i-1)R_L} = cV_i$	$(0,0,-1)$	Virion clearance, $V \rightarrow \emptyset$
$W_{9+(i-1)R_L} = p_vT_i^*$	$(0,0,1)$	Continuous virion production, $T_i^* \rightarrow T_i^* + V_i$
$W_{10+(i-1)R_L} = \epsilon kV_iT_i$	$(0,0,-1)$	Failed infection, $V_i \rightarrow \emptyset$
Transition rate	$r_j = \Delta X$	Description
$W_{1+10N_c+6(i-1)} = \mu_{L+}L_i$	$(0,\ldots,0,-1,0,0,1,0,\ldots)$	$L_i + L_{i+1} \rightarrow L_i - 1 + L_{i+1} + 1$
$W_{2+10N_c+6(i-1)} = \mu_{L-}L_i$	$(0,\ldots,0,1,0,0,-1,0,\ldots)$	$L_i + L_{i-1} \rightarrow L_i - 1 + L_{i-1} + 1$
$W_{3+10N_c+6(i-1)} = \mu_{T^*+}T_i^*$	$(0,\ldots,0,-1,0,0,1,0,\ldots)$	$T_i^* + T_{i+1}^* \rightarrow T_i^* - 1 + T_{i+1}^* + 1$
$W_{4+10N_c+6(i-1)} = \mu_{T^*-}T_i^*$	$(0,\ldots,0,1,0,0,-1,0,\ldots)$	$T_i^* + T_{i-1}^* \rightarrow T_i^* - 1 + T_{i-1}^* + 1$
$W_{5+10N_c+6(i-1)} = \mu_{V+}V_i$	$(0,\ldots,0,-1,0,0,1,0,\ldots)$	$V_i + V_{i+1} \rightarrow V_i - 1 + V_{i+1} + 1$
$W_{6+10N_c+6(i-1)} = \mu_{V-}V_i$	$(0,\ldots,0,1,0,0,-1,0,\ldots)$	$V_i + V_{i-1} \rightarrow V_i - 1 + V_{i-1} + 1$

$R_L = 10$, $T_i = 3 \cdot 10^9$, $r = 0.2\ \text{day}^{-1}$, $\eta = 0.001$, $\epsilon = 0.85$, $d_0 = 0.001\ \text{day}^{-1}$, $a_L = 0.1\ \text{day}^{-1}$, $c = 23\ \text{day}^{-1}$, $p_v = 2000\ \text{day}^{-1}$, $k = 4.8 \cdot 10^{-12}\ \text{day}^{-1}$. $\mu_{J\pm}$ is taken such that the diffusion coefficient, D_J of the species J $(= V, T^*, L)$, is $D_V = 5\,\mu\text{m}^2\,\text{s}^{-1}$, $D_{T^*} = D_L = 0.05\,\text{m}^2\,\text{s}^{-1}$, to take into account the directionality of blood flow $\mu_{j+} = 3\mu_{j-}$. Here, $X_i = (L_i, T_i^*, V_i)$

state $x_i(t_c) = (T_j^*(t_c), L_i(t_c), V_i(t_c))$ and $x_j(t_c) = (T_j^*(t_c), L_j(t_c), V_j(t_c))$. In order to account for possible delays between the time of extraction and the actual analysis, we assume that the extracted samples continue to evolve subject to the local (within-compartment) dynamics with the transition rates corresponding to between-compartment transitions $W_{6+10N_c+6(i-1)} = 0$. As the extracted sample is isolated for the mechanisms of the body to clear the virus we will consider a new $W_{8+10N_c+R_L(i-1)} = c^* V_i$ with $c^* < c$. This post-extraction dynamics is ran for a duration t_w.

3 Results

In order to study the Master Equation we perform numerical simulations by means of the Gillespie algorithm. The first thing we investigate is how the mean viral load affects the appearance of the viral blips: in Fig. 1 (top) we show that the probability

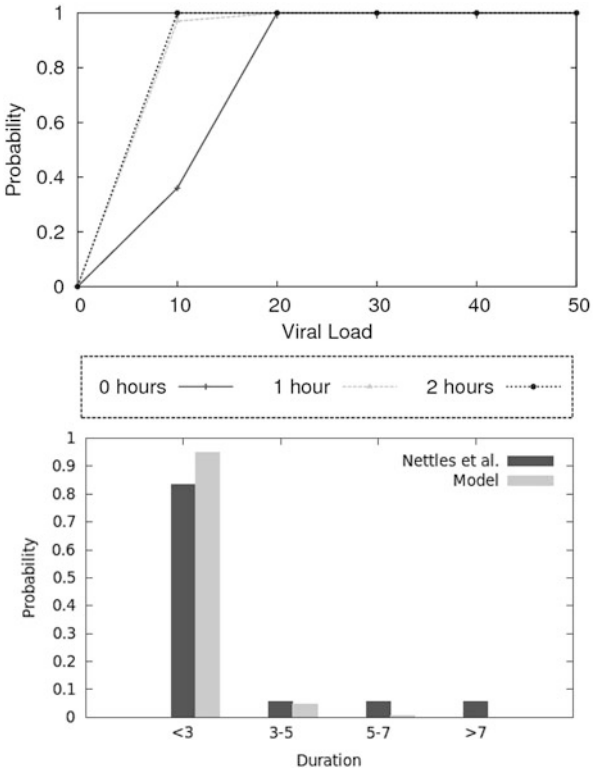

Fig. 1 *Top*: probability of observing at least one blip in our in silico blood sample analysis model as a function of the average virus load for different values of t_w. *Bottom*: comparison between blips statistics obtained in the study by Nettles et al. [2] and those obtained from our simulations, where $t_w = 0$

of the appearance of at least one viral blip increases with the mean viral load and the time between the extraction and the observation. Another important thing is the duration of this viral blips: in Fig. 1 (bottom) we show a comparison between the duration observed in the study by Nettles et al. [2] and our model predictions, the simulation results are in good agreement with experimental observations. However, appears to overestimate the frequencies of the shorter blips.

4 Discussion

Our aim is to discuss whether the effect of the inhomogeneous density fluctuations can be the origin of viral blips. To this end, we have presented an inhomogeneous stochastic HIV-1 infection dynamics model. We have further designed an in silico blood sample model, in order to reproduce as close as possible the experimental protocol of Nettles et al. [2].

Furthermore, our approach allows us to (partially) address the issue of whether laboratory and sample manipulation artifacts affect the observation of blips. We have investigated the effect that the post-extraction handling time, i.e., the time elapsed between sample extraction and the actual analysis, has on the statistics of the number of blips. According to our model, this factor contaminates the statistics of the number of blips, which supports the position regarding the effects laboratory artifacts on viral blip observation.

References

1. J.M. Conway and D. Coombs, "A stochastic model of latently infected cell reactivation and viral blip generation in treated HIV patients". *PLoS Comput. Biol.* **7** (2011), e1002033.
2. R.E. Nettles, T.L. Kieffer, P. Kwon, D. Monie, Y. Han, T. Parsons, J. Cofrancesco, J.E. Gallant, T.C. Quinn, B. Jackson, C. Flexner, K. Carson, S. Ray, D. Persaud, and R.F. Siliciano, "Intermittent HIV-1 viremia (blips) and drug resistance in patients receiving HAART". *JAMA* **293** (2005), 817–829.
3. L. Rong and A.S. Perelson, "Modeling latently infected cell activation: Viral and latent reservoir persistence, and viral blips in HIV-infected patients on potent therapy". *PLoS Comput. Biol.* **5** (2009), e1000533.

Models of Developmental Plasticity and Cell Growth

Graeme Wake

1 Introduction

In this note we discuss the following topics:

1. *Epigenetics*: How to alter your genes? This is evolution within a lifetime. Epigenetics is a relatively new scientific field; research only began in the mid nineties, and has only found traction in the wider scientific community in the last decade or so. We have long been told our genes are our destiny. But it is now thought a genotype's expression (that is, its phenotype), can change during its lifetime by habit, lifestyle, even finances. What does this mean for our children? So we consider *phenotype change*:
   (a) firstly in a stochastic setting, where we consider the expected value of the mean fitness;
   (b) then we consider a Plastic Adaptive Response (PAR) in which the response to an environmental cue is initiated after a period of waiting;
   (c) finally, we consider the steady-fitness states, when the phenotype is modelled on a continuous scale providing a structured variable to quantify the phenotype state.
2. Consider the steady-size distribution of an evolving cohort of cells and therein establish thresholds for growth or decay of the cohort.

G. Wake (✉)
Centre for Mathematics in Industry, Institute of Natural and Mathematical Sciences, Massey University, Albany, Auckland, The New Zealand

Gravida, National Centre for Growth and Development, Auckland, The New Zealand
e-mail: G.C.Wake@massey.ac.nz

M. Corbera et al. (eds.), *Extended Abstracts Spring 2014*, Trends in Mathematics 4,
DOI 10.1007/978-3-319-22129-8_27

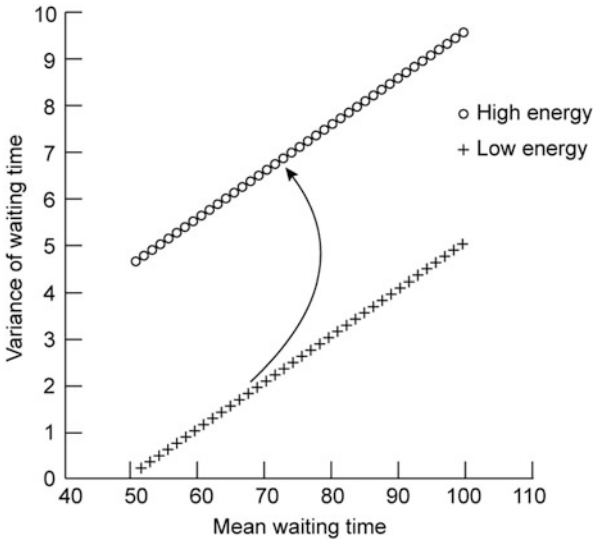

2 Details

2.1 Topic (1a)

In some species an inducible secondary phenotype will develop sometime after the environmental change that evolves it. Nishimura showed in [2] how an individual organism should optimise the time it takes to respond to an environmental change (the *waiting time*). If the optimal waiting time is considered to be a population attribute then there are implications for the mean fitness in that population. We do this in [4] where we assume that the waiting time is a normally distributed random variable because of the biological variance inherent in mounting the response. It is found that the value of the mean waiting time that maximises fitness depends linearly on the variance of the waiting time, an important issue where perturbed environments impact on the development of a Predictive Adaptive Response (PAR). See diagram below, where we have also shown the trade-off between the expected value of the time for plasticity and the variance of the time for plasticity in a population subjected to two different energy availabilities, and the optimal path of time to plasticity mean and variance when the energy available changes from low to high.

2.2 Topic (1b)

Here we consider a PAR in which the response to an environmental cue is initiated after a period of waiting and the induced phenotype develops completely before the eventual environmental change forecast by the cue. This is developed non-stochastically, in [3].

The realization that the induced response need not manifest itself immediately after the environmental cue has generally been under-appreciated by evolutionary biologists. Predictive adaptive responses are a form of developmental plasticity but differ from most in that the selective advantage of the response manifests later in life, well after the initiating environmental cue, when a second or "eventual" environment prevails. Note that this eventual environment may or may not be the same as that than induced the initial response. The archetypal case is adult coat thickness in the Meadow Vole, *Microtus pennsylvanicus*, which is induced before birth by the day length sensed by pregnant mothers, but which has an evolutionary pay-off in the highly seasonal post-natal environment.

Our modelling shows that, for a variety of formulations for the costs of development, predictive adaptive responses (PARs) maximize fitness when there is no anticipation (the time between the completion of the development of the induced phenotype and the onset of the eventual environment). In addition, when rapid development is costly, fitness is maximized when there is no delay between the environmental cue and the initiating of development, and hence all available time is allotted to development. Developmental costs appear to be privileged, fitness being maximized whenever the additional costs of development are minimized.

Second in the hierarchy is the delay time, with fitness maximized when any time not required for development is assigned to the delay (Fig. 1).

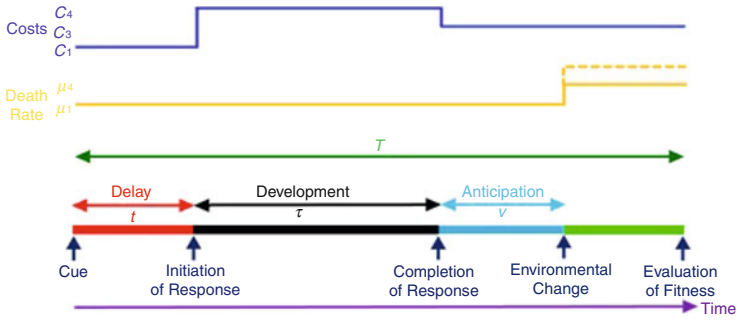

Fig. 1 Life history of the model organism. The dashed yellow line shows the death rate for an organism that fails to respond to the environmental cue

2.3 Topic (1c)

We consider steady-fitness states, in a model developed by Korobeinikov and Dempsey [1], in which the phenotype is modelled on a continuous scale providing a structured variable to quantify the phenotype state. This enables thresholds for survival/extinction to be established in terms of fitness. We note that methylation is a chemical process by which genes can be switched off-thereby changing our phenotype. There is also increasing evidence that certain cancers are caused by misplaced epigenetic tags. For development we switch to viral evolution which is probably the most significant single factor accountable for emergence of new pathogens and drug-resistant strains and preventing a development of effective drugs and vaccines. The ability of virus to evolve and leads to development of drug-resistant strains, thus making its treatment extremely difficult; it prevents development of an effective vaccine, and enables the virus to escape immune control. Moreover, it is believed that the dynamics of HIV is also mostly determined by the ability of HIV to evolve. Viruses mutate quickly so data is easy to obtain.

Phenotype expression can be modelled using these structured population models. These involve challenging nonlocal nonlinear eigenvalue problems, with thresholds able to be quantified. Algorithms are being developed at present.

An example of the type of the non-local problem that arises is

$$DV''(s) + \left(\frac{abs}{\mu + a \int_0^\infty sV(s)ds} - m \right) V(s) = 0, s > 0,$$

with $V'(0) = V(\infty) = 0$. Here, $V(s)$ is the steady state population of the infected cells, which in turn is structured by the phenotype variable s. This equation is a type of nonlinear *eigenvalue problem*.

2.4 Topic (2)

We look now at the steady-size distribution of an evolving cohort of cells, such as tumour cells in vitro, and therein establish thresholds for growth or decay of the cohort. Living cell populations which are simultaneously growing and dividing are usually structured by size, which can be, for example, mass, volume, or DNA content. The evolution of the number density $n(x, t)$ of cells by size, in an unperturbed situation, is observed experimentally to exhibit the attribute of that of an asymptotic Steady Size Distribution (SSD). That is, $n(x, t) \sim$ scaled (by time only) multiple of a constant shape $y(x)$ as $t \to \infty$ (Fig. 2).

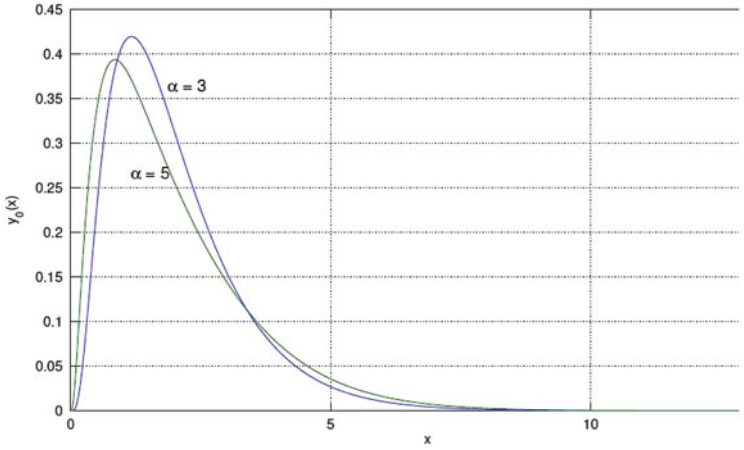

Fig. 2 SSD's for binary asymmetrical division $x \to (x/\alpha, x/\beta)$, where $1/\alpha + 1/\beta = 1$

3 The Cell Cycle

If $t_2 > t_1$ then the population is growing; and if $t_2 < t_1$ then the population is dying. By developing a simple evolutionary model to describe this outcome, criteria for the growth/decline of the cohort can be determined.

This work is relevant to the underlying understanding of cell tumour growth. The application is stimulating new mathematics, for example the spectral theory of non-local singular eigenvalue problems, see [5]. Cells dividing asymmetrically are essential for generating diverse cell types during development. The capacity for symmetric stem-cell self-renewal may confer developmental plasticity, increased growth and *enhance regenerative* capacity; however, it may also confer an inherent risk of cancer. When the machinery that regulates asymmetric divisions is disrupted, however, these cells begin dividing symmetrically and form tumours. This needs underpinning rigour to understand the dynamics of cancer-cell growth and regulation of cell-growth.

This is established using a new class of non-local (but linear) singular eigenvalue problems which have point spectra, like the traditional Sturm–Liouville problems. The first eigenvalue gives the threshold required. But these problems are first order unless dispersion is added to incorporate random perturbations; the same idea will also apply here. Current work involves binary asymmetrical division of cells, simultaneous with growth. It has implications to cancer biology, helping biologists to conceptualise non-local effects and the part they may play in cancer. This is developed in [6].

A new model is needed of cell-growth with asymmetrical division [two or more daughter cells of different sizes (usually DNA content)] from a single division event. This model must capture the key features from earlier models with symmetrical cell-division, where the cell-size distribution tends asymptotically to one of constant

shape when the cohort is not disturbed; this being a well-known observation. This is also still called a steady-size-distribution (SSD).

A model is proposed which does this for different types of cellular evolution and amounts to a hyperbolic integro-differential equation. Separated solutions again answer the question of SSD behaviour and the time-constant can be a principal eigenvalue of a singular first-order integro-first-order ODE. More general questions arise as to whether these solutions are attracting with time and whether they span the space of all solutions.

Acknowledgements The support of Gravida (NCGD) is gratefully acknowledged.

References

1. A. Korobeinikov and C. Dempsey, "A continuous phenotype space model of RNA virus evolution within a host". *Mathematical Biosciences and Engineering*, **11** (2014), 919–927.
2. K. Nishimura, "Inducible plasticity: Optimal waiting time for the development of an inducible phenotype". *Evolutionary Ecology Research* **8** (2006), 553–559.
3. H.G. Spencer, A.B. Pleasants, P.D. Gluckman, and G.C. Wake, "A model of optimal development time for a plastic response". *Preprint*.
4. G. Wake, A. Pleasants, A. Beedle, and P. Gluckman, "A model for phenotype change in a phenotype change in a stochastic framework". *Mathematical Biosciences and Engineering* **7** (2010), 719–728.
5. G. Wake, A. Zaidi, and B. van-Brunt, "Tumour cell biology and some new non-local calculus", in "The Impact of Applications on Mathematics", Proceedings of Forum Math-for-Industry 2013, Springer, (2014).
6. A.A. Zaidi, B. Van Brunt, and G.C. Wake, "A model for asymmetrical cell division". Math. Biosci. Eng. **12**(3) (2015), 491–501. doi:10.3934/mbe.2015.12.491.